OPTIMIZATION OF SENSITIVITY OF ELECTROSPRAY IONIZATION MASS SPECTROMETRY FOR METABOLITE ANALYSIS

By

NARE ALPHEUS MAUTJANA

A DISSERTATION PRESENTED TO THE GRADUATE SCHOOL
OF THE UNIVERSITY OF FLORIDA IN PARTIAL FULFILLMENT
OF THE REQUIREMENTS FOR THE DEGREE OF
DOCTOR OF PHILOSOPHY

UNIVERSITY OF FLORIDA

2009

To my Grandmother,
Selaki MaChuene Seemole Mautjana

ACKNOWLEDGMENTS

I am very grateful to my mother Melida Mautjana for motivating me since my beginning of school at gaMahoai village through college in Vanderbijl Park and Cape Town South Africa, up until graduate school here in Gainesville, Florida USA. I acknowledge with much gratitude the (parent-like and financial) support I received from Dr. Hunt Davis and his wife Jeanne Davis anytime I needed it during the course of my PhD studies.

I thank Dr. Anna Brajter-Toth for her teaching, her guidance, and for being my guardian in many respects. What seemed like a long haul in the beginning turned out to be a brief period of professional and personal growth. I also thank members of the Toth group (Mehj, Andrews, and Abraham) for interesting chemistry discussions and friendship.

I thank Dr. John Eyler for giving me total access to the FT-ICR mass spectrometer and for being available to assist me with experiments and to discuss my research. I also acknowledge the invaluable exchange of ideas with members of the Eyler group, particularly Cesar Contreras.

Sincere thanks go to Dr. Sergiu Palii for giving me the initial FT-ICR MS training and Dr. John Toth for giving me on-the-job mass spec training. I also wish to express my appreciation to Drs. Vaneica Young, Weihong Tan, John R. Eyler, and Haniph Latchman for serving on my PhD supervisory committee. I thank Dr. Williams for her invaluable comments and for proof reading this dissertation.

Special thanks go to my wife, Kgadi, for her ever-present support, her patience, friendship and her kind love. I appreciate immensely her spending time with our son Lesego, while I was working in the lab. To Lesego, I am happy to say “NOW I am done with my school work.” Everyone has been a blessing to me and I thank God!

TABLE OF CONTENTS

LIST OF TABLES

LIST OF FIGURES

LIST OF SCHEMES

Abstract of Dissertation Presented to the Graduate School
of the University of Florida in Partial Fulfillment of the
Requirements for the Degree of Doctor of Philosophy

OPTIMIZATION OF SENSITIVITY OF ELECTROSPRAY IONIZATION MASS SPECTROMETRY FOR METABOLITE ANALYSIS

By

Nare Alpheus Mautjana

May 2009

Chair: Anna Brajter-Toth
Major: Chemistry

Improvements in the sensitivity of on-line Electrochemistry Electrospray Ionization Fourier Transformation Ion Cyclotron Resonance Mass Spectrometry (EC/ESI FT-ICR MS) for uric acid, cysteine, homocysteine, and other low oxidation potential (lower than 1 V vs SHE) metabolites is presented. Inclusion of a variable resistor to the EC cell circuit to regulate applied voltage allowed more detailed elucidation of the mechanisms of electrochemical reactions occuring during ESI MS analysis of the stated metabolites. Various factors which can affect the detection sensitivity of these metabolites in positive ion mode ESI MS and EC/ESI MS are discussed. Changes in the intensity profiles of the various species as a function of applied EC cell potential, ESI flow rate, and analyte concentration provide information for signal optimization.

Additional improvements in sensitivity (over ten-fold intensity increases) were observed when the standard cylindrical MS capillary inlet was replaced with a cone-shaped inlet. This new design and the associated dynamics leading to increased sensitivity are discussed. The new modification of ESI inlet is particularly valuable for the analysis of small metabolites, which tend to be spatially distributed in the electrospray interface and are radially segregated. Some of

the metabolites used in this work have been reported as antioxidants, and results in this dissertation support antioxidant activity as indicated by the proposed radical mechanisms.

In addition to revealing antioxidant activity of selected analytes, step-wise one-electron, one-proton oxidation reactions are observed for dopamine and uric acid with the aid of electrochemistry coupled on-line with ESI MS. These results suggest that positive ion mode ESI MS offers a new radiation-free technique for studying radical pathways. On-line EC/ESI MS data also show that dopamine and purines follow similar oxidation pathways leading to the development of a generic model for their behavior during ESI MS.

CHAPTER 1
INTRODUCTION

Electrospray Ionization Mass Spectrometry (ESI MS)

Mass Spectrometry (MS) was introduced some 100 years ago by Thompson [1913], recipient of the 1906 Nobel Prize in physics for the discovery of the electron in 1898. The initial applications of mass spectrometry were carried out by F.W. Aston, a former member of Thompson's research group. Aston's work led to the discovery of naturally occurring isotopes and resulted in the awarding of the Nobel Prize in chemistry to Aston in 1922. Today, mass spectrometry is used to obtain molecular weight and structural information for a diverse range of compounds including peptides, proteins, pharmaceuticals, natural and synthetic products, metabolites, and more.

A key step in acquiring a mass spectrum is ionization of the analyte molecules [Vestal, 2001]. For non-volatile biological samples the most prominent ionization methods are matrix-assisted laser desorption/ionization (MALDI) [Karas and Hillenkamp, 1988] and electrospray ionization (ESI) [Whitehouse et al., 1985; Fenn et al., 1990]. Both MALDI and ESI allow MS detection of large proteins intact, which was previously nearly impossible to achieve. The convenient coupling to separation techniques and resultant analysis efficiency, particularly in proteome analyses, has given ESI MS a leading edge over MALDI MS, since this latter technique requires off-line identification of the analytes [Shen et al., 2005].

The electrospray phenomenon, whereby a sample solution is dispersed into small charged droplets by electrostatic field, was reported as early as 1917 by Zenely [1917]. However, its use to produce gas-phase ions was not demonstrated until about 50 years later by Dole et al. [1968] and Mack et al. [1970]. Fenn et al. [1989] were the first to couple electrospray ionization with

mass spectrometry (Figure 1-1). For his part in developing electrospray ionization mass spectrometry (ESI MS), Fenn received the Nobel Prize in chemistry in 2002 [Fenn, 2003].

Electrochemical Nature of Electrospray Ionization

Electrospray ionization is accomplished by applying high voltage (± 2-5 kV) to a solution flowing at a slow rate (μL/h) through a narrow metal capillary which faces a counter electrode. Electrospray can be generated by applying either a positive or negative voltage to the solution, producing either positively charged or negatively charged droplets.

Girault and coworkers [Rohner et al., 2004] have described three stages of the electrospray process. At first, before any voltage is applied, the liquid surface in the capillary has a curved front surface due to surface tension and the hydrostatic pressure. With application of a positive potential to the capillary, the liquid/air interface becomes polarized and the emerging liquid forms a Taylor cone (Figure 1-2) as the electric field drives the cations at the liquid surface away from the capillary. The cone-shaped formation by liquids in an electric field was first studied by G. I. Taylor [1964]; hence the designation "Taylor cone." At higher potentials the electric field strength overcomes the surface tension and the cone is destabilized, giving way to a liquid jet which breaks off into tiny segments that become charged droplets [Mutoh et al., 1979]. As the solvent evaporates, the droplets shrink, and the charge density at the droplet surface increases. Eventually, each droplet explodes due to Coulombic repulsion, leading to smaller droplets and ultimately to gas phase ions [Iribane and Thomson, 1976]. The removal of positively charged droplets from the emerging liquid causes charge imbalance in the analyte solution, resulting in electrochemical oxidation; i.e., transfer of electrons from the solution components into the wall of the electrospray needle, in order to maintain charge balance in solution.

The electrosprayed ions flow continuously under the influence of the electric field across the interface and give rise to electrospray current, i_{ES}. The high voltage applied to the

electrospray ion source has only a minimal effect on the electrospray current, because the electrical conductivity of air (~3.0 x 10^{-20} mS/cm or 3 fS/m) [Aplin, 2005] is very small. In fact, once established, the electrospray current is unaffected by further increase in applied, high ESI voltage. Although previously debated [Van Berkel et al., 2000; Van Berkel, Kertesz, 2007], the observed continuous flow of current suggests that the electrospray current is due to Faradaic processes in solution [Jackson and Enke, 1999]. Compounds with the lowest oxidation potential are oxidized first followed by those with higher oxidation potentials including water (in the carrier solution) and these maintain current at a constant level [Jackson and Enke, 1999]. Figure 1-3 shows a typical current versus applied voltage curve by an electrospray ion source similar to that of a current-limited device. The actual voltage drop associated with electrochemical processes [$V_{ec} = (iR)_{ec}$] at the tip region of the ES capillary has been measured by Pozniak and Cole [2004; 2007; Li et al., 2003] as ≤ 2.5V vs SHE, which covers the range of most electrochemical oxidation reactions.

The migration of charged droplets away from the electrospray capillary (a working electrode) under high applied ESI voltage leading to reduction of ions at the MS inlet (a counter electrode) makes the electrospray interface a special kind of an electrochemical cell and a voltage drop [$V_{app} = (iR)_{gap}$] is associated with this process [Blades et al., 1991; Van Berkel et al., 1995a; Van Berkel et al., 1995b; Van Berkel, Kertesz, 2007]. Migration of charged droplets across the ES-interface is analogous to diffusion in a conventional electrochemical cell. The rate of charge neutralization i.e. reduction which occurs at the MS inlet surface (V_{inl}) upon contact of radially distributed ions with the inlet surface determines the observed ESI current. Note that this does not include ions that enter the mass spectrometer since they are neutralized at the detector (V_{det}). Ions neutralized at the inlet and at the detector represent a total of all preformed ions,

including those formed as adducts and ions produced by oxidation at the tip of the ES capillary, provided no ion loss occurs along the MS transfer optics. Based on this assumption, a complete equivalent electrical circuit representation can be constructed (Figure 1-4) and the total voltage in the ES interface (V_{ES}) can be given by the following relationship [adapted from Jackson and Enke, 1999]:

$$V_{ES} = (iR)_{ec} + (iR)_{gap} + V_{inl} + V_{det} + V \qquad (1\text{-}1)$$

Direct control of the voltage responsible for electrochemical oxidations at the ES capillary (V_{ec}) is difficult. However, various experiments have been carried out to minimize undesirable electrochemical reactions which occur in the electrospray ion source without compromising the controlled-current properties. One way is the use of fused silica capillary (liner) inside the stainless steel capillary (sleeve), which is connected to the high voltage [Kertesz and Van Berkel, 2001]. Most commonly the end of the silica capillary liner is flush with the stainless steel sleeve or it is slightly protruding to restrict electrochemical processes to the stainless steel rim. When the fused silica capillary was pulled back by a few millimeters to expose the solution to more stainless steel, electrospray current sustaining reactions such as oxidation of water have been found to increase, indicated by the appearance of higher charge states of proteins [Konermann et al., 2001]. Kertesz and Van Berkel controlled undesired electrochemical reactions by using a copper electrospray capillary. This guaranteed that the electrode interface potential (V_{ec}) was held constant around the potential for equilibrium of the corrosion reaction of copper [Kertesz and Van Berkel, 2001]. Using this adaptation, the oxidation of N-phenyl-1,4-phenylenediamine to N-phenyl-1,4-phenylenediimine was inhibited because it occurs at a more positive potential than oxidation of copper [Kertesz and Van Berkel, 2001].

Yet another way to control the electrochemical processes at the ES capillary tip is the addition of redox buffering agents such as iodide (I^-; E^o (I^-/I_2) = -0.53V vs SHE) in the form of CsI [Van Berkel et al., 1997] or KI [Konermann et al., 2001] to the analyte solution. Redox buffers are electrolytes that are more easily oxidized than most analytes. Thus redox buffers play a sacrificial role, thereby preventing analyte oxidation.

In other applications, a potentiostat was incorporated into the ES capillary circuit [Van Berkel et al., 2004; Van Berkel et al., 2005] to control the voltage at the capillary/solution interface in order to study electrochemical processes occurring during ESI [Van Berkel et al., 2004; Van Berkel et al., 2005]. The earliest reports of incorporating a potentiostat into the ESI source are those of Cole and coworkers [Xu et al., 1996; Lu et al., 1997], who used this kind of ESI cell to study oxidation of polyaromatic hydrocarbons and to determine products of diphenyl sulfide oxidation. Kertesz and Van Berkel [2006] used a porous flow-through working electrode and a quasi-reference electrode, a battery plus a chain of resistors, to design a two-electrode cell [Kertesz and Van Berkel, 2006]. This on-line electrochemical cell was floated at the high voltage of the electrospray capillary and was used to follow the oxidation processes of methylene blue and reserpine at different current magnitudes [Kertesz and Van Berkel, 2006]. Nyholm's group developed a chip for on-line electrochemistry ESI MS (EC/ESI MS) by incorporating an array of gold microcoil electrodes into a polydimethylsiloxane (PDMS) substrate, which also formed the wall of a microchannel. A graphite tip intergated into the PDMS block served as an ESI emitter [Liljegren et al., 2005]. Control over on-line electrochemical reactions in the chip was gained by: 1) varying the number of turns of the gold coils to adjust the electroactive surface area, 2) including appropriate insulation, and 3) connecting the chip voltage (floated on the high ESI voltage) to a potentiostat. The capability of the microcoil electrode to control electrochemical

rections prior to ESI MS was demonstrated through changes in signal intensity of various oxidation products of dopamine.

A different approach is used in the present study. An electrochemical cell is coupled on-line with ESI MS to facilitate, instead of suppressing, electrochemical reactions in order to enhance ionization efficiency, particularly for neutral and negatively charged analytes. The system (described in detail in Chapter 2) includes a variable resistor to control voltage applied to the electrochemical cell. The orifice of the MS capillary inlet has been widened into a cone-shape to further augment the improvements in sensitivity due to the applied EC cell voltage. Advantages derived from potential control of this EC/ESI MS system are demonstrated in this work.

On-Line Electrochemistry Mass Spectrometry (EC/MS)

Electrochemistry plays an important role in quantitative determinations, and electroanalytical studies of electroactive metabolites and drugs in biological systems are necessary for better understanding of disease and drug development. Electrochemical processes are often studied in aprotic solvents, which are ideal for fundamental investigations, as well as in aqueous solutions, which allow evaluation of the behavior of different reaction products generated in biological systems. Furthermore, electrochemistry is relatively easy to control via external voltage. For these reasons, a number of electrochemical methods, including biosensors, have been developed and are used extensively in bioanalytical research. The bioanalytical utility of electrochemistry is further advanced when this technique is coupled to mass spectrometry, a universal detection system, in on-line electrochemistry mass spectrometry (EC/MS) [Lohman and Karst, 2008]. As described herein and elsewhere [Van Berkel, 2004; Diehl and Karst, 2002], EC/MS is a rapidly developing technique.

As described above, on-line electrochemistry has been incorporated into ESI MS to control electrochemical processes associated with electrospray ionization. But on-line electrochemistry mass spectrometry (EC/MS) has also been developed as an analytical technique in its own right [Volk et al., 1992]. Development of EC/MS started in the 1970s, when semi-permeable membranes were used as interfaces between the electrochemical cell and the mass spectrometer [Bruckenstein and Gadde, 1971; Brockman and Anderson, 1984]. At that time, the utility of EC/MS was limited only to those reduction-oxidation reactions that produce gaseous and volatile products which could pass through the membranes and enter the mass spectrometer. This was a severe limitation, because most electrochemical processes produce non-volatile products which remain in solution. One of the major challenges, perhaps the greatest, in the development of EC/MS was dealing with the liquid solvent containing the analyte prior to performing mass spectrometry which is a low-pressure gas phase technique. The same challenge confronted the developers of liquid chromatography-mass spectrometry (LC/MS), who designed several types of interfaces, including thermospray, which was invented in 1983 by Blackley and Vestal [1983], particle beams, and electrospray. All three of these interfaces have also been successfully applied to EC/MS.

Figure 1-5 is a diagram of a typical thermospray interface. Resistive heating of a metal capillary leads to rapid volatilization of the analyte solution flowing through it. Analyte molecules are subsequently ionized by electron impact and directed towards the mass spectrometer by electrostatic repulsion from the repeller electrode while neutral solvent molecules are pumped away.

A typical particle beam interface is shown in Figure 1-6. A flow of helium concentric to the LC outlet generates an aerosol/spray by nebulization. Upon exiting the aerosol/spray

chamber, the lighter solvent molecules and helium drift outward from the concentric center and are pumped away, leaving heavier analyte molecule beam which enters the ionization chamber. This is the point in particle beam ionization process referred to as the momentum separation stage. Either electron impact (EI) or chemical ionization (CI) methods can be used to generate charged analyte species which are directed to the mass spectrometer. The development of the particle beam interface, formerly called a monodisperse aerosol generation interface (MAGIC), was described by Willoughby and Browner [1984; 1988] and has also been reviewed by Creaser and Stygal [1993], and Capiello and Bruner [1993].

On-Line Electrochemical Cell Designs

Volk et al. [1992] reviewed on-line EC/MS instrumentation available prior to 1992, when electrospray ionization was yet developing, for monitoring reactants, short-lived intermediates and products of electrochemical reactions of biologically active molecules as a function of electrode potential.

Thermospray Interface: On-line electrochemistry-thermospray ionization mass spectrometry (EC/TSI MS) was first designed in 1986 by Hambitzer and Heitbaum [1986] who investigated the oxidation of dialkylanalines. Their EC/TSI MS system included an HPLC pump which was used to pump the carrier solution from the reservoir and to force the analyte solution out of the three-electrode thin-layer electrochemical cell through the working electrode placed at the cell outlet (Figure 1-7). The analyte solution was then introduced into the thermospray ion source.

Following Hambitzer and Heitbaum's successful demonstration of EC/TSI MS, Yost, Brajter-Toth and Volk [1986; 1990] reported the mechanism of oxidation of purines and thiopurines studied using EC/TSI MS/MS. This group used a commercially available three-electrode flow-through cell with porous reticulated vitreous carbon working electrode and

palladium reference and counter electrodes. A similar electrochemical cell was used by Getek et al. [1989] to investigate on-line electrochemical reactions producing the acetaminophen-glutathione conjugate. Similar flow cells for on-line EC MS are commercially available from companies such as ESA Inc. and Antec Leyden, Netherlands.

Particle Beam Interface: The first demonstration of on-line electrochemistry particle beam ionization mass spectrometry (EC/PBI MS) was reported by Regino and Brajter-Toth [1997] who developed a homemade thin-layer, flow-through electrochemical cell that could withstand the high back pressures encountered in PBI MS (Figure 1-8). Their electrochemical cell could also be used with TSI MS and had removable electrodes for surface cleaning and/or modification. The conversion efficiency of the cell, as well as the sensitivity and reproducibility of the EC/PBI MS were found to be affected by solvent composition, including aqueous-to-organic solvent ratio and supporting electrolyte. A significant enhancement of the signal was observed for triphenylamine when tetrabutylammonium perchlorate was used as an electrolyte [Zhang and Brajter-Toth, 2000].

Electrospray Interface: While well established and commercialized (e.g. by Vestec), thermospray and particle beam techniques are not as popular as electrospray for EC/MS interfacing today. The advantages of on-line electrochemistry electrospray ionization mass spectrometry (EC/ESI MS) were realized in 1995 by Bond et al. [1995] who used a simple flow through tubular two-electrode EC cell on-line with ESI MS to study metal diethylcarbamate complexes. That same year, Zhou and Van Berkel [1995] described three different types of on-line EC cells, which include a tubular two-electrode cell which is floated at the ESI high voltage. Working electrodes included the ES capillary emitter, as well as the ESI-decoupled thin-layer and porous working electrode types, both of which require a potentiostat. As described above,

Xu et al. [1996] and Lu et al. [1997] designed an EC/ESI MS system with three-electrode EC cell incorporated into the ES emitter, and they demonstrated its performance using polyaromatic hydrocarbons, diphenyl sulfide and nitrobenzene. Zhang, Brajter-Toth and co-workers designed a two-configurations-in-one on-line EC cell using a polyetheretherketone (PEEK) 4-way channel (Figure 1-9) [Zhang et al., 2002]. Two palladium electrodes were mounted along one axis of the PEEK cross, with stainless steel (ss) capillaries along the other axis. The cell operated as a thin-layer configuration when Pd-electrodes were used and as a tubular two-electrode configuration when the stainless steel capillaries were used. Using the latter cell configuration with triphenylamine as analyte, this group demonstrated the enhancement in sensitivity of ESI MS by on-line electrochemical reactions [Zhang et al., 2002]. Karst's review of applications reported prior to 2004 [Karst, 2004], describes clearly the diversity and superior information content of EC/ESI MS in metabolic research.

Control of EC Cell Potential in EC/ESI MS

It is demonstrated in this work that a variable resistor can be incorporated into the EC cell circuit portion of the EC/ESI MS system to adjust voltages applied to the EC cell from a 9 V battery. Applied EC cell voltage enhances analyte ionization efficiency in EC/ESI MS by providing electrochemical reactions in addition to those occurring at the ES capillary tip. Coupling of the electrochemical cell to ESI MS expands the coverage of this technique to include formerly neutral and negatively charged analytes as discussed above. Furthermore, electrochemistry coupled on-line to ESI MS diversifies the range of ESI MS applications to studies of electrochemical reactions of many analytes of pharmaceutical and biological interest. The need to acquire insight into biological oxidation reactions and to discover different pathways related to normal growth, aging and disease, which are the hall-marks of metabolomics, calls for

techniques such as EC/ESI MS, which can mimic enzyme-catalyzed oxidation reactions [Permentier et al., 2008].

The EC/ESI MS of Dopamine

The performance of the EC/ESI MS designs has been evaluated using dopamine as the model analyte, both in previous reports [Deng and Van Berkel, 1999; Liljegren et al., 2005] and in this research.

Dopamine (3,4-dihydroxyphenethylamine, DA) has three dissociable protons (pKa1, pKa2 and pKa3 of 8.9, 10.6 and 12.1, respectively) associated with the deprotonation reactions (Scheme 1-1). A distribution diagram of the different DA species (Figure 1-10) shows that DA exists as the H3DA+ ion (referred to as [DA]+ in this thesis) in acidic to neutral solutions [Sanchez-Rivera et al., 2003].

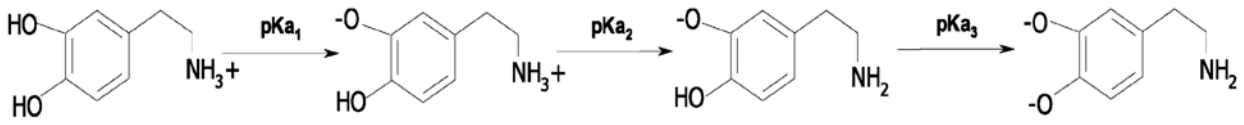

Scheme 1-1. Three proton dissociations of DA [Sanchez-Rivera et al., 2003].

The oxidation potential of DA ($E^0_{(DA)}$ = -0.12V vs SHE) [Blank et al., 1976] is lower than E^0 of most metabolites. Being a preformed ion and having a low E^o value, which indicate relatively easy ESI MS detection and oxidation, have made DA a suitable model analyte for testing new EC/ESI MS systems [Liljegren et al., 2005; Deng, Van Berkel, 1999; Mautjana et al., 2008a]. Oxidation of DA in EC/MS systems produces $1e^-$, $1H^+$ and $2e^-$, $2H^+$ oxidation products.

Endogenous DA functions as a neurotransmitter in the nervous system. Oxidation of DA in vivo by loss of $2e^-$ and $2H^+$ to produce dopamine quinone (DAQ) has been associated with the development of Parkinson's disease [Spina et al., 1989]. It has been proposed that DAQ can

modify essential proteins through electrophilic addition at the sulfhydryl group of cysteine residues, leading to dopaminergic neuron deaths and a neurodegenerative condition [Whitehead et al., 2001; LaVoie and Hastings, 1999]. The electrophilic addition of quinones to thiols was first proposed by Dryhurst and co-workers [Shen et al., 1996; Shen and Dryhurst, 1996a,b], based on cyclic voltammetry in conjunction with off-line nuclear magnetic resonance (NMR) spectrocopy for structure elucidation. In the present research, the use of EC/ESI MS to investigate DA oxidation and the addition reaction of DAQ to thiols provides direct evidence for this reaction via exact mass determination of electrochemically generated products, and observation of finer mechanistic details.

The EC/ESI MS of Uric Acid

Another important test compound for EC/ESI MS is uric acid which exists in two tautomeric forms, the keto- and enol-forms (Scheme 1-2) [Simic and Javanovic, 1989]. The keto-form is predominant at very low pH values, while the enol-form becomes more predominant as the pH approaches pK_{a1} (= 5.4) [Allen et al., 2004].

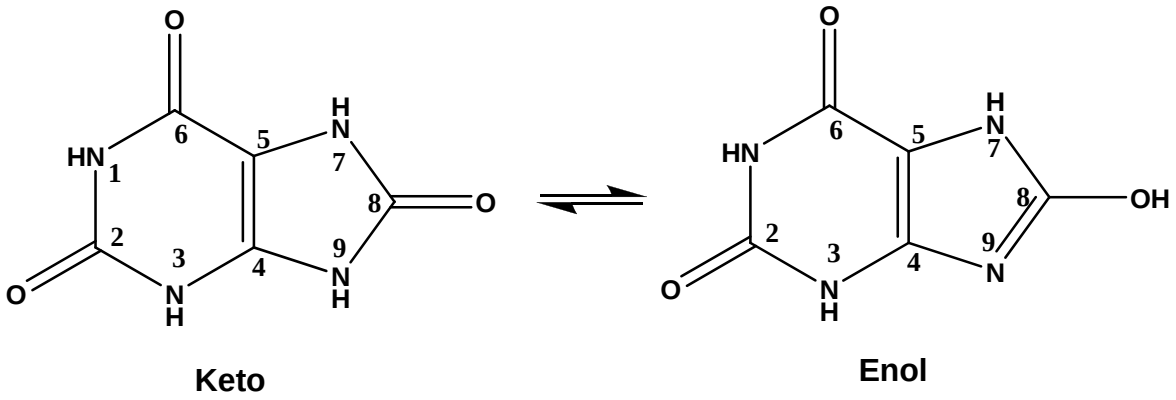

Scheme 1-2. Tautomeric structures of uric acid

It has been proposed that upon one-electron oxidation, uric acid loses a proton from the hydroxyl group, which is more acidic than the secondary amine group, to form a neutral radical

[Simic and Javanovic, 1989] (Scheme 1-3). The lone electron in uric acid radical is therefore centered on the oxygen bonded to C_8.

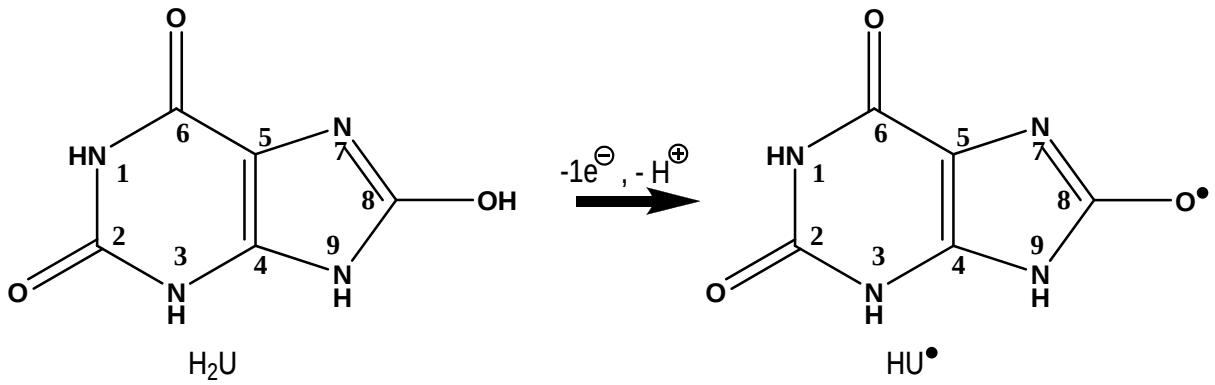

$E^o = 0.59V$ vs SHE

Scheme 1-3. Proposed one-electron, one-proton oxidation of uric acid [Buettner and Jerkiewicz, 1996].

One-electron oxidation pathways have also been suggested by Ames et al. [1981] in their proposal that uric acid is an antioxidant. The experiments carried out by Ames et al. [1981] included purging a uric acid solution with singlet oxygen prepared by irradiation of oxygen gas with a tungsten/halogen lamp. Their HPLC results showed that singlet oxygen oxidized urate, and they observed the same behavior for the reaction of urate with hydroxyl radicals produced from gamma (γ)-irradiated water. Uric acid radicals were detected by Maples and Mason [1988] using electron spin resonance spectroscopy as well as by Simic and Javanovic [1989] who used pulse radiolysis to elucidate the antioxidant mechanism. The present work demonstrates that positive ion mode ESI MS is a radiation-free alternative to these techniques for investigating pathway mechanisms of metabolites with low E^0 which undergo $1e^-$, $1H^+$ oxidation during ESI. While difficulties in detection of uric acid by standard ESI MS often leads to its omission in purine assays [La Marca et al., 2006; Ito et al., 2000], the EC/ESI MS system developed in this

work produces uric acid mass spectra with intense peaks at m/z 169 and 337, due to proton adducts of uric acid and uric acid dimer formed through electrochemical reactions.

In man and other primates, uric acid is the final product of the breakdown of energy-carrying molecules, adenosine triphosphate (ATP) and guanosine triphosphate (GTP) [Becerra and Lazcano, 1998] (Scheme 1-4). While there are salvage pathways for other purines (adenine, hypoxanthine, and guanine), excess uric acid is removed from the body by excretion through the kidneys and intestines.

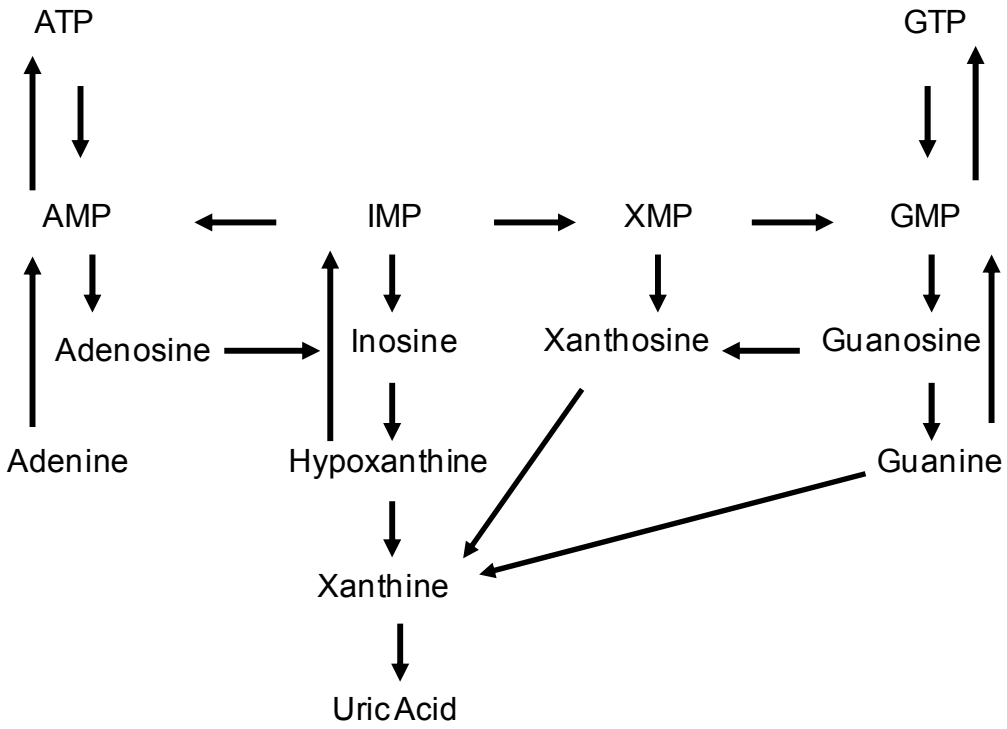

Scheme 1-4. Metabolic pathway of purines in humans (ATP, adenosine triphosphate; GTP, guanosine triphosphate; AMP, adenosine monophosphate; IMP, inosine monophosphate; XMP, xanthosine monophosphate; GMP, guanosine monophosphate).

The EC/ESI MS of Thiols

The low molecular weight thiol compounds, glutathione (GSH), cysteine (CySH) and homocysteine (hCySH) are involved in many important physiological and pathological processes [Rahman et al., 2005]. GSH and CySH are found at millimolar concentrations in different types

of cells and in blood plasma. Physiological functions of endogenous thiols include protecting cells against reactive oxygen species (ROS) and reactive electrophiles [Forman and Dickinson, 2003]. Decrease in concentrations of GSH and CySH from normal (1 – 10 mM) correlate with numerous disease conditions including Parkinson's and Alzheimer's diseases [Shen and Dryhurst, 2001]. Abnormally high concentrations of hCySH, which is an intermediate in the metabolism of methionine to CySH [Nekrassova et al., 2003; Himmelfarb et al., 2002], a precursor for GSH, have been found to correlate with atherosclerosis and venous thrombosis [Demuth et al., 2002; Van den Brandhof et al. 2001]. However, the mechanism of vascular injury is still unknown and could possibly involve GSH and CySH, given the common biosynthetic pathway of these three thiols (Scheme 1-5) [Himmelfarb et al., 2002]. Simultaneous analysis of thiols in biological samples is therefore important for clinical applications, as well as for understanding their roles in physiology.

Using ESI MS and EC/ESI MS to detect thiols allows direct and simultaneous detection of all three thiols, which is challenging when using electrochemical methods, given similar oxidation potentials, or using liquid chromatography with UV or fluorescence detectors which require derivatization because thiols do not possess any chromopores in their sructures.

Study Overview

This thesis investigates the sensitivity aspects of positive ion mode electrospray ionization mass spectrometry (ESI MS), including on-line electrochemistry(EC/ ESI MS), focusing on uric acid, thiols and other purine metabolites, which are clinically important metabolites but are not reliably detected by positive mode ESI MS. The electrochemical processes inherent to the electrospray ionization operation are described in relation to their effects on the detection of easily oxidized analytes. The application of electrochemistry coupled on-line with ESI MS

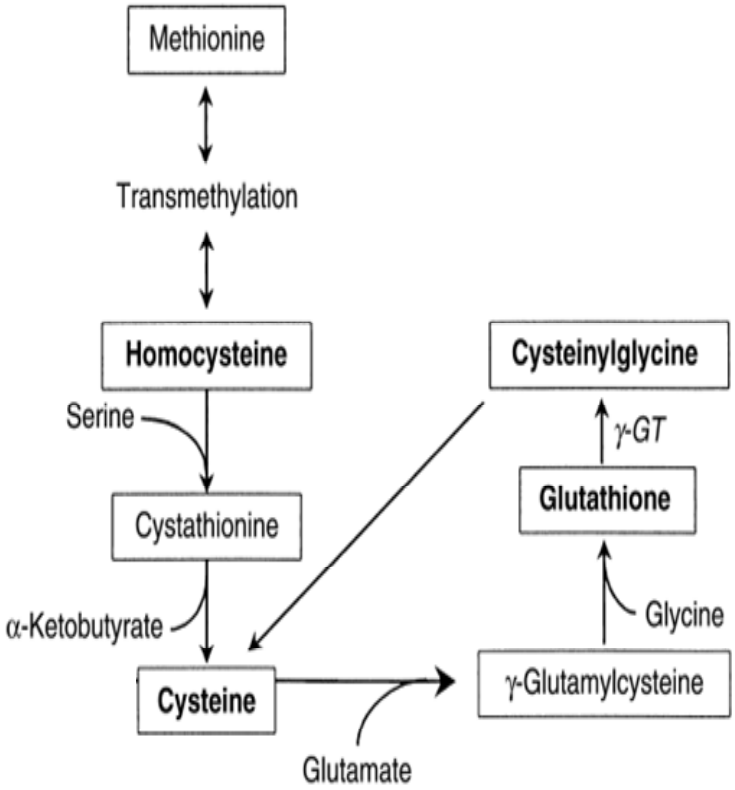

Scheme 1-5. Biosynthesis of homocysteine, cysteine and glutathione [adapted from Himmelfarb et al., 2002]

(EC/ESI MS) to the analysis of the abovementioned analytes and the resulting enhancement in sensitivity is demonstrated.This chapter has provided background information about ESI MS and the attempts towards gaining control of the electrochemical processes associated with electrospray ionization. Efforts to gain control over these processes culminated into on-line electrochemistry, which has become a technique in its own right.

Chapter 2 explains the experimental methods and instrumentation. Detailed schematics are given and fundametals of the techniques used are described to help the reader appreciate the science behind experiments conducted in this research. Chapter 3 describes the performance of EC/ESI MS at different flow rates, concentrations and applied EC cell voltages, using dopamine as the test compound. Oxidation processes that are all too evident are explained in terms of ion formation pathways.

Oxidation and sensitivity of uric acid in ESI MS is the subject of Chapter 4. In this chapter factors involved in the detection of uric acid are discussed and corresponding changes in observed mass spectra are explained. Results for EC/ESI MS of three thiol metabolites, glutathione, cysteine and homoxysteine, discussed in Chapter 5, show that ESI mass spectrometry is more selective than any of the other commonly used methods. Chapter 6 discusses ESI MS of other purines (guanine, adenine, hypoxanthine and xanthine) and mechanisms of oxidation of these purine metabolites during ESI MS are proposed. Chapter 7 summarizes conclusions drawn from the research results of the entire thesis and proposes ideas for future work.

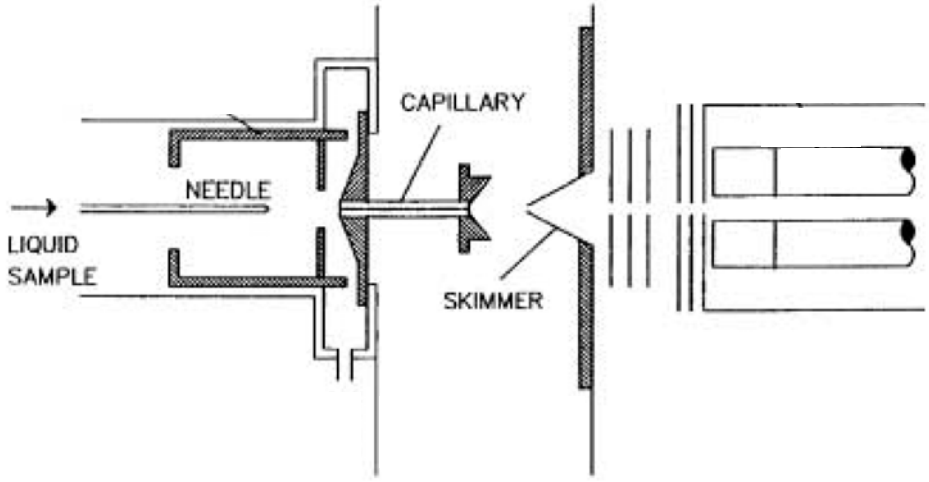

Figure 1-1. Electrospray Ionization Interface for LC/MS [Adapted from Fenn et al., 1989]

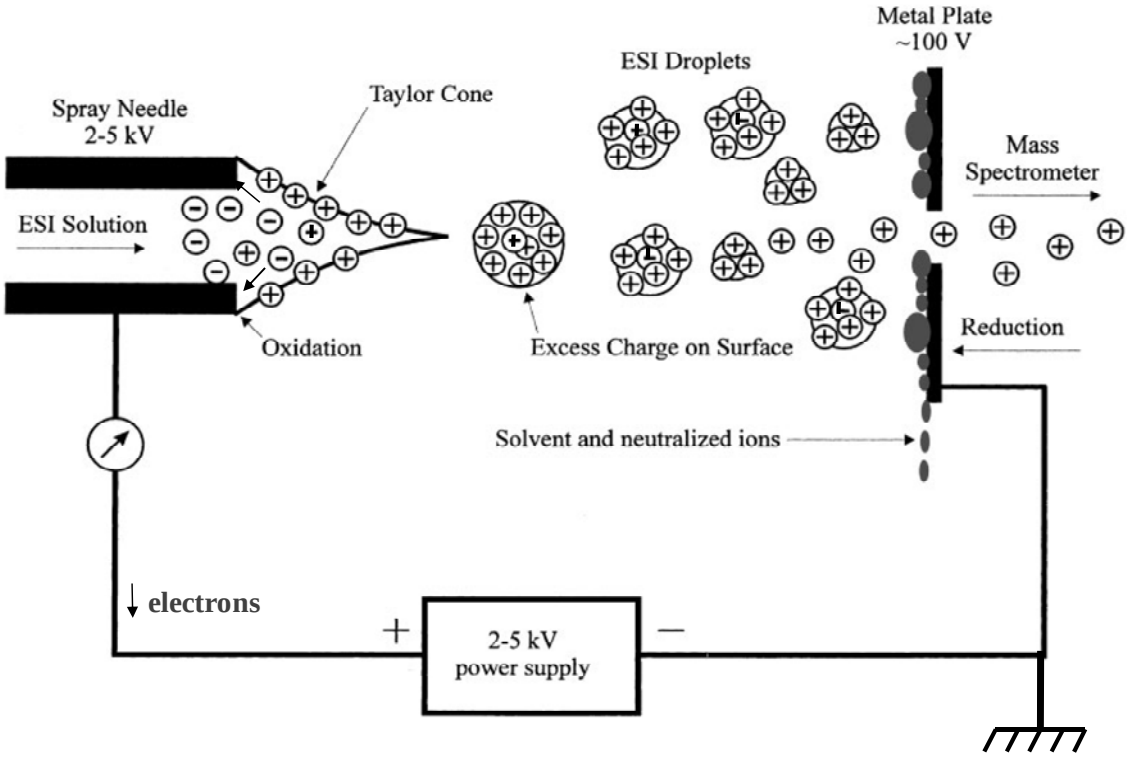

Figure 1-2. Electrospray ionization process [Adapted from Cech and Enke, 2001]

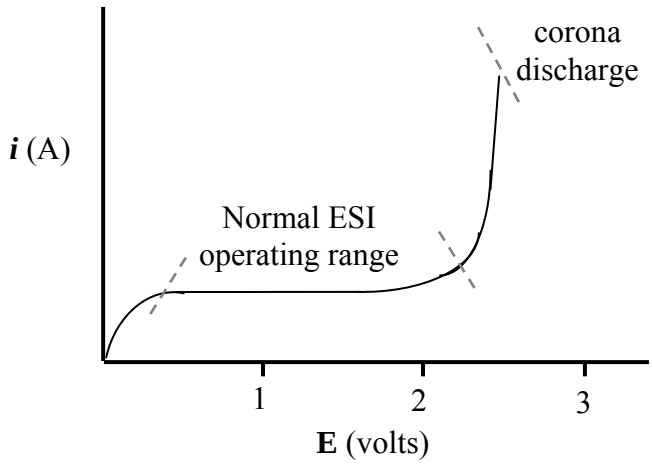

Figure 1-3. Current vs voltage curve for a current-limited device

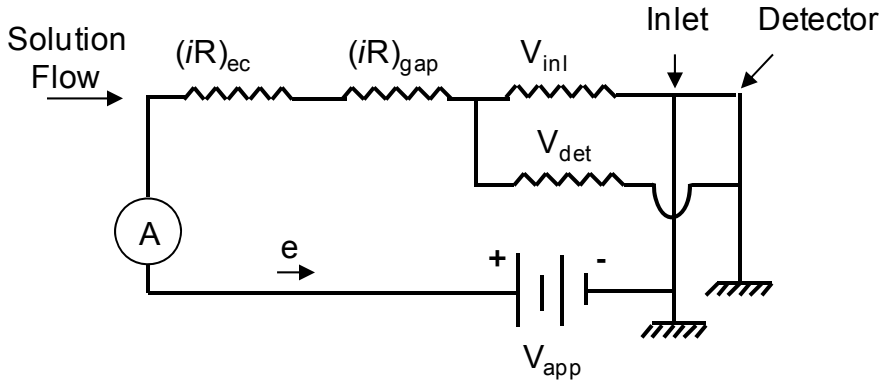

Figure 1-4. Equivalent electric circuit representation of the ESI process

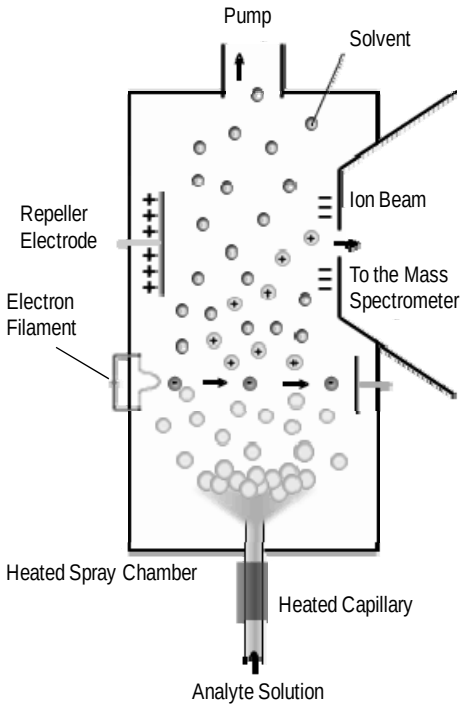

Figure 1-5. Thermospray interface for LC/MS

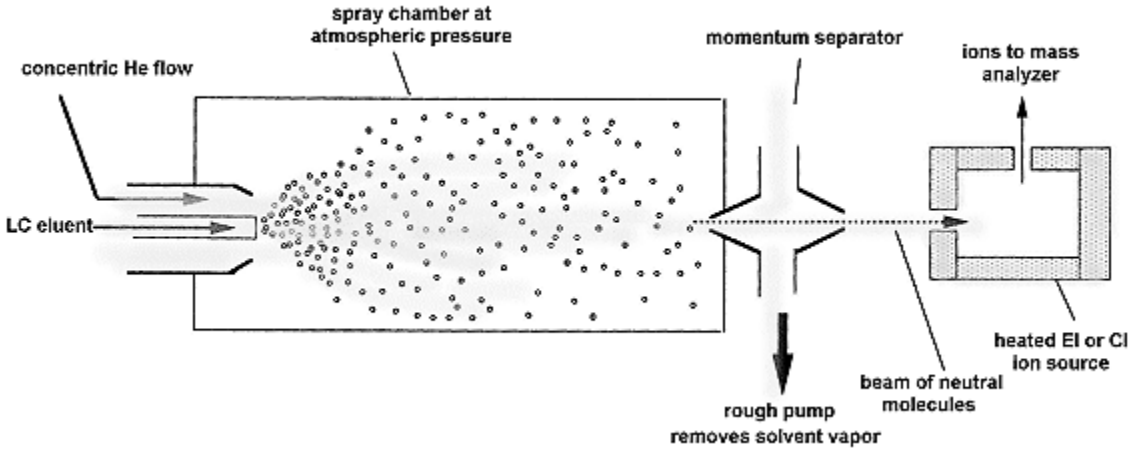

Figure 1-6. Particle beam interface for LC/MS

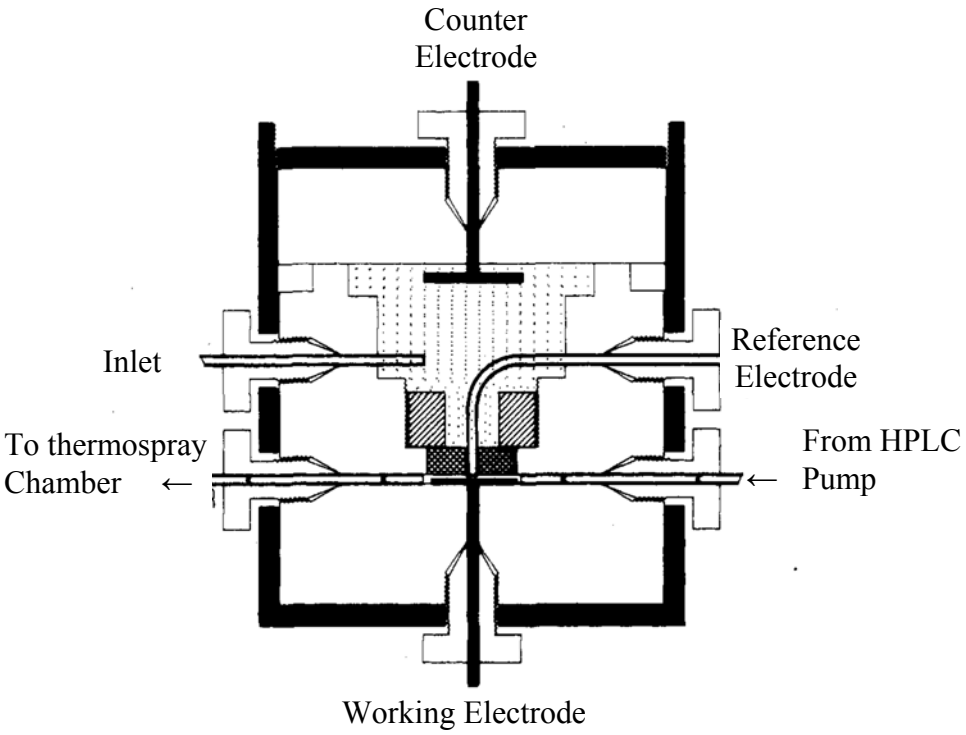

Figure 1-7. On-line electrochemical cell for EC/TSI MS [Adapted from Hambitzer and Heitbaum, 1986]

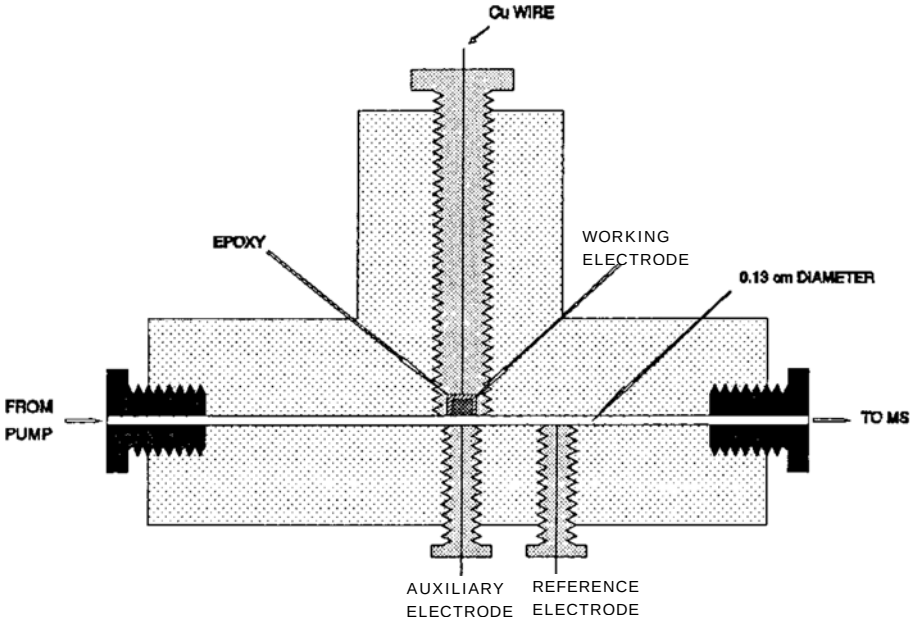

Figure 1-8. On-line electrochemical cell for EC/PBI MS and EC/TSI MS [Adapted from Regino and Brajter-Toth, 1997]

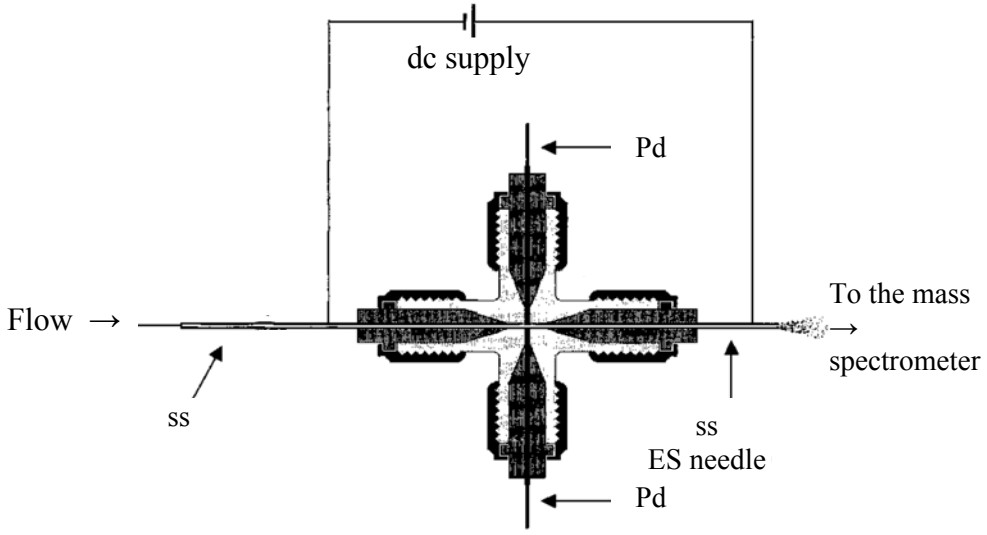

Figure 1-9. On-line electrochemical cell for EC/ESI MS (ss, stainless steel capillary; Pd, palladium electrode) [Adapted from Zhang et al., 2002]

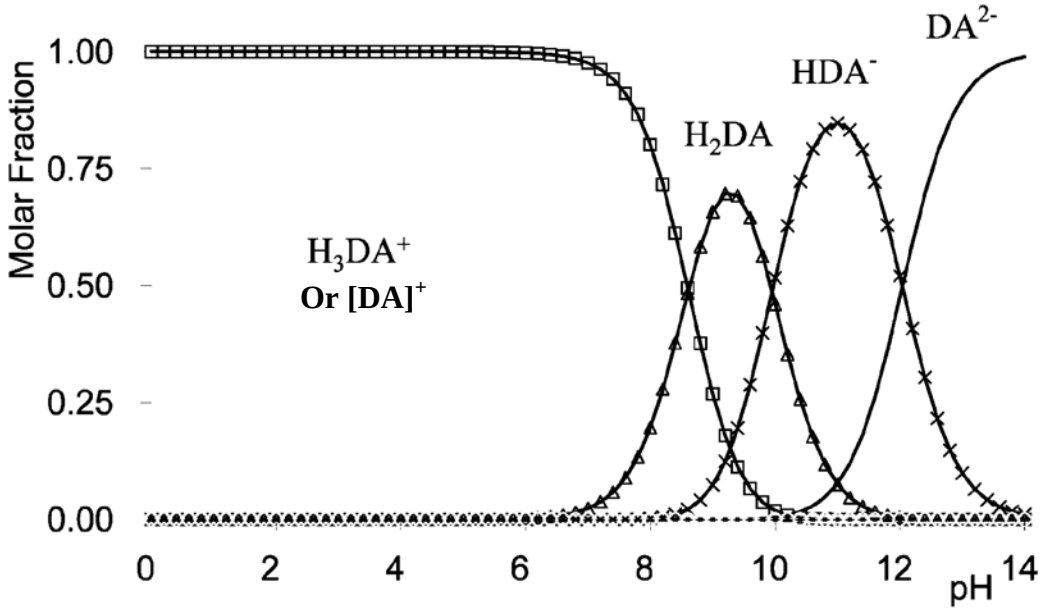

Figure 1-10. Distribution diagram of different dopamine species as a function of pH [Adapted from Sanchez-Rivera et al., 2003]

CHAPTER 2
EXPERIMENTAL

Methods and Instrumentation

Construction of the EC/ESI MS System

An on-line electrochemistry/electrospray ionization Fourier transform ion cyclotron resonance mass spectrometry (EC/ESI FT-ICR MS) system was developed in this work, with the EC cell integrated into the ion source (Figure 2-1). A simple series, two-electrode EC cell circuit was incorporated into the ES emitter by dividing the stainless steel ES capillary (80 μm i.d.) into two (4 and 5 cm long) sections (ss1 and ss2). These were joined with plastic tubing (100 μm i.d.) approximately 0.5 mm in length. A 9V battery was connected via a variable resistor (50 kΩ max.) to the two stainless steel ES capillaries to supply low, controlled, varying dc voltages. This produced an electrochemical cell with ss1 as the anode (working electrode) and ss2 as the cathode (counter electrode) and total cell volume (left end of ss2 to the ESI gap) of approximately 0.46 μL. The EC cell was fixed onto an adjustable *xyz*-micropositioner (World Precision Instruments, Sarasota, FL, USA). The electrical circuit of the entire system is shown in Figure 2-2. There is no upstream grounding point (i.e. between the counter electrode and the syringe). With the long plastic tubing (~140mm) between the syringe and ss2, and without upstream ground, electrochemical oxidations cannot occur at the counter electrode but are limited to the working electrode [Van Berkel and Kertesz, 2007].

The resistors R_1 (50 KΩ max) and R_2 (10 KΩ max) are commercially available, standard linear track variable resistors with manually movable (via a spindle) third contact (Figure 2-3). Connected as shown in Figure 2-2, resistors R_1 and R_2 form a two-turn rheostat for rough and fine adjustment, respectively, of the voltage applied to the on-line electrochemical cell. The voltage drop across the electrochemical cell (between counter and working electrodes) is

represented as $(iR)_{ec\ online}$, and that due to solution at the tip of the electrospray capillary is $(iR)_{ec}$, while $(iR)_{gap}$ represents the voltage drop due to the air gap. Charge neutralization at the inlet and detector are represented by V_{inl} and V_{det}, respectively. Jackson and Enke [1999] found that the amount of current flowing from the electrospray capillary back to the syringe during positive ion mode ESI MS is very small and negligible in theoretical equations for modeling the electrical behavior of ESI MS.

Cone-Shaped MS Capillary Inlet

A cone-shaped MS capillary inlet (Figure 2-1A) which is similar to the flared inlet introduced by Wu et al. [2006], was formed by reaming out about 25 mm depth of the orifice of the standard cylindrical inlet. This produced an orifice diameter of 6.12 mm, which tapers to 1.58 mm with a cone angle of 50o. As described below, the results obtained with the cone-shaped inlet were compared to those of a standard cylindrical metal capillary MS inlet with 1.58 mm i.d. Both metal capillary inlets are made of brass.

Fourier Transform Ion Cyclotron Resonance (FT-ICR) Mass Spectrometry

An APEX 4.7-T FT-ICR mass spectrometer (Bruker Daltonics, Billerica, MA, USA) was used with an operating ESI ion source region pressure of ~5.3 x 10-6 mbar. The other parameters included the ion transfer region and the ICR cell pressure ~3.4 x 10-10 mbar, needle voltage ~3 kV, and capillary inlet temperature of 120oC. A syringe pump (Cole Parmer 74900, Vernon Hills, IL, USA) provided constant flow rate of carrier solution continuously into the electrospray. Mass spectra for comparison of the cylindrical and cone-shaped inlets were acquired using identical settings for transfer of the ions through the optics in the external source and for the ICR detector.

Operational Safety

Safety protocols for high voltage and superconducting magnets were observed.

Cyclic Voltammetry

A Bio-Analytical Systems (BAS-100) electrochemical analyzer (Bioanalytical Systems, Inc., West Lafayette, IN, USA) was used for slow scan (50 mV/s) cyclic voltammetry. A homemade stainless steel disk electrode (r = 50.8 μm) was used as the working electrode, with a standard calomel electrode (SCE) as reference.

Electrode Fabrication: Stainless steel microelectrodes were fabricated according to the method reported by Bravo et al. [1998]. The stainless steel wire was inserted into a micropipette tip and sealed using an epoxy mixture of Shell Epon 828 resin (Miller-Stephenson Chemicals, Danbury, CT, USA) and m-phenylenediamine hardener (Miller-Stephenson Chemicals, Danbury, CT, USA). The mixture was heated at 70 oC in a water-bath until the epoxy was liquid and transparent. The liquid epoxy was transferred into the micropipette tip with embedded stainless steel wire, and the electrode was left to dry for 72 hrs and then cured in an oven at 150 oC for 1h. After curing, the electrode tip was sanded using an Ecomet I polishing wheel (Buehler, Evaston. IL, USA) with 600-grit silicon carbide paper, followed by an Alpha-A felt cloth (Mark V Labortory, East Granby, CT, USA) for smooth-polishing.

Fundamentals of Methods Used

ESI MS

The flow of ions generating the ES current (i_{ES}) depends on the potential difference (E) between the ES capillary and the MS inlet, the carrier solution conductivity (κ), surface tension (γ), flow rate (ν_f), permittivity (ε); and on permittivity of the vacuum (ε_o) according to Equation 2-1 [Rohner et al., 2004].

$$i_{ES} = [(4\pi/\varepsilon)^3(9\gamma)^2\varepsilon_o{}^5](\kappa E)^{3/7}(\nu_f)^{4/7} \quad (2\text{-}1)$$

When droplet sizes and charges are considered, the effect of the potential difference is negligibly small compared to solution conductivity, and E can be neglected leading to Equation 2-2 [de la Mora, 1992]

$$i_{ES} = f(\varepsilon_r)(\gamma\kappa\nu_f\varepsilon_r)^{1/2} \tag{2-2}$$

where $f(\varepsilon_r)$ is a function of the dielectric constant ($f(\varepsilon_r) \approx 18$ for water and methanol whose dielectric constant, $\varepsilon_r \geq 30$). Because the resistance of the gap between the ES capillary and the MS inlet is very large [Aplin, 2005] and the observed current (i_{ES}) is constant, it is apparent that the observed current (i_{ES}) is mostly due to the Faradaic processes. Part of the electrospray current (i_{ES}) is due to preformed ions which are simply repelled at the ES capillary tip and migrate to the MS inlet. This fraction is negligible because of the weak influence of the electric field. Therefore the Faradaic current (i_F) at the ES capillary tip, which is sustained by oxidation of compounds with lowest oxidation potentials (E^o) first, and progressively by those with higher E^o values, can be assumed approximately equal to the electrospray current (i_{ES}):

$$i_F = i_{ES} \tag{2-3}$$

The diffusion controlled Faradaic current of reactants is given by

$$i_F = F\sum_j n_j c_j m_j \tag{2-4}$$

where F is the Faraday constant (9.6485 x 10^4 C/mol), j the number of different electrolysis reactions that occur, n_j the number of electrons involved in the production of one mole of electrolysis product in reaction j, c_j the concentration of the reduced species and m_j the mass transfer (diffusion) coefficient of the reduced species in reaction j [Van Berkel and Kertesz, 2007; Rohner et al., 2004]. The equivalence of Faradaic and observed electrospray currents stated in Equation 2-3 was verified by Blades et al. [1991] who measured i_{ES} for electrochemically generated Zn^{2+} and found it to be equal to that from a calibration of Zn^{2+}

standards. However, it is difficult to determine the exact magnitude of the potential of the capillary electrode, because it is not fixed during the ESI MS experiment, but it adjusts according to the number of interactive variables to mainatin the required current [Van Berkel and Zhou, 1995].

The concentration of excess charge in the ES droplets [Q] (mol/L), which leads to coulombic explosion and release of ions into the gas phase, can be calculated from Faraday's first law of electrolysis [Van Berkel and Kertesz, 2007, Rohner et al., 2004]:

$$[Q] = i_F/(F\nu_f) \tag{2-5}$$

Therefore, the largest coulombic explosions occur in experiments where the lowest flow rate (ν_f) of carrier solution is used.

In addition to the parameters already mentioned, surface activity, proton affinity (PA) and the electrochemical properties of analytes, can also influence the number of ions produced in positive ion mode ESI and the detection sensitivity. Surface activity refers to the tendency of the analyte to migrate from the droplet center to the surface, where it can easily enter the gas phase. Relatively non-polar, hydrophobic metabolites show a greater degree of surface activity than polar, hydrophilic compounds. Polar metabolites generally acquire charge by forming H^+-, Na^+-, K^+-, Li^+-, or NH_4^+-adducts in solution and they enter the gas phase as adduct ions.

Proton affinity (PA) refers to the favorable enthalpy change (negative ΔH) for protonation of a given metabolite in the gas phase. In the gas phase, molecules with high PA, which were not already protonated in solution, can abstract protons from solution-protonated molecules with low PA. Analytes of interest can be detected reliably if they are dissolved in solvents with lower PA values [Cech and Enke, 2001]. Analytes that are neutral or even negatively charged but have

relatively low oxidation potentials (E^o) can be oxidized in positive ion mode ESI MS and form species that give a response [Mautjana et al., 2008b].

MS capillary inlet design: For an MS inlet capillary with a small orifice, uniform ion intensities for metabolites with different PAs and surface activities are obtained using very low flow rates (μL/h) and narrow ES capillaries to promote formation of small droplets. Efficient ion desolvation is achieved by heating the MS inlet capillary to about 120 ^oC for efficient evaporation of the carrier solution, which often includes water.

However, large losses in ion transmission can occur at the MS capillary inlet because of the small area (internal diameter) of the orifice of the inlet relative to the size of the charged droplet/ion plume produced by electrospray. Internal diameters of standard MS capillary inlets are kept small to preserve low pressure (vacuum) conditions. But there is no observable effect on the pressure (no additional vacuum pumping is required) if the inlet capillary orifice is enlarged into a cone (Figure 2-1A) [Mautjana et al., 2008a,b] or has a flared orifice [Wu et al., 2006]. Under conditions where positive ions are electrostatically repelled from the ES capillary tip rather than attracted to the capillary inlet surface (since the inlet is held at a lower, but still positive, potential), a wide orifice allows collection of radially distributed ions [Nemes et al., 2007] and increases ESI MS sensitivity several fold. In contrast to other ion transmission enhancing approaches, such as focusing the ES droplet/ion plume with static dc fields at the inlet [Zhou et al., 2006; Schneider et al., 2001] or adding electrodynamic funnel at the skimmer position [Kelly et al., 2007; Kim et al., 2000], the cone-shaped capillary inlet is easy to make and use.

EC/ESI MS

As a result of the applied EC cell voltage, other electrochemical reactions occur, in addition to those at the tip of the electrospray capillary (Figure 2-8). Cole's group has shown that

the electrode-solution interface potential is highest at the tip of the electrospray capillary [Pozniak and Cole, 2007; Pozniak and Cole, 2004]. Their measurements indicate that voltage decreases exponentially from highest (≤ 2.5 V vs SHE) at the ES capillary tip (± 0.25mm from the ES capillary tip opening) and approaches zero in the upstream direction, so that much of the inner surface of the ES capillary is not electrochemically active during ESI. Application of voltage to the other end of the capillary (left end of ss1 in Figure 2-1) increases the active inner surface area of the ES capillary (see Figure 2-4), as indicated by the increase in ES current as applied EC cell voltage is increased [Mautjana et al., 2008a]. It has also been pointed out in a recent review [Van Berkel and Kertesz, 2007] that the magnitude of potential reached at all points along the ES capillary is directly related to the ES current.

FT-ICR Mass Spectrometry

Pioneered by Marshall et al. [1974] a Fourier transform ion cyclotron resonance (FT-ICR) mass spectrometer uses combined magnetic and electric fields to determine the mass-to-charge (m/z) ratio of an ion. Ions in an FT-ICR mass spectrometer possess very low kinetic energy and, unlike the case in the magnetic sector mass spectrometer, they do not pass through the magnetic field but are actually trapped in the magnetic field. When entering a region of constant magnetic field strength in a direction that is perpendicular to the field, the ion path is bent into a circle, a motion referred to as cyclotron motion and mathematically described by

$$\omega_c = qB/m \tag{2-6}$$

where ω_c is the angular frequency, q the charge, B the magnetic field and m is the mass of the ion. Ion cyclotron motion is spatially confined and thus made observable by applying an electric field at frequency (rf) that is the same as (or resonating with) the ion cyclotron frequency. Application of rf excitation field causes the ions to spiral outward to larger orbits, and all ions of a given mass move coherently (as a clump). Distinct ion oscillation (or image) currents are

induced at (and therefore detected by) the plates of the cell (Figure 2-5) generating the ICR (time domain) signal whose digital form is converted by Fourier transformation into a frequency-domain spectrum and further (using the magnetic field strength value) to a mass spectrum [Grosshans and Marshall, 1991; Marshall et al., 1998; Baykut and Eyler, 1986]. The high precision of digital frequency measurement, in conjunction with large magnetic field strengths (> 7 Tesla), results in very high mass resolution (10000+), a very desirable and important property of FT-ICR MS. Furthermore, because the image current is induced as long as the ions are moving coherently, the frequencies can be measured hundreds of times, thereby improving the signal-to-noise (S/N) ratio.

Hydrogen/Deuterium (H/D) Exchange Methods

Hydrogen/deuterium exchange methods are used for distinguishing covalently bonded species from non-covalently bonded structures and for elucidation of the formation of complexes in solution. Solution phase H/D exchange is used for structures with hydrogen-bond donor and acceptor groups. The donor group usually contains oxygen (O), nitrogen (N), sulfur (S) or a strong electron-withdrawing group to which the hydrogen (denoted H in H/D exchange terms) is attached. If an active H forms an H-bond either with another atom or group in the same molecule (i.e intra-molecular H-bonding) or with an atom or goup of another molecule forming a complex, that H is protected and will not be replaced by deuterium [Liu et al., 2008; Jiang et al., 2007].

Generally, active (or acidic, or labile) hydrogens that are bonded to heteroatoms (not carbon) in organic molecules are replaced by deuterium when exposed to high deuterium concentrations (e.g. in D_2O). The reaction can be written as

$$R\text{-}XH + D_2O \rightarrow R\text{-}XD + DOH \qquad (2\text{-}7)$$

where R represents a partial molecular structure, X represents oxygen, nitrogen or sulfur, H is hydrogen and D, deuterium. When *n* active hydrogens (*n* x 1Da) of a given molecule are exchanged with *n* deuterium atoms (*n* x 2Da), the molecular mass increases by *n*. The increase in mass due to H/D exchange corresponds to the number of exchageable hydrogens, because the neutral molecule $M_{n\mathrm{H}}$ (where *n*H represents the number of exchangeable hydrogens) becomes $M_{n\mathrm{D}}$ after the exchange. In ESI MS, residual $M_{n\mathrm{H}}$ and $M_{n\mathrm{D}}$ form proton adducts (given the presence of acid electrolytes, e.g. acetic acid, or H^+-producing solvent oxidation during ESI). The relative intensities of $[M_{n\mathrm{H}}+H]^+$ and $n[M_{\mathrm{D}}+H]^+$ ions reflect molar fractions of molecules with exchanged hydrogens [Liu et al., 2008; Jiang et al., 2007].

Tandem Mass Spectrometry (MS/MS or MS^n)

Tandem mass spectrometry (MS/MS or MS^n) involves at least two stages of mass spectrometry. The ion of interest is isolated in the first MS. It is then activated to the point of dissociation either by collisions with neutral atoms (collision-activated dissociation – CAD or collision-induced dissociation – CID) or by irradiation with a laser (e.g. 10.6 μm photons from a CO_2 laser; infrared multiple photon dissociation – IRMPD). Activation results in secondary (or daughter) ions which are analyzed by the second MS stage to identify the primary (parent) ion. The generation of secondary ions is represented by

$$m_p^+ \rightarrow m_d^+ + m_n \qquad (2\text{-}8)$$

where m_p^+ is the primary (or parent) ion, m_d^+ the secondary (or daughter) ion, and m_n is a neutral fragment. IRMPD has the advantage of being vacuum-friendly which allows immediate FT-ICR detection of the secondary ions. Other activation techniques include sustained off-resonance irradiation (SORI) where selected ions are irradiated off-resonance (i.e. at a different, non-resonating frequency) causing them to collide as they spiral away from and back into orbit, and

black-body infrared dissociation (BIRD) in which ions are confined in a hot (40 – 215°C) ICR cell for 10 – 1000 s, during which time they absorb black-body photons, are excited, and undergo unimolecular dissociation [Price et al., 1996; Glish and Vachet, 2003; Marshall, 1998].

Cyclic Voltammetry

In cyclic voltammetry, the current is monitored as potential is scanned linearly in the forward and reverse directions repetitively, thus following a triangular waveform in time, typically with sub-second scan cycles. A potential (E) scan towards more positive values results in oxidation of the analyte which displays an anodic (oxidation) peak current (i_{pa}) at E_{pa}. Reverse potential scan, towards less positive values, results in a cathodic (reduction) peak current (i_{pc}) at E_{pc}, provided the electrochemical process is reversible. A typical cyclic voltammogram is shown in Figure 2-8. For reversible reactions $i_{pa} = i_{pc}$ and the potentials corresponding to the peaks are related by

$$E_{pa} - E_{pc} = 2.22RT/nF \tag{2-9}$$

where n is the number of electrons in each (either oxidation or reduction) half-reaction. For a reversible reaction at 25 °C, the peak current is given by

$$i_p = (2.69 \times 10^8) n^{3/2} A c D^{1/2} \nu^{1/2} \tag{2-10}$$

whereas for electrochemically irreversible (i.e very slow) reactions peak current is given by

$$i_p = (2.99 \times 10^8) n(\alpha n_a)^{1/2} A c D^{1/2} \nu^{1/2} \tag{2-11}$$

where A is electrode area (m^2), c is concentration (mol/L), D and α are the diffusion coefficient (m^2/s) and the transfer coefficient of the analyte (unitless), respectively, ν is the scan rate (V/s), and n_a is the number of electrons in the rate determining step [Bard and Faulkner, 2001]. As Equations 2-10 and 2-11 show, peak current is proportional to $\nu^{1/2}$.

Cyclic voltammetry is used both for quantitative determination of analytes and for studying the kinetics of reactions occurring at the electrode surface. The use of microelectrodes, which have very small active surface area and very small *iR* drops, is advantageous for analysis of samples with poor conductivity, including nonaqueous solutions. Furthermore, the low capacitance associated with the very small surface areas allows very small charging currents relative to the Faradaic currents of many oxidation reactions, resulting in significant improvement in limits of detection [Harris, 2007; Willard et al., 1988].

Experimental Conditions

Solution Preparation

All solutions were prepared and stored in glass volumetric flasks. When stored in plasticware, solutions produced mass spectra with numerous unidentifiable peaks.

Reagents: Dopamine hydrochloride (98%), sodium dihydrogen phosphate (99%), uric acid (H_2U) (99%), glutathione (99%), L-cysteine hydrochloride (98%), DL-homocysteine (95%), and disodium hydrogen phosphate (99%) were purchased from Aldrich (St. Louis, MO, USA); ammonium acetate (NH_4Ac), glacial acetic acid (HAc) (99.9%), KOH (88%)and methanol (HPLC grade) were from Fisher (Pittsburgh, PA, USA); deuterium oxide (99.9%) was from Cambridge Isotope Laboratories (Andover, MA). All chemicals were used as received.

Dopamine: The carrier solution was 50/1/49vol%, water/acetic acid/methanol with a pH of 4.2 (by a pH-meter). Dopamine solutions were prepared in the carrier solution unless specified otherwise. Specific conductivity was measured with a conductivity meter (Wissenschaftlich Technise Werkstatten, Weilheim, Germany) as 103 and 312 $\mu S\ cm^{-1}$ for the carrier solution and 2.5 mM dopamine solutions, respectively.

Uric acid (and other purines): The carrier solution was 40/60 vol%, water/methanol containing 10^{-3} M NH_4Ac, pH ~6.3 or containing 0.10 M KOH and 0.04 M HAc, pH ~12.7. Uric

acid was dissolved in the water fraction (40% of final volume) of the carrier solution with moderate heating followed by dissolution of NH_4Ac. Methanol was added and the solution was allowed to cool to room temperature and then was made up to volume with methanol. Any uric acid solution that appeared turbid was discarded. Specific conductivities of the pH 6.3 and the pH 12.7 carrier solutions were measured using a conductivity meter (Wissenschaftlich Technise Werkstatten, Weilheim, Germany) as 0.132 mS/cm and 3.30 mS/cm, respectively.

Thiols: Analyte solutions were made in 40/60 vol%,, water/methanol containing 0.001 M ammonium acetate, pH ~6.3 or 50/49/1 vol%,, water/methanol/acetic acid, pH~4.2.

Cyclic Voltammetry

A BAS-100 electrochemical analyzer was used for analysis of both dopamine and cysteine (either without or with 100 μM Fe^{2+}). A 50 mV/s scan rate was used for all anlyses, and the typical potential scan window was -0.2 V to 1.3 V vs SCE. Duplicate cyclic voltammograms were recorded for each smple. For analysis of dopamine, a total of four 400 μM DA solutions were prepared in: 31 mM sodium dihydrogen phosphate/disodium hydrogen phosphate buffer, pH~7.4; in the carrier solution (50/49/1 vol% water/methanol/acetic acid, pH~4.2); and 99/1 vol%, water/acetic acid, pH~4.0. For cysteine analysis 0.5 mM cysteine solution was prepared in 50/49/1 vol%,, water/methanol/acetic acid, pH~4.2.

FT-ICR MS Data Analysis

The Predator (version 1.2) [Blakney et al., 2005] and Modular ICR Data Acquisition and Analysis System (MIDAS) software [Senko et al., 1996], written at the National High Magnetic Field Laboratory (Florida State and University of Florida) were used to obtain frequency-domain (ion peak height) mass spectra, following magnitude mode Fourier Transformation of the time-domain (transient signal) spectra. The data from 100 scans were signal averaged. In order to confirm peak assignments, the IsoPro 3.0 program [http://members.aol.com/msmssoft/] was used

for comparison of theoretical relative isotope peak intensities and measured isotope abundances. Averages of at least duplicate measurements are reported.

Photo-Induced Dissociation and MS/MS

A 7W grating-tuned CO_2 laser (Access Laser Company, Marysville, WA, USA) with its output set to either 10.65 and 10.16 μm (corresponding to dopamine and uric acid IR absorption bands, Figures 2-6 and 2-7), was used for infra-red multiple photon dissociation (IRMPD).

H/D Exchange Experiment

A 0.5 mM DA solution was prepared in 50/1/49 vol%, D_2O/acetic acid/methanol and was allowed to stand overnight for proton/deuterium exchange. To verify the structure of the uric acid dimer (MW 336.06), a proton/deuterium exchange experiment was carried out using a solution of uric acid in 40/60 vol%,, D_2O/MeOH, 10^{-3} M NH_4Ac. The reaction was allowed to proceed overnight (18 hrs) to ensure completion of H/D exchange.

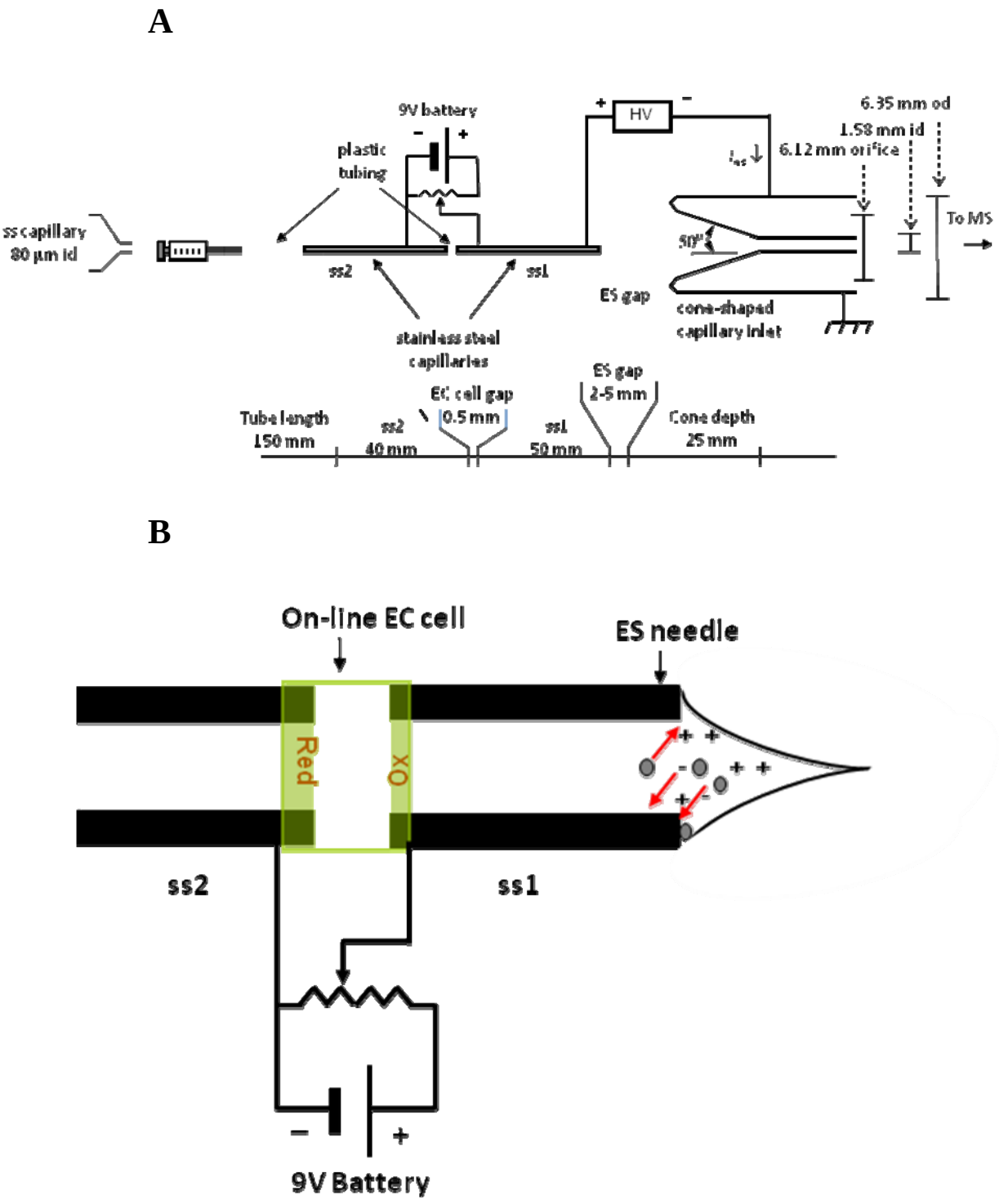

Figure 2-1. The EC/ESI MS system with the electrochemical cell intergrated into the electrospray capillary. A) Schematic with dimensions; B) Expansion of on-line EC cell.

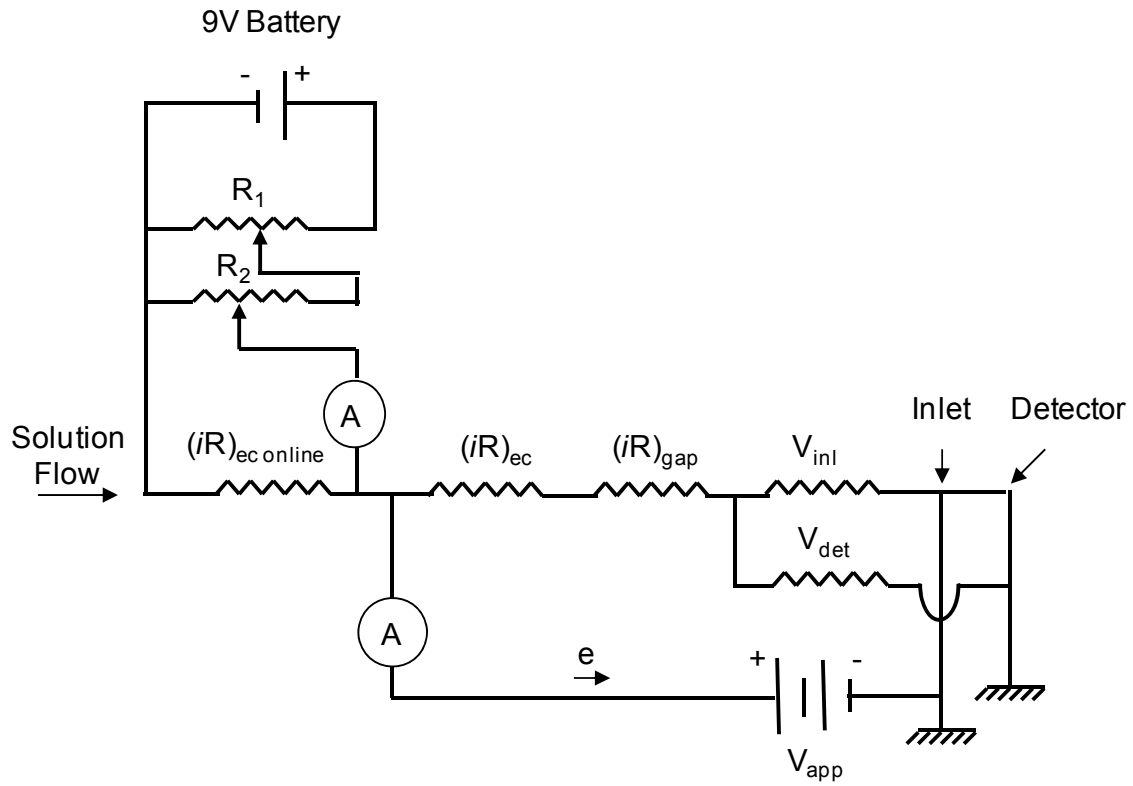

Figure 2-2. Electrical circuit diagram of the on-line EC/ ESI MS system

Figure 2-3. Standard linear track variable resistor.

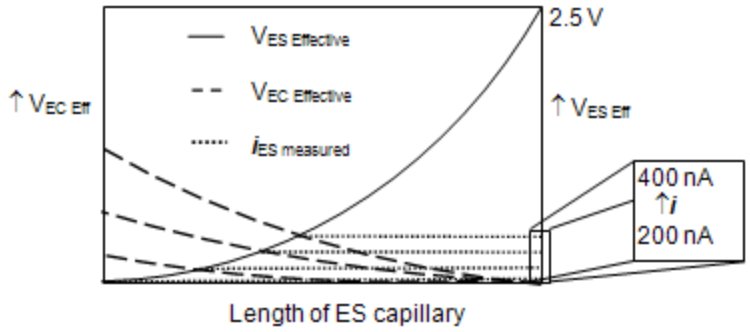

Figure 2-4. Projected voltage profiles along the ES capillary with ~0.5V increments of applied EC cell voltage (V_{app}). The low EC cell voltage is floated at the high voltage (HV) of the electrospray. The solid line represents the reported voltage profile of a standard ES emitter [Pozniak and Cole, 2007].

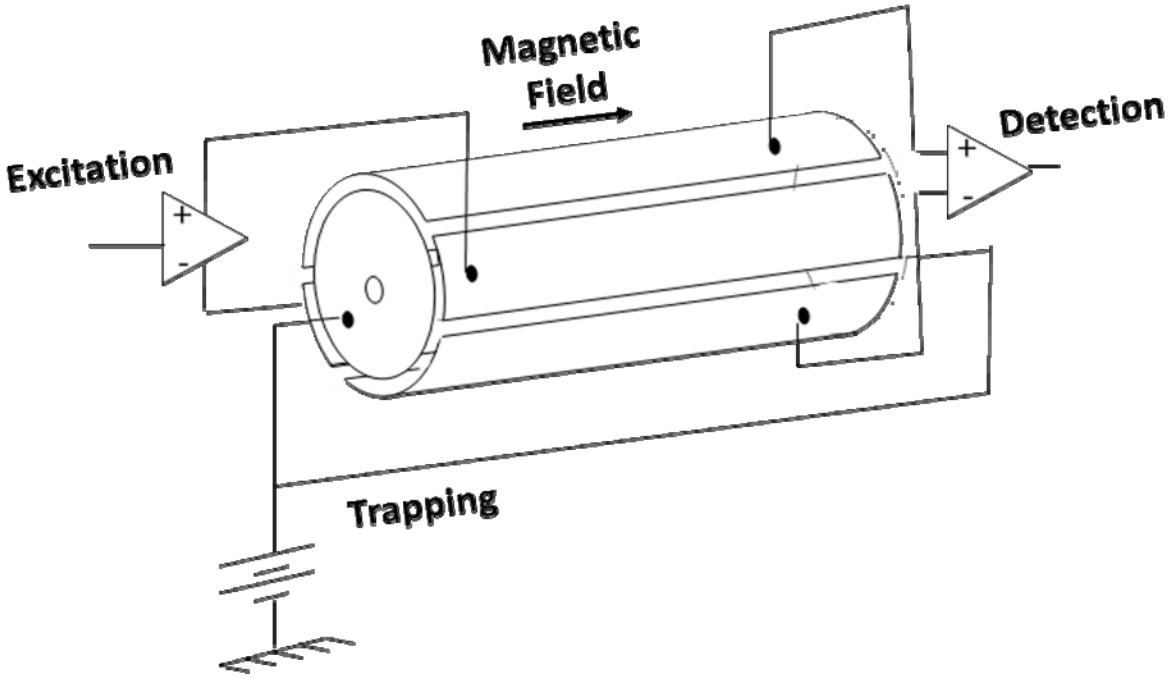

Figure 2-5. The ICR cell showing the electronic circuit through which rf electric field is applied to excite, trap and detect ions.

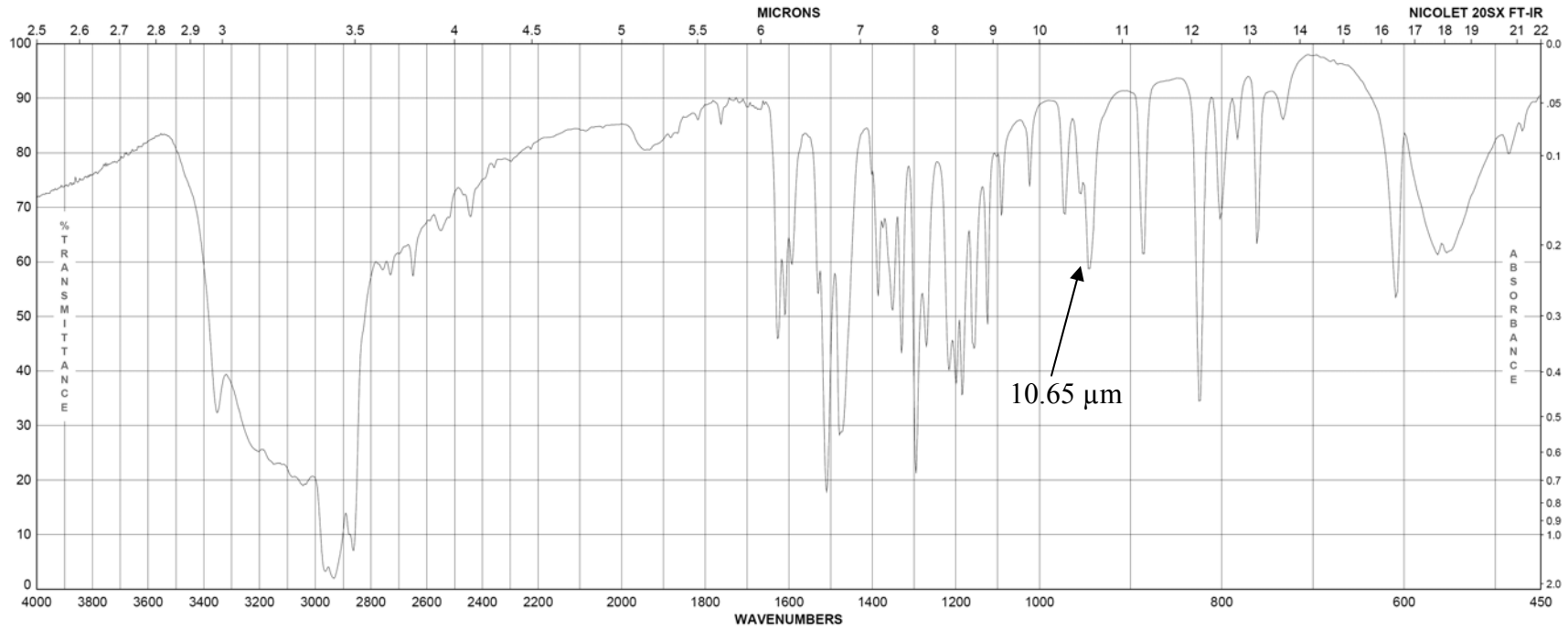

Figure 2-6. Fourier transform IR absorption spectrum of dopamine. The band at 10.65 µm was laser targeted for the IRMPD MS/MS experiment.

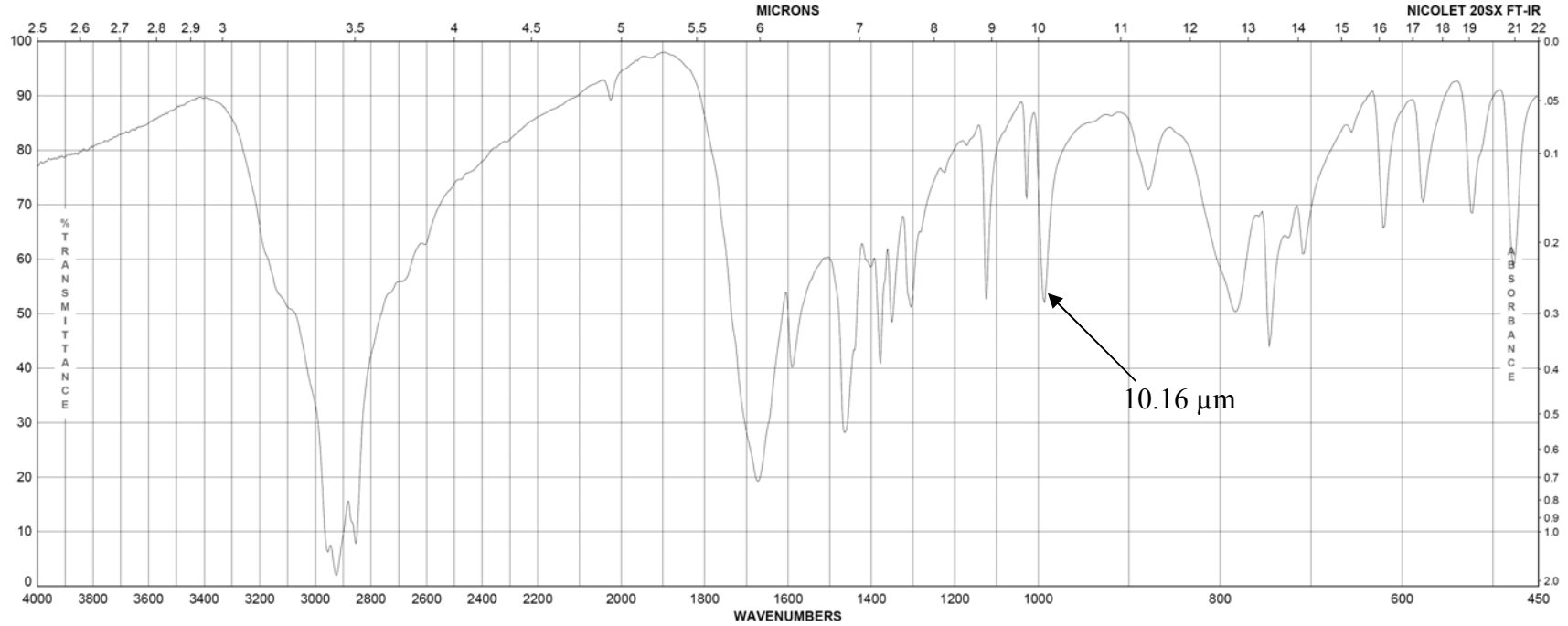

Figure 2-7. Fourier transform IR absorption spectrum of uric acid. The band at 10.16 µm was laser targeted for the IRMPD MS/MS experiment.

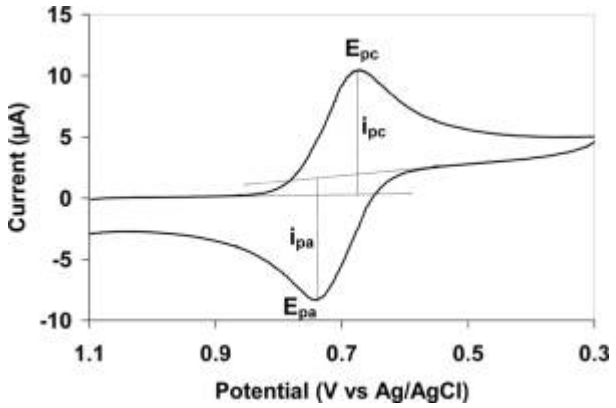

Figure 2-8. Typical cyclic voltammogram.

CHAPTER 3
ONE-ELECTRON OXIDATION OF DOPAMINE IN ESI AND EC/ESI MS

Introduction

Electrospray ionization mass spectrometry (ESI MS) is an important tool in proteomics [Aebersold and Mann, 2003; Bogdanov and Smith, 2005] and, because of its high throughput characteristics and relative ease of coupling to capillary liquid chromatography and microfluidic devices, it is attractive for the analysis of complex mixtures in metabolomics [Shen et al., 2005]. Electrochemical processes encountered during ESI, reviewed recently by Van Berkel and Kertesz [2007], have been exploited in proteomics research [Roussel et al., 2004; Maleknia et al., 1999] and are of interest in metabolomics [Gamache et al., 2004].

In ESI MS, high voltage (HV) is applied to a metal capillary through which the analyte solution is pumped. In positive mode ESI MS, charge separation of ions in solution results when positively charged droplets form [Blades et al., 1991; Xu et al., 1994]. As discussed in Chapter 1, electrochemical (oxidation) reactions maintain charge balance during ESI and the ESI interface operates as an electrochemical cell.

Electrochemical reactions which occur during ESI are unique and can be exploited in analysis [Karst, 2004]. Water, which is commonly present in aqueous/organic carrier solutions, is oxidized during positive mode ESI generating protons (H^+) [Moini et al., 1999; Konermann et al., 2001]. As mentioned in Chapter 1, oxidation buffers can be added to the carrier solution in order to control electrochemical reactions of the analyte during ESI. Lately though, new instrumental designs are being considered [Kertesz and Van Berkel, 2006; Liljegren et al., 2005].

In on-line electrochemistry ESI MS (EC/ESI MS) experiments described in this dissertation, low voltage is applied to the electrospray needle in addition to the HV of ES (Chapter 2, Figure 2-1). The ES capillary, connected through low volume plastic tubing to a

second capillary section into which the sample is injected, is the working electrode and the second capillary section is the counter/reference electrode [Zhou and Van Berkel, 1995; Zhang et al., 2002]. Thus the low voltage cell is floated on the HV of the ES. When low voltage is applied, ionization efficiency increases as does the electrospray current and sensitivity improves [Zhang et al., 2002; Kertesz, Van Berkel, 2005].

Radicals of dopamine (2,4-dihydroxyphenethylamine; DA), a catecholamine neurotransmitter, have been proposed to function as biological antioxidants against reactive oxygen species [Anderson and Harris, 2002]. In addition, the formation of Cys radicals by $1e^-$, $1H^+$ oxidation processes has been proposed from electrochemical studies of cysteine (CySH), a known biological antioxidant [Spataru et al., 2001; Zhou et al., 2007]. Sensitive and selective measurements of these molecules as markers of disease, including by LC MS methods [Zhou et al., 2007; Ogasawara et al., 2007], are of interest; and development of sensitive LC MS methods can be facilitated through information provided by ESI MS.

The formation of one-electron ($1e^-$) oxidation products of DA and CySH, as well as DA quinone-CySH adduct, via a radical pathway during positive mode ESI are described in this chapter. ESI MS thus provides direct insight into $1e^-$ oxidation processes of biological interest. The DA quinone-CySH adduct has been identified as an important metabolite in studies of oxidative stress in the brain [Zhang and Dryhurst, 1994; LaVoie and Hastings, 1999; Spencer et al., 1998]. The ESI MS system used in this work, with a cone-shaped capillary inlet (Figure 2-1) allowed efficient collection of the electrospray plume of ions. The use of cone-shaped inlet results in significant enhancement in sensitivity compared to the standard cylindrical capillary inlet, which only collects the axially centered portion of the ES plume. Higher sensitivity aids the investigations of $1e^-$ processes inherent to ESI.

Results and Discussion

The ESI MS of Dopamine (DA)

Figure 3-1 shows ESI mass spectra of DA using a cylindrical inlet (A) and a cone-shaped inlet (B). The three major peaks in either spectrum were assigned to deaminated dopamine $[DA\text{-}NH_3]^+$ m/z 137 (peak 1), the DA cation $[DA]^+$ m/z 154 (peak 2) and the DA dimer $[2DA\text{-}H]^+$ m/z 307 (peak 3). A small peak (peak 4) at m/z 152 was assigned to DA quinone $[DAQ]^+$. Scheme 3-1 shows the proposed ion formation pathways, which are discussed in more detail later in this chapter. Since DA is a cation in the carrier solution ($pK_a = 8.9$) [Sanchez-Rivera et al., 2003; Linert et al., 1996; Hawley et al., 1967] it forms gas phase $[DA]^+$ ions simply through solvent evaporation. The $[DA\text{-}NH_3]^+$ ions likely form in the heated MS capillary inlet due to gas phase expansion within a small space. The low formal oxidation potential ($E^{o'}$= 0.12V vs SCE) [Tse et al., 1976] favors DA oxidation during ESI [Van Berkel et al., 2007]. However, the low pH reached during ESI [Moini et al., 1999] can inhibit $2e^-$, $2H^+$ oxidation of DA, which may explain low intensity of the DA quinone $[DAQ]^+$ signal. Studies show that the initial electrolytic $1e^-$ oxidation occurs with a concomitant loss of H^+ regardless of pH [Constentin et al., 2007]. Therefore, oxidation of DA by $1e^-$, $1H^+$ processes can produce radicals and then, rapidly, the DA dimer $[2DA\text{-}H]^+$ by nucleophilic reactions common to catecholamines [Hawley et al., 1967; Tse et al. 1976] (Scheme 3-1). Further $1e^-$ oxidation of the DA dimer (Scheme 3-1) during ESI, to a doubly charged dimer $[2DA\text{-}H]^{2+}$ (m/z 153.5), is indicated by EC/ESI MS results discussed below. In EC/ESI MS, as shown below, $2e^-$, $2H^+$ oxidation of DA to DA quinone (DAQ) is made more efficient than in ESI MS, and DA dimer intensity decreases as a result.

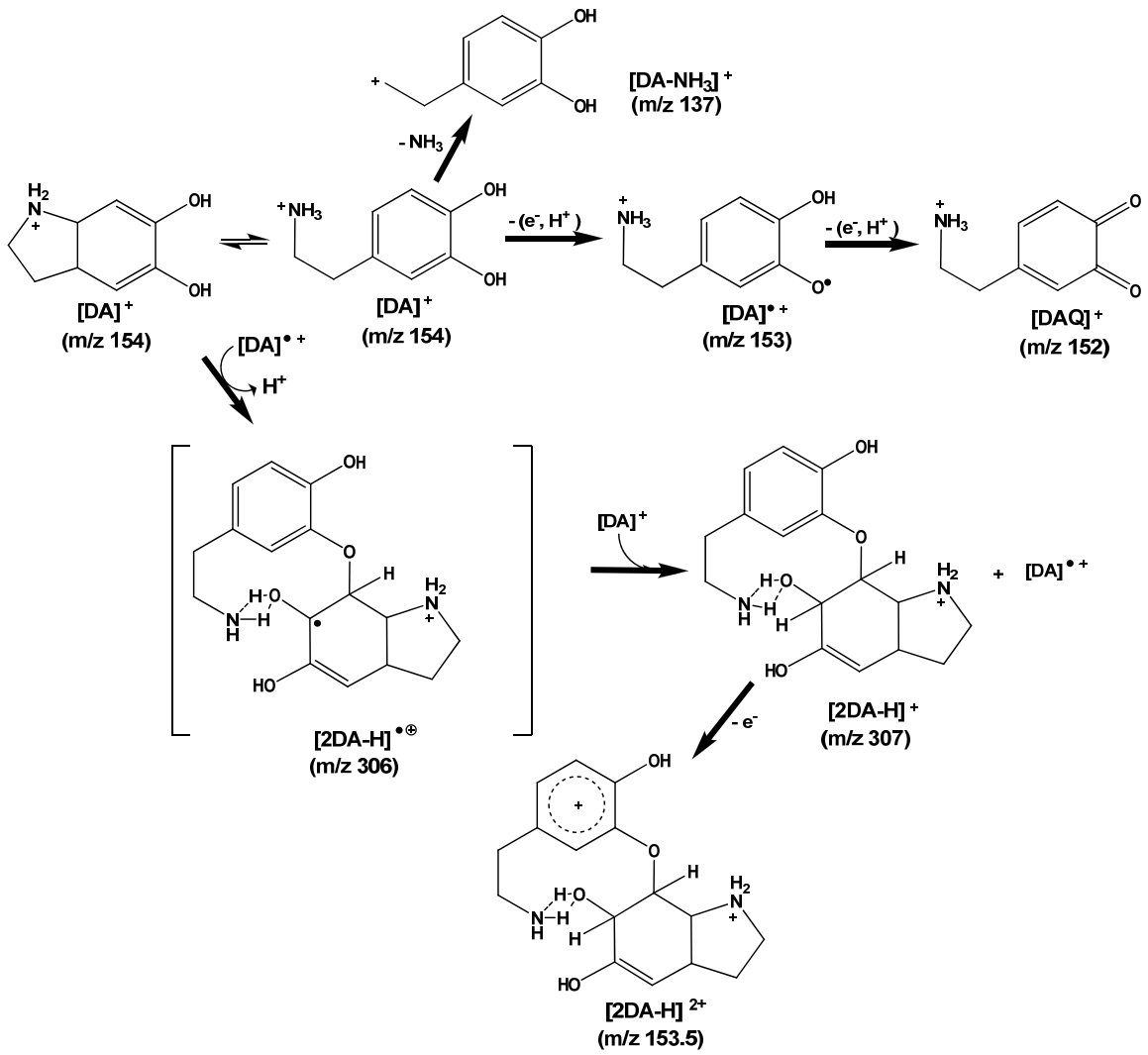

Scheme 3-1. Dopamine oxidation in positive mode ESI MS. Hydrogens that form H-bonds are not exchangeable with deuterium in the presence of D_2O (see mass spectra in Figure 3-2).

Cone-Shaped vs Cylindrical Inlet

A significant improvement in detection sensitivity for dopamine (> 100% increase in intensity of the base peak) is observed when the cone-shaped inlet is used (Figure 3-1B) compared to a standard cylindrical inlet (Figure 3-1A). A small peak at m/z 152 (Figure 3-1B peak 4), which corresponds to the dopamine quinone $[DAQ]^+$ (Scheme 3-1), is observed with the cone-shaped inlet ESI MS owing to its great sensitivity.

In the normalized version of spectra shown in Figure 3-1, the relative intensity of the dopamine dimer $[2DA-H]^+$ (m/z 307) is higher in the cylindrical inlet ESI MS, most likely due to loss of radially disributed lighter ions [Nemes et al., 2007]. The smaller ions of unoxidized dopamine are spatially distributed upon coulombic explosion of electrospray droplets [Rohner et al., 2004, Watson, 1997] and are not collected in the cylindrical inlet. When radially distributed ions re collected using the cone-shaped MS inlet, the sensitivity and the relative intensity of $[DA]^+$ ions increases (Figure 3-1), which allows detection of low concentrations of dopamine. Considering that the loss of the NH_3 group from $[DA]^+$ likely occurs during the expansion and desolvation of the electrospray droplets in the MS inlet capillary, it is not surprising that higher intensity of the $[DA-NH_3]^+$ ion (peak 1) relative to intact $[DA]^+$ ion (peak 2) is observed in the more confined cylindrical inlet (Figure 3-1A). The DA dimer, a $[2M-H]^+$ species (not to be confused with a proton-bound dimer $[2M + H]^+$) can only be explained by a covalently bound arrangement such, as that shown in Scheme 3-1, given that DA (pK_a =8.9) exists as a cation at pH 4.2 [Sanchez-Rivera et al., 2003; Linert et al., 1996]. Furthermore, dopamine hydrochloride was used in this work, which dissociates into positive dopamine ions and negative chloride ions in solution. It is unlikely therefore, that at pH 4.2 a dopamine dimer formed by two electrically neutral dopamine molecules exists.

The H/D Exchange of DA

The H/D exchange experiments show that the DA dimer has five exchangeable protons (Figure 3-2D), in agreement with the proposed covalent structure of the dimer shown in Scheme 3-1. In addition, H/D exchange shows that $[DA]^+$ has four exchangeable protons (Figure 3-2C), consistent with a closed ring structure of $[DA]^+$ in the gas phase. Scheme 3-1 shows the closed ring structure in equilibrium with the open ring for ions of DA, which is common among catecholamines [Blank et al., 1976]. High sensitivity is achieved with the cone-shaped inlet ESI

MS. The lowest measured concentration is 0.02 mM (20 μM), where only the $[DA]^+$ (m/z 154) ion is observed (Figure 3-3). The intensities of DA ions change with experimental conditions and with DA concentration (Figure 3-3).

The MS/MS of DA Dimer

That the O-C and intramolecular hydrogen bonds link the dopamine semi-quinone and dopamine (see structure of $[2DA-H]^+$ in Scheme 3-1) is supported by results of the H/D exchange experiment much more explicitly than MS/MS experiment. The MS/MS spectrum of the DA dimer, obtained after activation and subsequent dissociation of DA dimer by CO2 laser irradiation (for > 0.5s) showed both the $[DA]^+$ (m/z 154) and the DA dimer $[2DA-H]^+$ (m/z 307) peaks (Figure 3-4). Considering that the two DA molecules are bound by one covalent bond and a hydrogen bond, this result is expected since the new covalent bond is more likely to cleave than any of the covalent bonds in the DA dimer structure. The persistent presence of the DA dimer under prolonged irradiation indicates the presence of a (difficult to cleave) covalent bond holding together the dimer structure, presumably the O-C covalent bond linking the two DA structures. The proposed cleavage mechanism is shown in Scheme 3-2. If the H-bound DA dimer were present, it would be cleaved readily and the DA dimer peak (m/z 307) would disappear completely upon laser irradiation.

The EC/ESI MS of DA

In EC/ESI MS, the intensity of DA ions is determined by the low voltage applied in the on-line EC cell. As shown in Figure 3-5, the intensities of $[DA]^+$ and $[DA-NH_3]^+$ ions increase with the applied voltage. Electrospray current is higher in EC/ESI MS than in ESI MS, an indication of improved ionization efficiency and conditions that are conducive to the release of preformed $[DA]^+$ ions from solution to the gas phase and corresponding increase in fragmentation of $[DA]^+$ to $[DA-NH_3]^+$. In EC/ESI MS the DA quinone signal increases and the DA dimer signal

decreases as applied EC cell voltage is incresed. Thus $2e^-$, $2H^+$ oxidation of DA is promoted in EC/ESI MS.

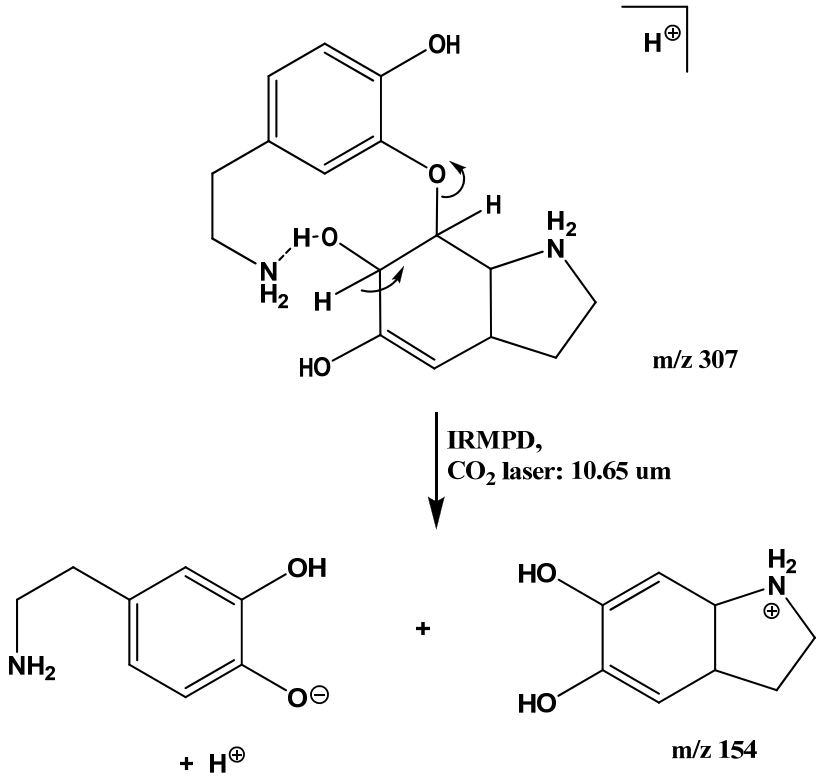

Scheme 3-2. Proposed cleavage mechanism of the DA dimer in the infrared multiphoton dissociation (IRMPD) experiment.

During EC/ESI MS of 2.5 mM DA, the electrospray current increases to ~400 nA from ~200 nA in ESI MS. Assuming a uniform current distribution in a capillary of a circular cross section, the limiting current should be ~26 μA, based on

$$i_{lim} = 1.61zFC(DA/r)^{2/3} v^{1/3} \quad (3\text{-}1)$$

[Bard and Faulkner, 2001] where i_{lim} is the mass transport-limited current during laminar flow, $z = 1$ (number of electrons), $F = 96485$ C mol^{-1} (Faraday constant), $l = 5.0\text{x}10^{-2}$ m (length of the capillary tube), $C = 2.5$ mol m^{-3} (concentration), $D = 6.0\text{x}10^{-10}$ m^{2}s^{-1} [Gerhardt and Adams, 1982] (diffusion coefficient), $v = 8.3\text{x}10^{-12}$ m^{3}s^{-1} (30 μL/h) (flow rate), $r = 4.0\text{x}10^{-5}$ m (cross sectional capillary radius) and $A = 2\pi rl = 1.3 \text{ x } 10^{-5}$ m^2 (area inside the capillary). However, the

observed electrospray current in EC/ESI MS of DA is lower than the theoretical i_{lim} calculated from Equation 3-1. The presencxe of large signals of $[DA]^+$ and $[DA\text{-}NH_3]^+$ ions verify that in both ESI and EC/ESI MS, oxidation efficiency of DA is less than 100% (Figure 3-1), which reflects non-uniform distribution of current in the electrospray capillary needle.

Effect of Flow Rate

Sensitivity of ESI MS depends on flow rate [Tang et al., 2001]. In ESI MS with the cylindrical capillary inlet, the ion signal (and thus sensitivity) does not depend strongly on flow rate as shown by Figure 3-6A. With the cone-shaped inlet (Figure 3-6B), the ion signal is a stronger function of flow rate because of efficient collection of spray droplets by the large orifice of the MS inlet. In EC/ESI MS, the maximum signal is reached at lower flow rates (Figure 3-6C), because higher current increases ion signal at all flow rates. With a cylindrical inlet, good sensitivity has been reported at flow rates ≤ 200 nL/min (or 12 μL/h) [Vanhoutte et al., 1998]. These results show that the cone-shaped inlet ESI MS system developed in this work accommodates much higher optimum flow rates, which is practical for ESI MS coupling to micro-column HPLC and other micro-fluidic separations.

Cyclic Voltammetry of DA

A cyclic voltammogram of DA in pH 7.4 phosphate buffer at a stainless steel disk electrode (r = 50.8 μm) shows one broad shoulder at ~400 mV vs SCE before the increase in the background current at positive potentials (Figure 3-7). This wave is not observed for DA in the carrier solution (50/1/49 vol% H2O/HAc/MeOH, pH 4.2) (Figure 3-7B) or in 99/1 vol% H2O/HAc, pH 4.0 (Figures 3-7C). DA electrooxidation is thus slow in the 50/1/49 vol% H2O/HAc/MeOH, pH 4.2 carrier solution at a stainless steel electrode, and it likely occurs together with oxidation of water.

The ESI MS of DA in the Presence of Cysteine (CySH)

The ESI mass spectrum of CySH (Figure 3-8A; discussed in detail in Chapter 5) shows the base peak at m/z 241, assigned to the proton adduct of the cysteine dimer $[CySSCy+H]^+$ (Scheme 3-3), and the proton adduct of CySH $[CySH+H]^+$ (m/z 122). Peak 6 of the proton adduct of monomeric CySH $[CySH+H]^+$ (m/z 122) is much smaller compared to DA ions because CySH is neutral in the carrier solution. ESI MS sensitivity to CySH is low under the present conditions, which are optimized for DA, and the background signal is relatively high. The ESI mass spectrum of DA with CySH reflects the individual mass spectra of DA and CySH (Figure 3-8B). In addition, an m/z 273 ion is detected and assigned as the DAQ/CySH adduct $[DAQ+CySH]^+$. The intensities of this adduct and of the DA dimer increase at higher CySH concentration from 0.1 to 2.0 mM at a constant DA concentration (2.5 mM). Thus, during ESI, oxidation of DA to DAQ is facilitated by the presence of CyS. radicals, probably because of the difference in Eo values of DA (Eo = -0.12 V vs SHE) [Tse et al., 1976] and CySH (0.92 V vs SHE) [Buettner and Jerkiewicz, 1996], and is followed by nucleophilic addition of CySH to DAQ, which produces the DAQ/CySH adduct. As shown in Figure 3-8A a disulfide dimer CySSCy forms during ESI of CySH. Ionization of CySH is facilitated by higher electrospray current and by the presence of DA, which chemically reduces CyS. radicals. In this case, DA acts as an antioxidant. Ion formation pathways are summarized in Scheme 3-3. Nucleophilic addition of CySH to DAQ is significant in Alzheimer's and Parkinson's disease [Shen and Dryhurst, 1996a; Shen and Dryhurst, 1996b; Shen et al., 1996;]. In these ESI MS experiments (where CySH is present), high intensities of the DA oxidation products, DA dimer and DAQ, relative to the CySH oxidation product and the disulfide dimer of cysteine, may be due in part to faster oxidation of DA^+ to DA^+ (k ~ 7.2x109 M-1s-1) [Anderson and Harris, 2002] relative to oxidation of CySH to CyS. (k ~ 1.2x 103 M-1s-1) [Uchiyama and Sekioka, 2005].

The EC/ESI MS of DA in the Presence of CySH

High electrospray current in EC/ESI MS improves ES efficiency of DA and CySH ionization. There is less formation of the DA and CySH oxidation products, DA and CySH dimers, and DAQ-CySH adduct (Figure 3-9). At higher applied voltages (≥ 1.0V), oxidation of DA by $2e^-$, $2H^+$ is facilitated, and the intensity of the DAQ/CySH adduct increases while the intensity of the DA dimer decreases.

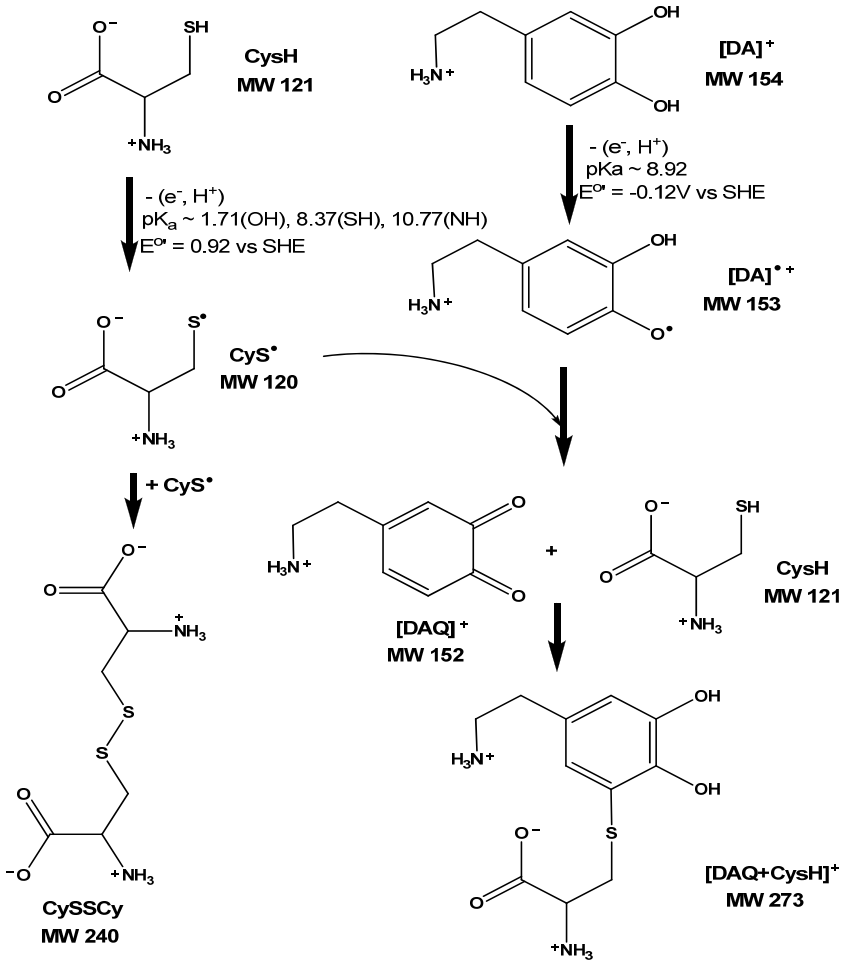

Scheme 3-3. Formation of DAQ-CySH adduct in positive ion mode ESI MS.

Conclusions

In positive mode ESI of DA and CySH in aqueous/methanol carrier solution, DA and CySH dimer signals are detected. Thus during ESI, DA and CySH radicals appear to form and

rapidly dimerize. Cone-shaped capillary inlet ESI MS is more sensitive than the standard cylindrical capillary inlet ESI MS. Formation of DA quinone by a $2e^-$, $2H^+$ process is not efficient, possibly because of the low pH during ESI. Real-time chemical identification of products of $1e^-$ and $2e^-$ ionization processes is possible in ESI and EC/ESI MS. High flow rates that can be used with cone-shaped inlet ESI MS can be practical for direct coupling of ES to microcolumn separations.

New insights into oxidation and antioxidant activity can be obtained by ESI and EC/ESI MS. The limiting step in the overall $2e^-$, $2H^+$ oxidation of DA, which is positively charged, may be the first $1e^-$, $1H^+$ loss. In vivo $2e^-$, $2H^+$ oxidation of DA in the presence of CySH was shown to form DAQ-CySH adducts [LaVoie and Hastings, 1999] which may lead to the depletion of the cysteine pool. ESI MS results suggest that this reaction can be relatively slow.

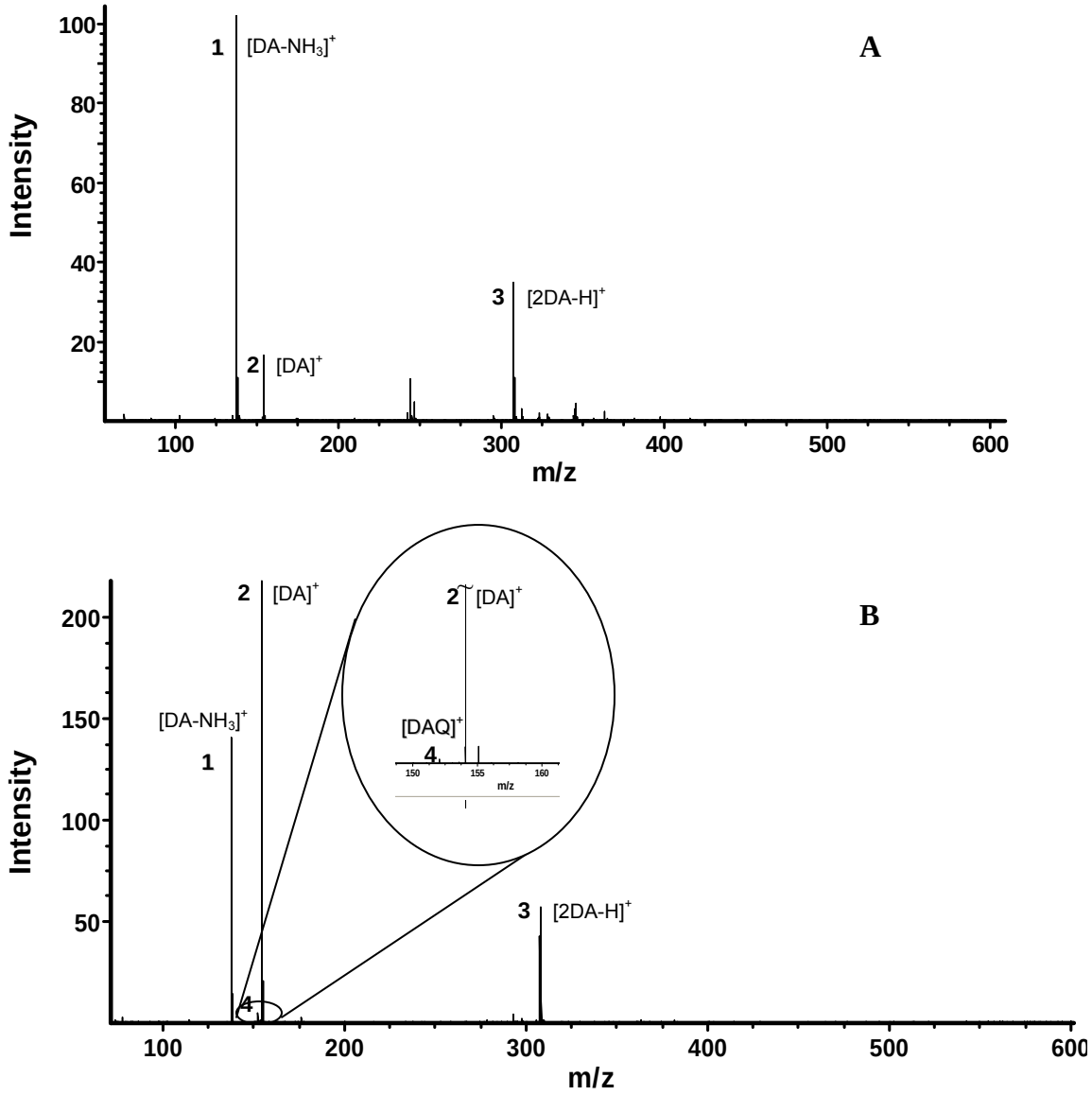

Figure 3-1. Positive ion ESI MS of DA (2.5 mM) with (A) cylindrical inlet and (B) cone-shaped inlet; flow rate 30 μL/h; 50/1/49 (vol %) H_2O/HAc/MeOH, pH~4.2; HV ~3 kV.

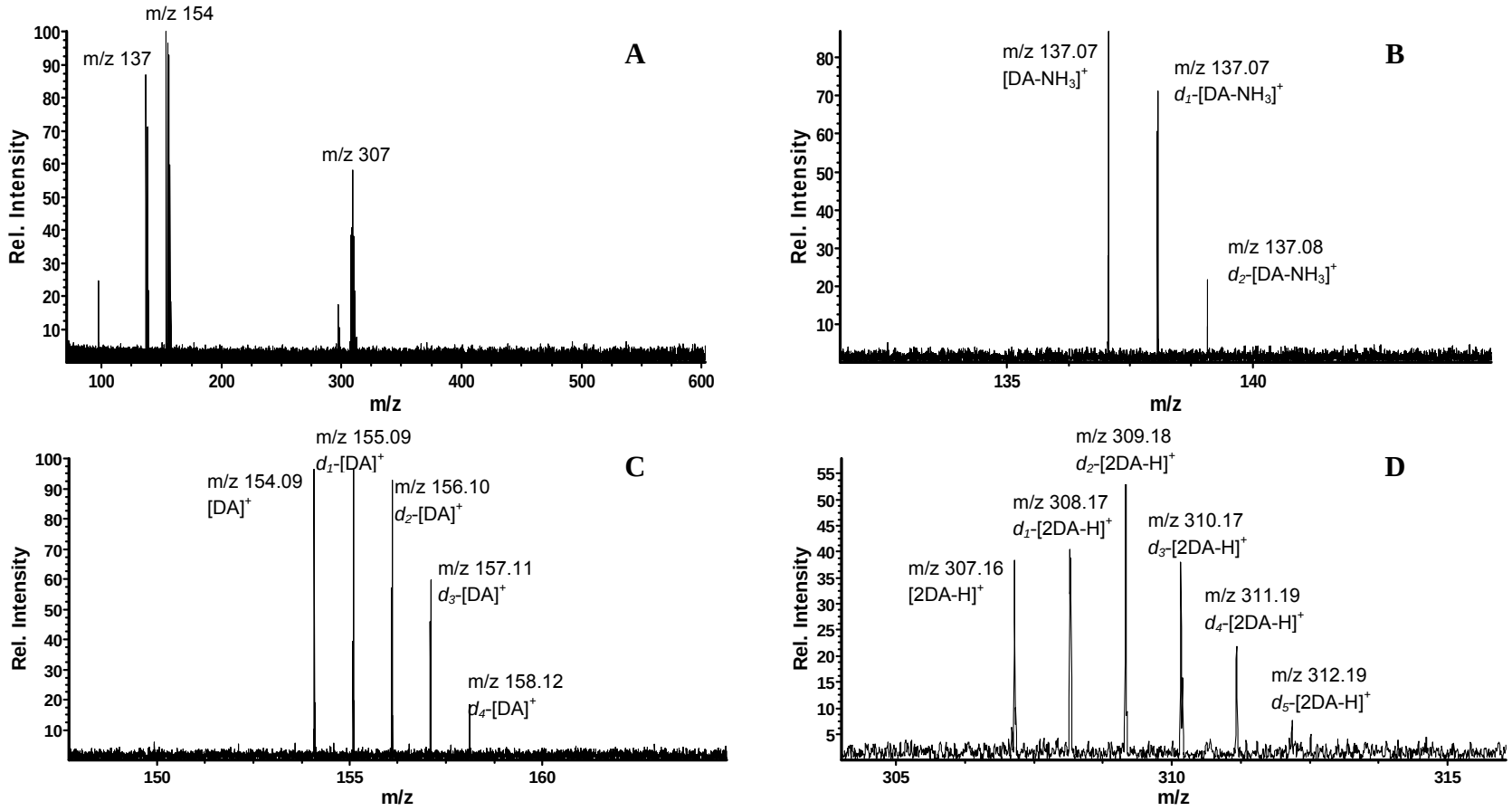

Figure 3-2. The ESI mass spectrum of dopamine (0.5 mM) in 50/49/1 vol%, D_2O/methanol/acetic acid (A). Peaks representing the number of exchangeable protons for the ions $[DA\text{-}NH_3]^+$, $[DA]^+$ and $[2DA\text{-}H]^+$ are shown in (B), (C) and (D), respectively. See structures in Scheme 3-1.

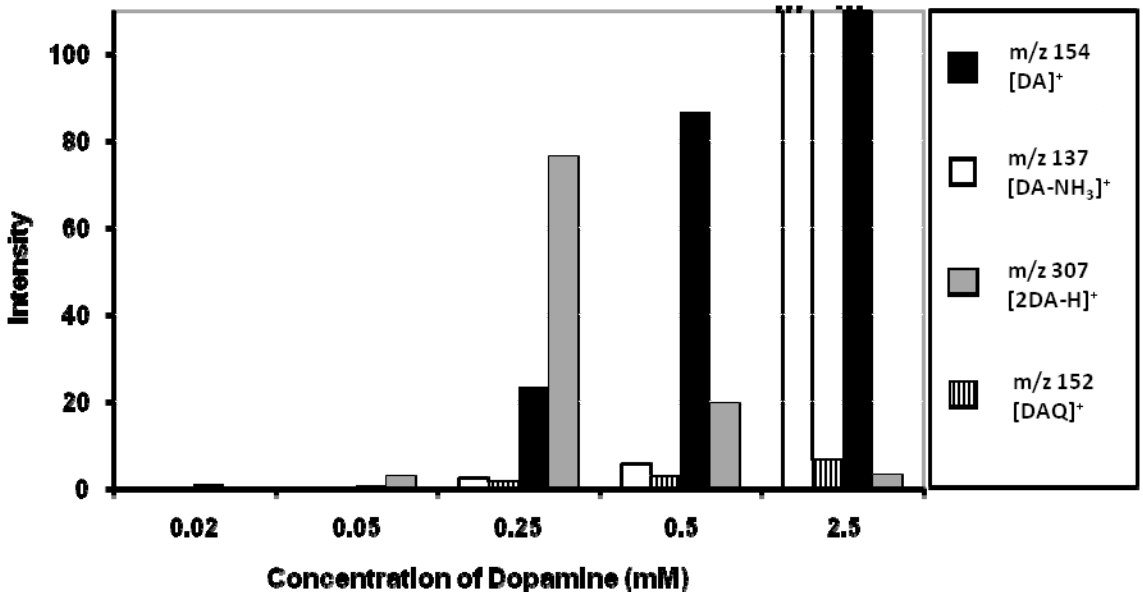

Figure 3-3. Changes in ion intensities in ESI mass spectra of DA due to change in concentration. Dots indicate off-scale intensity. Flow rate 60 μL/h; cone-shaped capillary inlet; 50/1/49 (vol %) H_2O/HAc/MeOH, pH~4.2; HV ~3 kV.

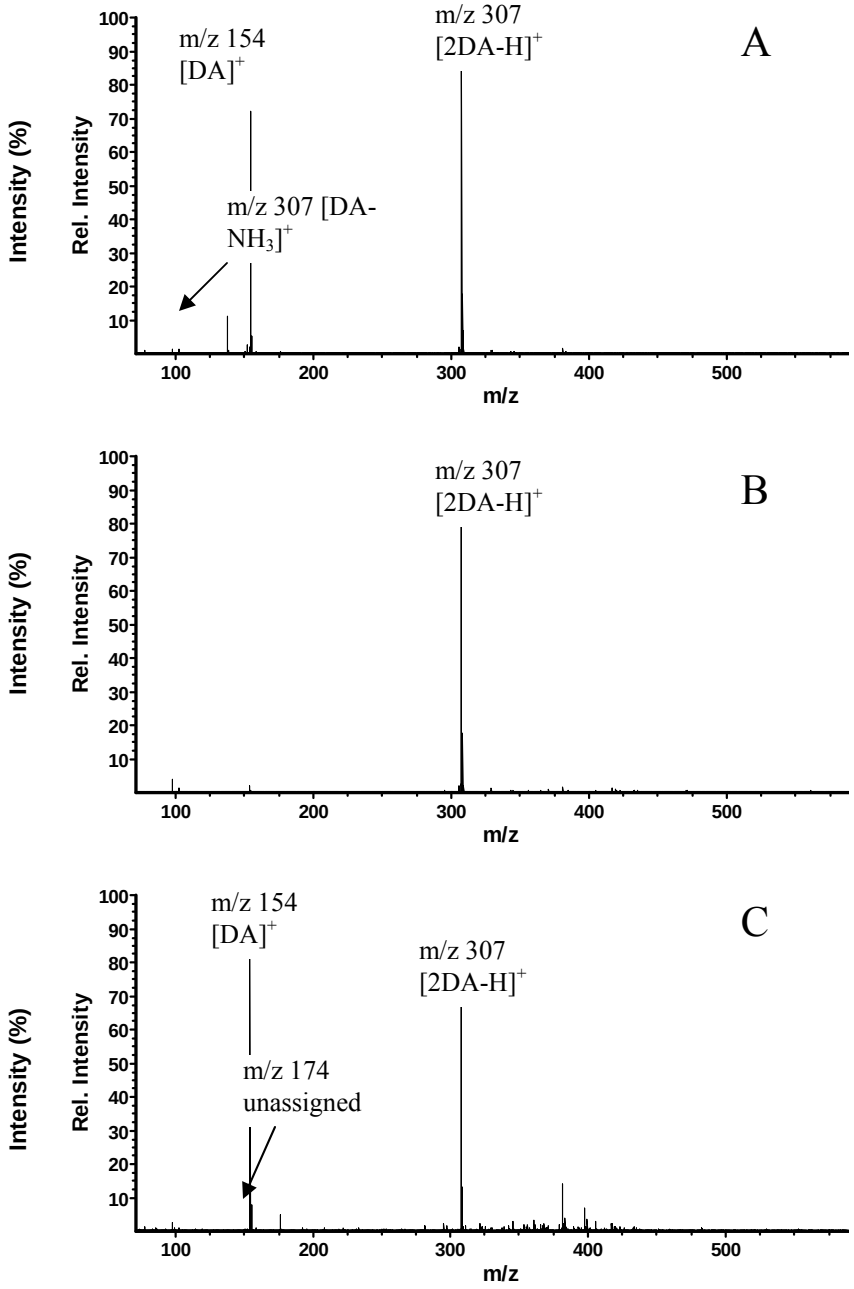

Figure 3-4. The ESI MS of 2.5 mM dopamine (A); ESI MS after ejection of m/z < 307 and m/z > 307 ions i.e isolation of dopamine dimer $[2DA-H]^+$ (m/z 307) ion (B); MS/MS of $[2DA-H]^+$ following CO_2 laser irradiation (>0.5s) - Notice product ion peaks at m/z 154, most likely $[DA]^+$ and at m/z 174, unassigned (C).

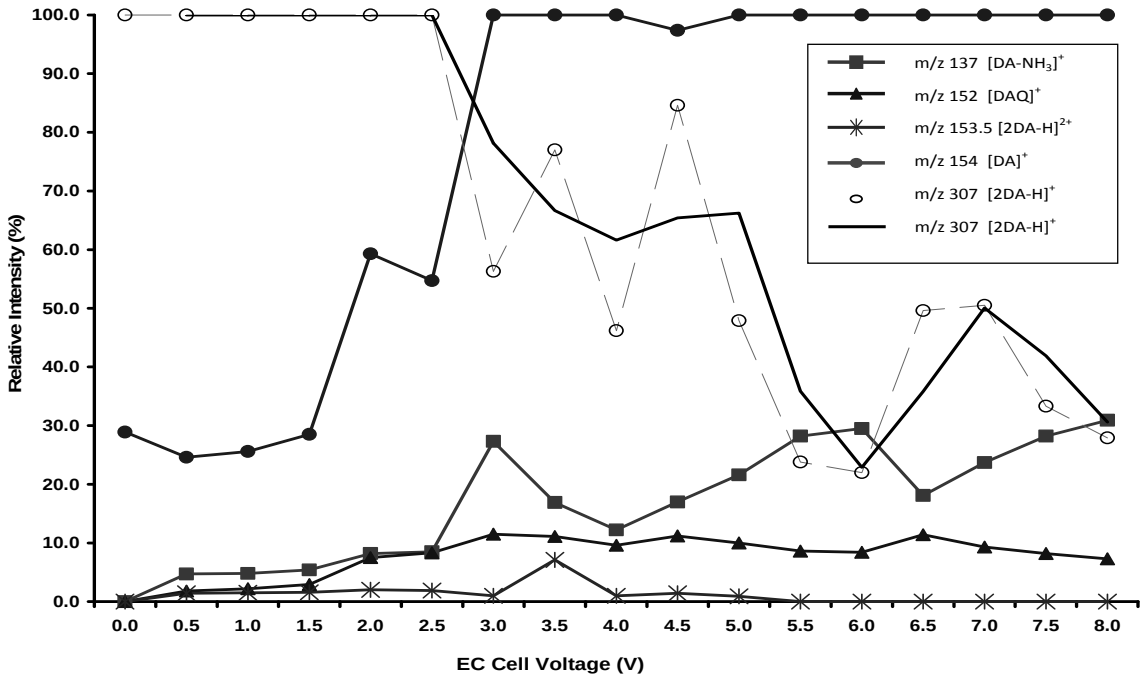

Figure 3-5. The EC/ESI MS of DA (0.25 mM). Conditions as in Figure 3-3; moving average in black.

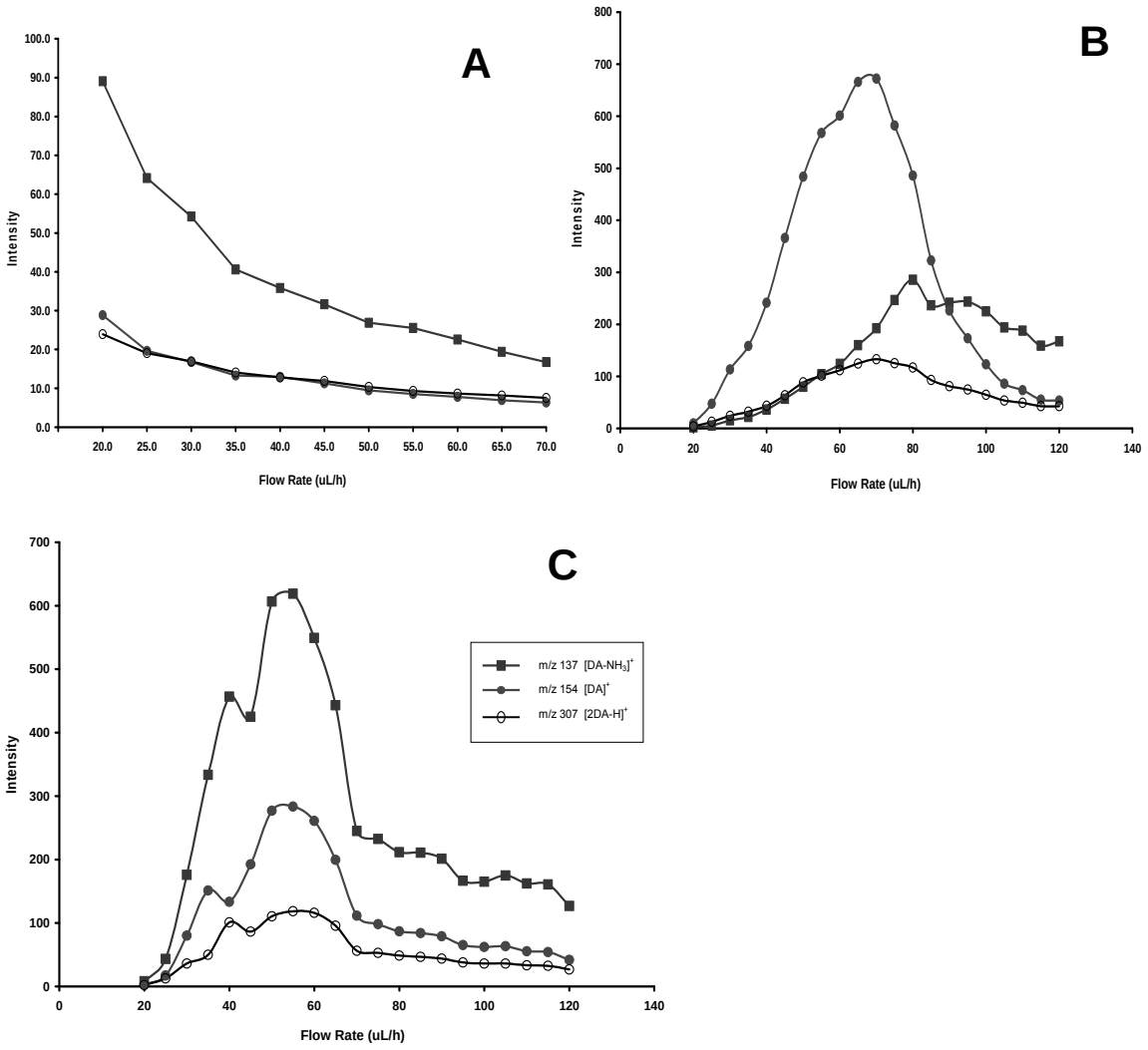

Figure 3-6. The ESI MS of DA (2.5 mM) as a function of flow rate: (A) cylinder capillary inlet; (B) conical capillary inlet; (C) conical capillary inlet in EC/ESI MS (1.5 V). Other conditions as in Figure 3-3.

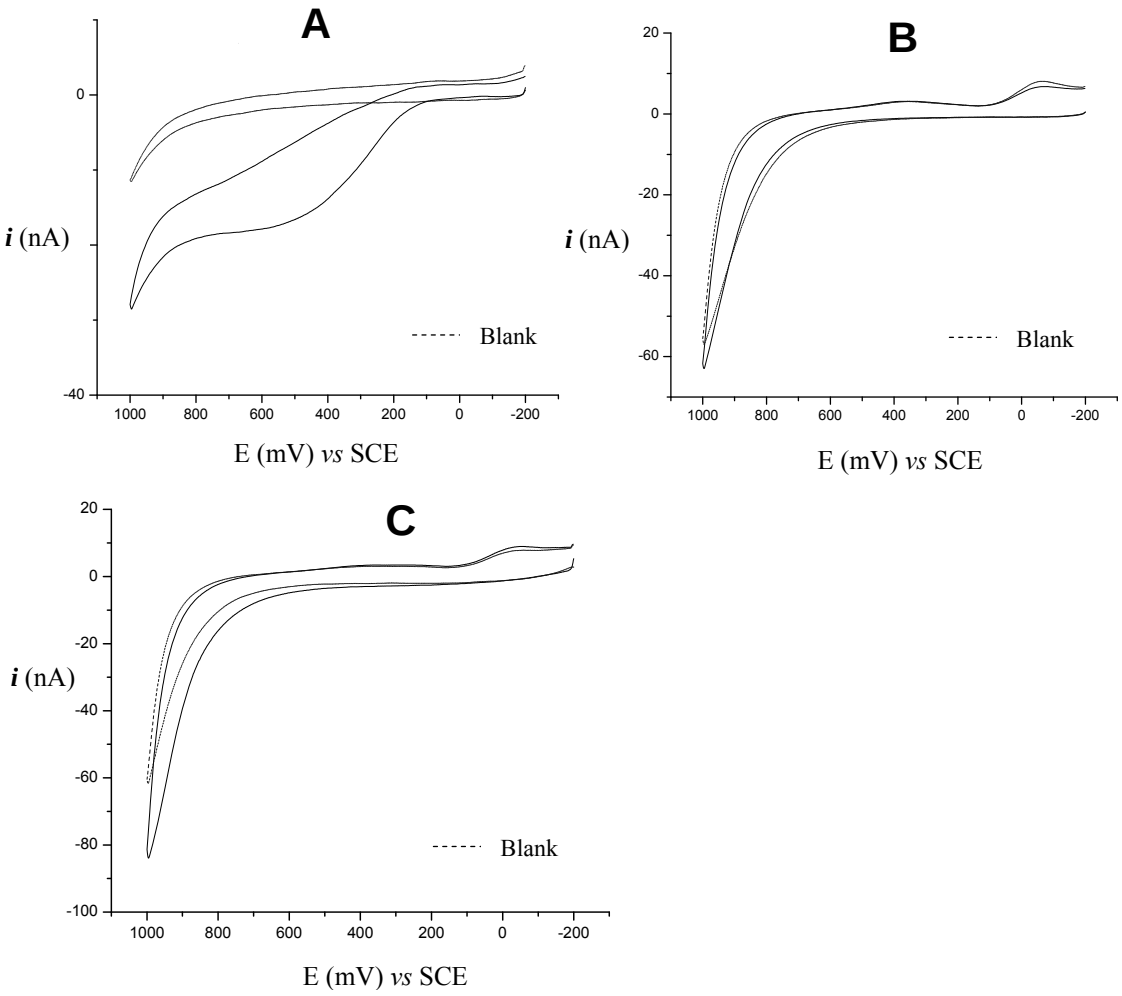

Figure 3-7. Cyclic voltammetry of DA (400 μM) at stainless steel electrode in (A) phosphate buffer (31 mM), pH~7.4; (B) 50/1/49 vol%, water/acetic acid/methanol, pH~4.2; (C) 99/1 vol%, water/acetic acid, pH~4.0. Disk radius 50.8 μm; scan rate 50 mVs^{-1}.

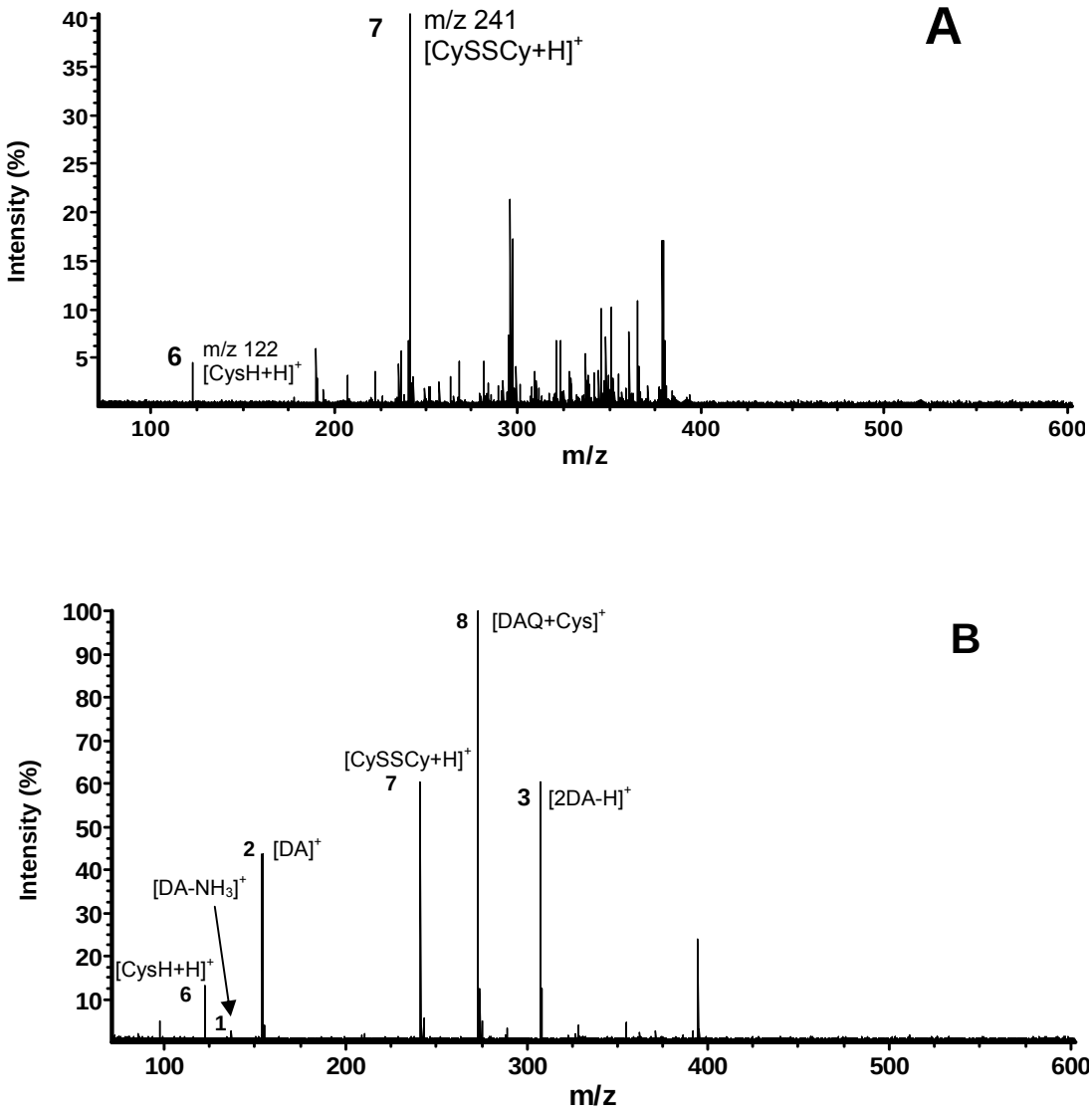

Figure 3-8. The ESI MS of cysteine (CySH) and DA with CySH: (A) CySH (0.5 mM); (B) DA (2.5 mM), CySH (0.5 mM). Flow rate 45 µL/h. Other conditions as in Figure 3-3.

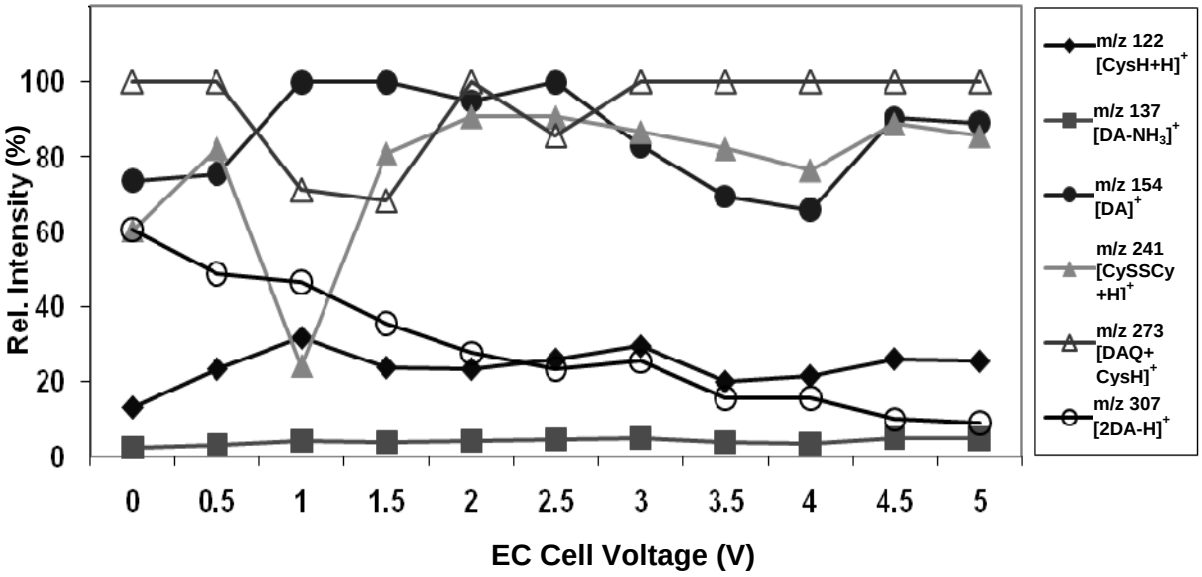

Figure 3-9. The EC/ESI MS of DA with CySH. Conditions as in Figure 3-3.

CHAPTER 4
ONE-ELECTRON OXIDATION AND DETECTION SENSITIVITY OF URIC ACID IN ESI AND EC/ESI MS

Introduction

Purine metabolites are important as markers of physiological disorders, and their analysis is of interest in clinical diagnostics and metabolomics [Simmonds et al., 1997; La Marca et al., 2006; Gamache et al., 2004]. Uric acid, which is the final product of nucleotide catabolism in humans [La Marca et al., 2006], has been identified as a marker of cardiovascular disease [Waring et al., 2000; Alderman and Kala, 2004]. Uric acid has also been reported to have protective functions during oxidative stress, when high concentrations of superoxide (O2.-) drive the reaction of O2.- with nitric oxide (NO.) to peroxynitrite (ONOO-) [Skinner et al., 1998; Hooper et al., 2000]. The consumption of NO., which regulates blood vessel dilation, is undesirable. However, uric acid appears to scavenge the peroxynitrite and liberate NO. [Skinner et al., 1998]. Thus uric acid may minimize tissue damage via the release of NO. [Hooper et al., 2000].

Purine metabolites can be analyzed by high performance liquid chromatography (HPLC) [La Marca et al., 2006; Gamache et al., 2004, Hartman et al., 2006; Ito, et al., 2000] and capillary electrophoresis (CE) [Benavente, et al., 2006] with ESI MS detection. However, uric acid is difficult to detect by ESI MS, in spite of its relatively high concentration in biological fluids [La Marca et al., 2006]. Uric acid was identified as a potent biological antioxidant from HPLC and UV analysis of $1e^-$ oxidation products in singlet oxygen and hydroxyl radical reactions [Ames et al., 1981]. In the previous work $1e^-$ oxidation and radical formation was confirmed by ESR and by transient UV measurements [Maples and Mason, 1988; Simic, Javanovic, 1989]. To enhance the sensitivity of uric acid detection in ESI MS, on-line electrochemistry ESI MS (EC/ESI MS), described in Chapter 2, was used in this work (see Figure 2-1).

As has been shown in Chapter 3 [Mautjana et al., 2008a], ESI and EC/ESI MS can provide unique insights into $1e^-$ reactions relevant to biological antioxidant properties. Furthermore, it has been demonstrated that oxidation of analytes during electrospray ionization can enhance the sensitivity in ESI MS measurements, because the higher electrospray current increases ionization efficiency [Mautjana et al., 2008a; Zhang et al., 2002]. In EC/ESI MS, the sensitivity can be further improved because the electrospray current increases when current flows in the on-line EC cell. A conical MS inlet capillary [Wu et al., 2006], used for study of one-electron oxidation reactions of dopamine [Mautjana et al., 2008a], can be used in the measurements of uric acid. Low m/z ions of biological metabolites, such as uric acid, are radially distributed in the electrospray and are not collected by the standard cylindrical inlet ESI MS, resulting in low detection sensitivity. The enhancement of sensitivity is expected as a result of improved collection of ions by the large-orifice conical MS inlet capillary [Wu et al., 2006] compared to the standard cylindrical capillary inlet.

Positive ion mode ESI MS is used in this work because of its high sensitivity to proton adducts of analytes. The results of this work suggest that during positive mode ESI MS, uric acid, which is negatively charged in the carrier solution, is oxidized by $1e^-$ processes to neutral radicals, which form dimers. The signals of the protonated monomeric and dimeric species contribute to the total uric acid signal. Furthermore, the low solubility of uric acid (~0.009g/100mL or 5.35×10^{-4} M at 25°C in water) [Mentasti et al., 1983] which can limit sensitivity in ESI MS, was addressed here through control of the carrier solution's composition.

Results and Discussion

Ionization of Uric Acid in Electrospray (ES)

Figure 4-1 shows the positive ion mass spectra of uric acid in a 40/60 vol%, H_2O/MeOH carrier solution with 1 mM NH_4Ac, pH~6.3 (A and B) and with 0.10 M KOH, 0.04 M HAc, pH

~12.7 (C). The base peak at m/z 169 (Figure 4-1A) was assigned to the proton adduct of uric acid $[H_2U+H]^+$ and the peak at m/z 337 [Skinner et al., 1998; Binyamin et al., 2001] was assigned to the proton adduct of uric acid dimer $[2H_2U+H]^+$. The dimer can form during ESI by $1e^-$ oxidation of urate followed by rapid dimerization of the radicals that are formed during oxidation. The proposed ion formation pathway is shown in Scheme 4-1. A small peak at m/z 231 (Figure 4-1A) was identified as the protonated adduct of 5-hydroxyhydantoin with parabanic acid $[OHhyd+Parab+H]^+$ (Scheme 4-2). Thus, $2e^-$, $2H^+$ oxidation of uric acid (Scheme 4-2) [Volk et al., 1992; Volk et al., 1999], can occur during ESI, but with low efficiency, as indicated by the low intensity of the $[OHhyd+Parab+H]^+$ adduct.

A consecutive $1e^-$ oxidation, with radical formation, has been reported in the electrochemical and chemical oxidation of uric acid and other purines [Subramanian, et al., 1987; Griffiths, 1952]. In agreement with the $1e^-$ oxidation and radical dimerization during ESI, formation of covalent dimers has been reported in ESI MS of dopamine (E^o = -0.12 V vs SHE), caffeic acid (E^o = 0.20 V vs SHE) and cysteine (E^o = 0.92 V vs SHE) [Mautjana et al., 2008a; Arakawa et al., 2004]. H/D exchange experiments show that three hydrogents of uric acid (H_2U) are exchangeable (Figure 4-2B) in 40/60 vol%, H_2O/MeOH, 1 mM NH_4Ac. The N_1-proton between C_2=O and C_6=O groups is the least acidic of all protons in the uric acid molecule and might be exchangeable if a completely deuterated solvent 40/60 vol%, D_2O/CD_3OD, 1 mM ND_4(CD3CDOO). The uric acid dimer ($2H_2U$) has five exchangeable protons (Figure 4-2D), in agreement with the structure proposed in Scheme 4-1. See molecular structures in Scheme 4-1 and their H/D exchange mass spectra in Figure 4-2. A hydrogen-bonded dimer (unlikely for purines due to the energetically unfavored 90^o arrangement of the bonded molecules) would have

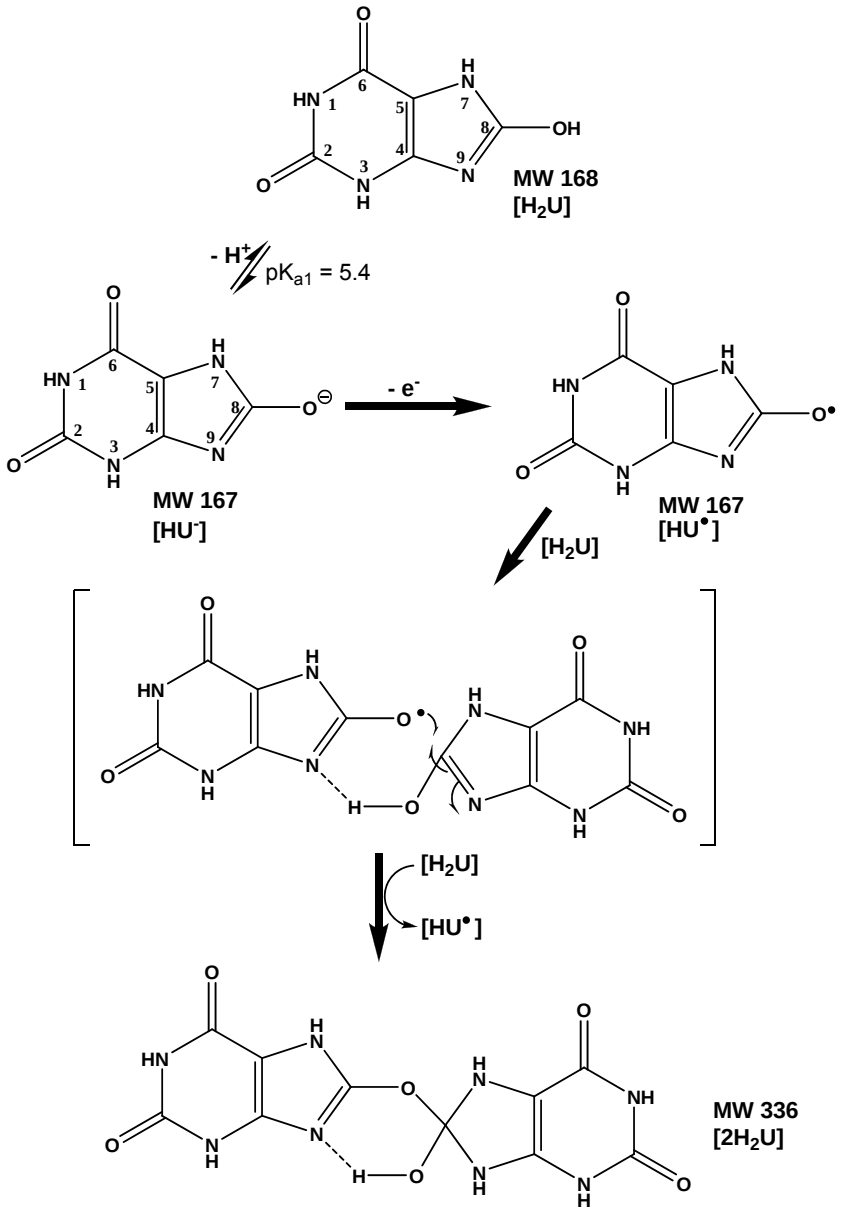

Scheme 4-1. Proposed reactions during ESI of uric acid (H_2U). Urate (HU^-) is present in the pH 6.3 carrier solution of H_2U (pK_{a1}=5.4). Hydrogens that form H-bonds and those between C=O groups are not exchangeable with deuterium in the presence of D_2O (see mass spectra in Figure 4-2). Proton adducts of uric acid $[H_2U+H]^+$ (m/z 169) and uric acid dimer (m/z 337) are detected in this carrier solution in ESI MS. The H^+ is generated during positive ion mode electrospray.

fewer exchangeable protons. Stable H-bonding between purines requires four molecules (Chapter 6). At higher uric acid concentrations, Na^+ and K^+ adducts of uric acid species were detected in addition to H^+ adducts (Figure 4-1B). The formation of adducts of various analytes

with Na^+ and K^+ is commonly observed because of Na^+ and K^+ ions from glass which have been estimated to reach concentrations of ~10^{-5} M [Kebarle, 1997]. The Na^+ and K^+ adducts become more apparent at higer pH values where the proton concentration is relatively small (~10^{-6} M at pH 6.3).

Similar to the dopamine dimer discussed in Chapter 3, MS/MS of the uric acid dimer ion $[2H_2U+H]^+$ (m/z 337) following its dissociation under infrared CO_2 laser irradiaton (~ 0.5s) in an infrared multiple photon dissociation (IRMPD) experiment, shows an ion peak at m/z 169 without complete disappearance of the uric acid dimer peak at m/z 337 (Figure 4-3). This result could be an indication of the relative strength of the covalent bond linking the two uric acid molecules as opposed to H-bonds. The proposed cleavage mechanism of uric acid dimer is shown in Scheme 4-2.

The 40/60 vol%, water/methanol, 10^{-3} M NH_4Ac carrier solution was chosen because it provides the maximum solubility of H_2U with feasible electrospraying conditions. In this carrier solution, the ectrospray current is 100 – 200 nA and the solubility of H_2U is 50 – 150 μM. When the water fraction is lower (<40%) uric acid precipitates; a larger water fraction (≥50%) causes arcing.

To avoid the low sensitivity for uric acid in the 50/50 vol%, water/methanol carrier used for negative ion mode HPLC ESI MS [La Marca, et al., 2006; Ito, et al., 2000; Shi, et al., 2003], 0.1 M KOH was used to dissolve uric acid [Binyamin, et al., 2001], and 0.04 M HAc was added to stabilize the current in 40/60 vol%, water/methanol. The high specific conductivity of the 40/60 vol%, water/methanol, 0.1 M KOH, 0.04 M HAc, carrier solution of ~3.30 mS/cm, compared to ~0.132 mS/cm for 40/60 vol%, water/methanol, 10^{-3} M NH_4Ac, and ~0.103 mS/cm

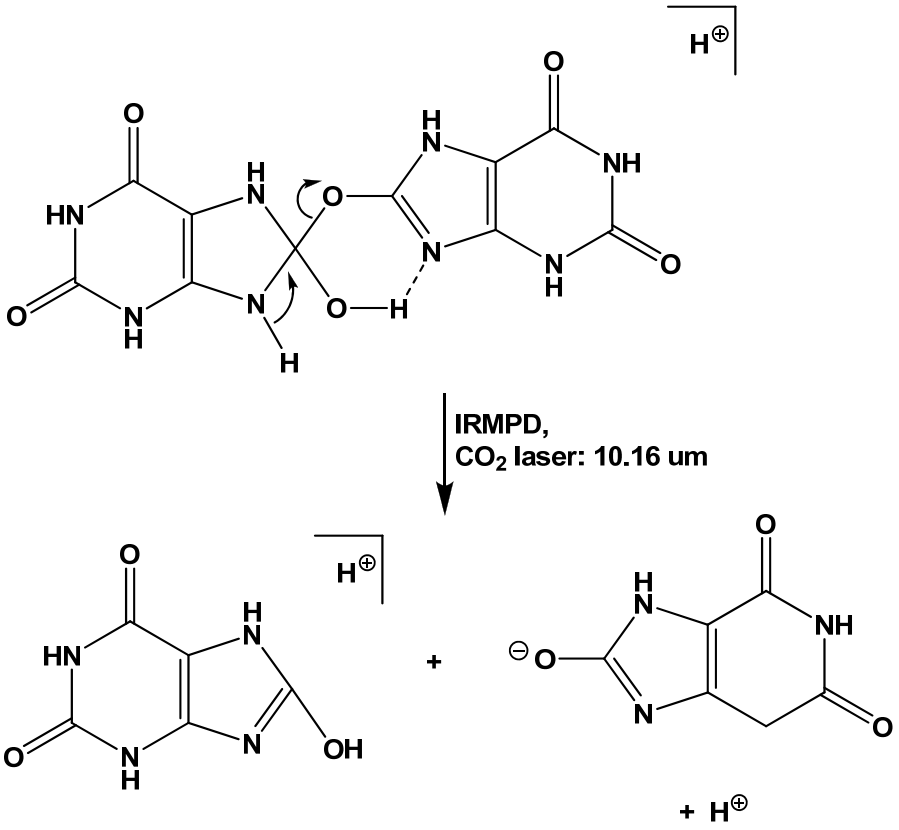

Scheme 4-2. Proposed cleavage mechanism of the uric acid dimer in the infrared multiphoton dissociation (IRMPD) experiment.

for 50/49/1 vol%, water/methanol/acetic acid, can contribute to the high electrospray current that was observed. In the carrier solution with KOH of pH ~12.7, $2e^-$, $2H^+$ oxidation of uric acid (Scheme 4-3) generates allantoin (MW 158; pK_a ~8.96), which was detected as $[K(Allnt)+K]^+$ (Figure 4-1C). A K^+ adduct of unoxidized urate (U^{2-}) (pK_{a1} 5.4; pK_{a2} 9.8) [Simic and Javanovic, 1989] was detected with a standard cylindrical capillary inlet ESI MS, where the electrospray current is lower (not shown). This adduct was not detected under the experimental conditions of Figure 4-1C, however. Allantoin and parabanic acid observed in this work have also been

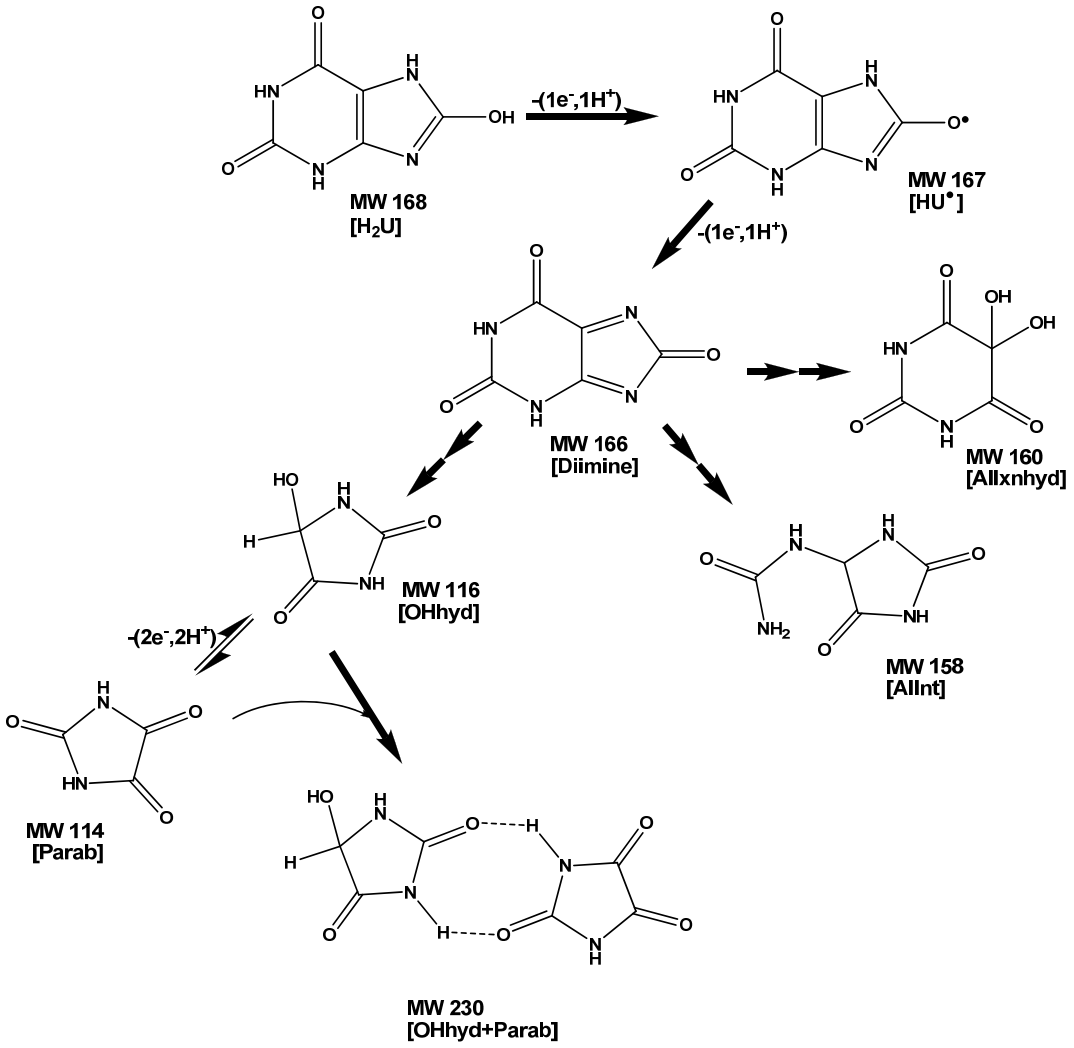

Scheme 4-3. Oxidation pathway of uric acid to 5-hydroxyhydantoin–parabanic acid adduct [OHhyd+Parab], alloxan monohydrate [Allxnhyd], and allantoin [Allant] [Volk et al., 1992; Volk et al., 1999]. Protonated hydroxyhydantoin–parabanic acid adduct (m/z 231) is detected in ESI MS. Allantoin and alloxan monohydrate are detected as K^+ adducts $[K(Allnt)+K]^+$ (m/z 235) and $[K(Allxnhyd)+K]^+$ (m/z 237), respectively.

observed during radiolytic oxidation of uric acid at pH 3.4 and 7.4 using HPLC with UV detection,where significantly more parabanic acid than allantoin was produced at pH 3.4 [Hicks et al., 1993]. Radiolysis produces high concentration of OH radicals at pH 7.4 which can attack allantoin to give parabanic acid, but Hicks et al. observed little change in allantoin concentration at the higher pH. It is possible that the formation of allantoin at the high pH (~12.7) seen in this work is accompanied by the formation of undetectably low amounts of parabanic acid, and that

formation of parabanic acid at pH~6.3 used in this work is accompanied by formation of undetectably low amounts of allantoin, in which case the two studies produce consistent results.

The ions identified in ESI MS of uric acid are summarized in Table 4-1. Assignments are based on the relative intensity of M+2 ions of the K-41 isotope and are in good agreement with theoretical isotope abundances. The $[K(Allxnhyd)+K]^+$ (m/z 237) signal overlaps with the M+2 isotope signal of K-41 of $[K(Allnt)+K]^+$ (m/z 235) and the intensity of the M+2 isotopic cluster $[K(Allnt)+Ac+2K]^+$ (m/z 333) is inflated by the overlapping signal of K^+-alloxan-acetate cluster $[K(Allxnhyd)+Ac+2K]^+$ (m/z 335) (Table 4-1). Alloxan monohydrate (MW 160) is a product of the $2e^-$, $2H^+$ oxidation of uric acid (Scheme 4-2) and was also detected as $[K(Allxnhyd)+K]^+$. A linear relationship with an average correlation (R2) > 0.7 was observed between ln(ion intensity) and ln(uric acid concentration) for $[K(Allnt)+K]^+$ (m/z 235) as well as $[K(Allnt)+Ac+2K]^+$ (m/z 333) (Figure 4-4).

The EC/ESI MS of Uric Acid

In EC/ESI MS, the ion intensities of the proton adducts of uric acid $[H_2U+H]^+$ (m/z 169), uric acid dimer $[2H_2U+H]^+$ (m/z 337) and $[OHhyd+Parab+H]^+$ (m/z 231) adduct are a function of the voltage applied to the on-line low voltage EC cell (Figure 4-5). Thus ion distribution is determined by the efficiency of electrooxidation. At higher applied voltages the dimer signal decreases while the $2e^-$, $2H^+$ oxidation of uric acid increasingly generates parabanic acid (Figure 4-5). Since purine dimers can be oxidized at high positive potentials [Subramanian et al., 1987], oxidation of the dimer may contribute to the increase in the parabanic acid signal at higher applied voltages. The intensities of Na^+ and K^+ adducts of uric acid species follow those of H^+ adducts (not shown).

A general stepwise $1e^-$, $1H^+$ oxidation pathway [Hicks et al., 1993] can account for the ionization of urate, forming neutral radicals [$HU^{\bullet}$], which rapidly dimerize to the $[HU^{\bullet}+H_2U+H]^+$ radical and then to the $[2H_2U+H]^+$ (m/z 337) dimer. Scheme 4-4A summarizes this pathway. The pathway may involve H-atom transfer (Scheme 4-4B) [Siegbahn et al., 1997].

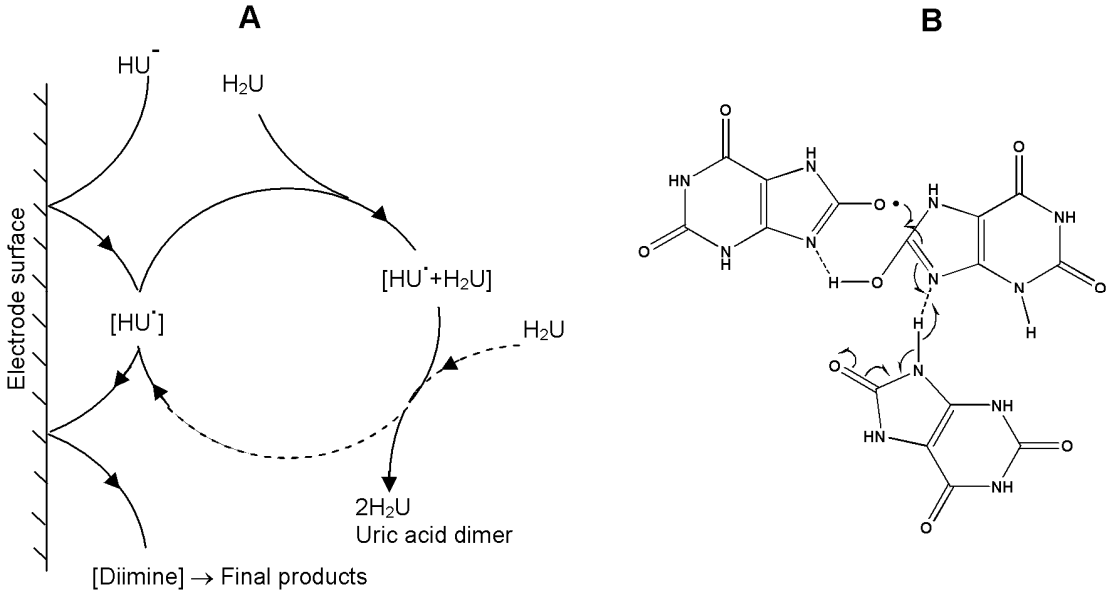

Scheme 4-4. Proposed dimer formation pathway (A) during ESI of uric acid (H_2U). HU^- is present in pH 6.3 carrier solution of H_2U (pK_{a1}=5.4). Protonated uric acid $[H_2U+H]^+$ (m/z 169) and the protonated dimer (m/z 337) are detected in ESI MS. The H^+ is generated during positive ion mode electrospray. (B) H-atom transfer leading to the uric acid dimer and the neutral radical, which further gives diimine and final oxidation products.

The ESI MS of Uric Acid in Urine

In 1000-fold diluted normal urine (pH 5.3 – 8.0) the concentration of uric acid is 2–7 μM [Yue-Dong, 1998; Kupeli, et al., 2005]. Direct ESI MS analysis of a more concentrated urine sample leads to irreproducible mass spectra. In 1000-fold diluted urine, the concentration of uric acid is lower than that of the solutions of standards that were tested (~20 μM). Nevertheless a K^+ adduct of Na^+ urate $[NaHU+K]^+$ (m/z 229) was detected in 40/60 vol%, water/methanol, 1 mM

NH4Ac, pH ~6.3 carrier solution (Figure 4-6A). In 1000-fold diluted urine spiked with 20 μM uric acid, protonated uric acid $[H2U+H]^+$ (m/z 169) was detected together with $[NaHU+K]^+$ (Figure 4-6B). Na^+ and K^+ found in urine may form the urate complexes (NaHU, pKsp ~ 4.6 at 25oC) [Wang and Konigsberger, 1998] and $[NaHU+K]^+$ that were detected.

Conclusions

In the positive ion conical capillary inlet ESI MS of uric acid, ion signals of the protonated uric acid dimer and two-electron oxidation products of uric acid, parabanic acid, hydantoin, allantoin and alloxan monohydrate were detected. The results thus indicate that negatively charged urate ions are oxidized during positive ion mode ESI to neutral uric acid radicals, which form the uric acid dimer. The dimer and the unoxidized uric acid are detected, which improves the sensitivity in ESI MS of uric acid. H/D exchange experiments indicate a covalent structure of the uric acid dimer. ESI of uric acid may involve stepwise $1e^-$, $1H^+$ oxidation and dimerization pathway similar to those for dopamine [Mautjana et al., 2008a] and caffeic acid [Arakawa et al., 2004]. Thus ESI MS can provide insight into the 1e--oxidation reactions of biological interest, especially to individuals studying the antioxidant properties of easily oxidized biological analytes, such as uric acid. The results additionally show that concentration and composition of the carrier solution determine ion distribution and ESI MS signal intensity of uric acid ions. In EC/ESI MS with an on-line EC cell voltage floated on the HV of the ES, the $2e^-$, $2H^+$ oxidation of uric acid is more efficient than in ESI MS, and the intensity of the 1e- oxidation product, the protonated dimer, decreases. The high sensitivity of the conical capillary inlet ESI MS allows measurements of uric acid. In 1000-fold diluted normal human urine 2–7 μM uric acid was detected as a Na^+ urate complex with K^+.

Table 4-1. Theoretical and average measured m/z values of identified ions and their isotopic abundances (n = 15).

	Theoretical				Measured			
	m/z		Isotopic abundance(%)		m/z		Isotopic abundance(%)	
Ion Identity	M	M+1	(M+1)/M	(M+2)/M	M	M+1	(M+1)/M	(M+2)/M
[a][H_2U+H]$^+$	169.04	170.04	7.20	-	169.04	170.04	5.44	-
[a][H_2U+Na]$^+$	191.02	192.02	7.19	-	191.02	192.03	5.39	-
[a][$2H_2U$+H]$^+$	337.06	338.07	14.39	-	337.07	338.08	11.73	-
[a][$2H_2U$+Na]$^+$	359.05	360.05	14.46	-	359.05	360.05	10.28	-
[a][OHhyd+parab+H]$^+$	231.04	232.04	8.46	1.51	231.08	232.08	7.09	1.19
[a][OHhyd+parab+Na]$^+$	253.02	254.02	8.45	1.51	253.06	251.06	6.55	n/d
[b][K_2U+K]$^+$	282.90	283.90	7.13	22.47	282.91	283.91	5.22	22.35
[b][K(Allnt)+K]$^+$	234.96	235.96	6.08	15.19	234.92	235.92	3.40	18.28[c]
[b][K(Allxnhyd)+K]$^+$	236.93	237.93	5.37	15.44	236.94	237.94	*d*	*d*
[b][K(Allnt)+Ac+2K]$^+$	332.94	333.94	8.44	22.96	332.90	333.90	7.61	33.45[c]
[b][KAllxnhyd+Ac+K]$^+$	334.91	335.91	7.68	23.24	334.92	335.92	*d*	*d*

[a]Carrier solution: 40/60 vol%,, H_2O/CH_3OH containing 0.001 M NH_4CH_3COO, pH~6.3.

[b]Carrier solution: 40/60 vol%,, H_2O/CH_3OH containing 0.10 M KOH and 0.044 M CH_3COOH, pH~12.7.

[c]Uncharacteristically high abundances due to spectral overlap of M+2 peaks with those of ions of equivalent m/z values, [K(Allxnhyd)+K]$^+$ (m/z 236.93) and [K(Allxnhyd)+Ac +K]$^+$ (m/z 334.91), respectively.

[d]Values were omitted because these peaks were observed with poor S/N ratio in some mass spectra.

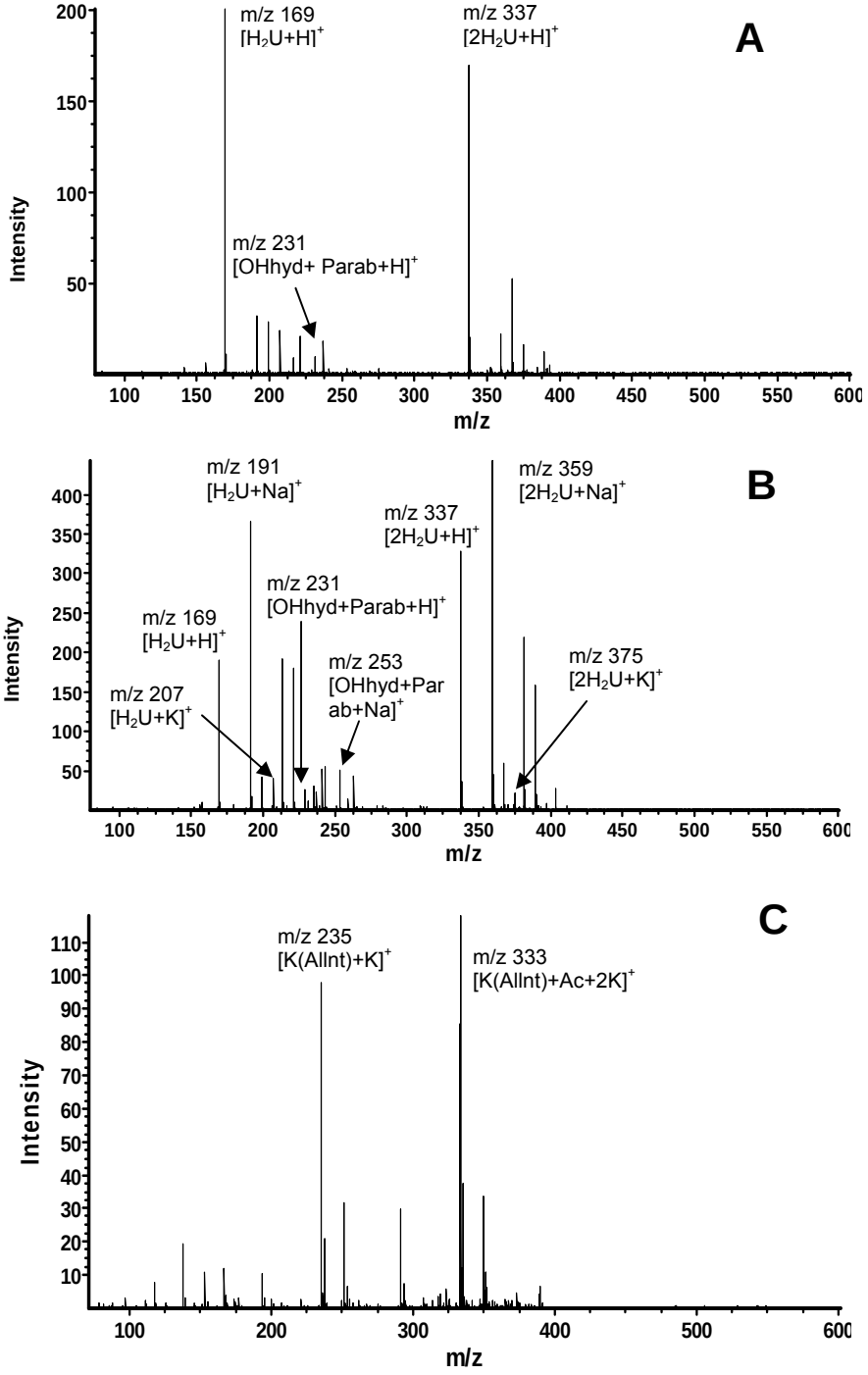

Figure 4-1. Positive ion mass spectra of uric acid. Cone-shaped capillary inlet; 40/60 vol%, water/ methanol, 0.001M ammonium acetate, pH~6.3* ; flow rate 40µL/h; HV 3kV.

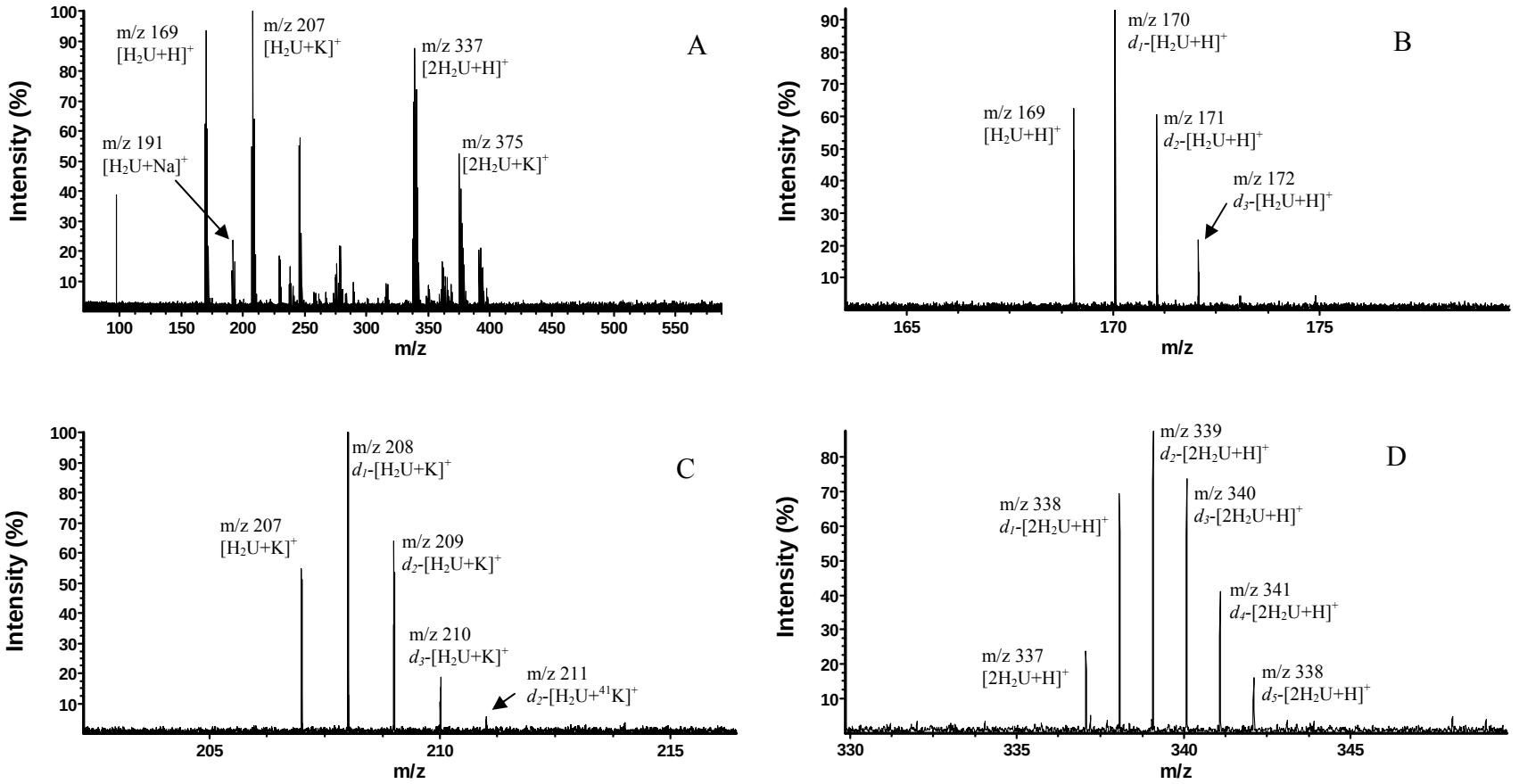

Figure 4-2. The ESI mass spectrum of uric acid (50 μM) in 40/60 vol%, D_2O/MeOH, 1mM NH_4Ac (A). Peaks representing the number of exchangeable protons for the ions $[H_2U+H]^+$, $[H_2U+K]^+$ and $[2H_2U+H]^+$ are shown in (B), (C) and (D), respectively. See structures in Scheme 4-1.

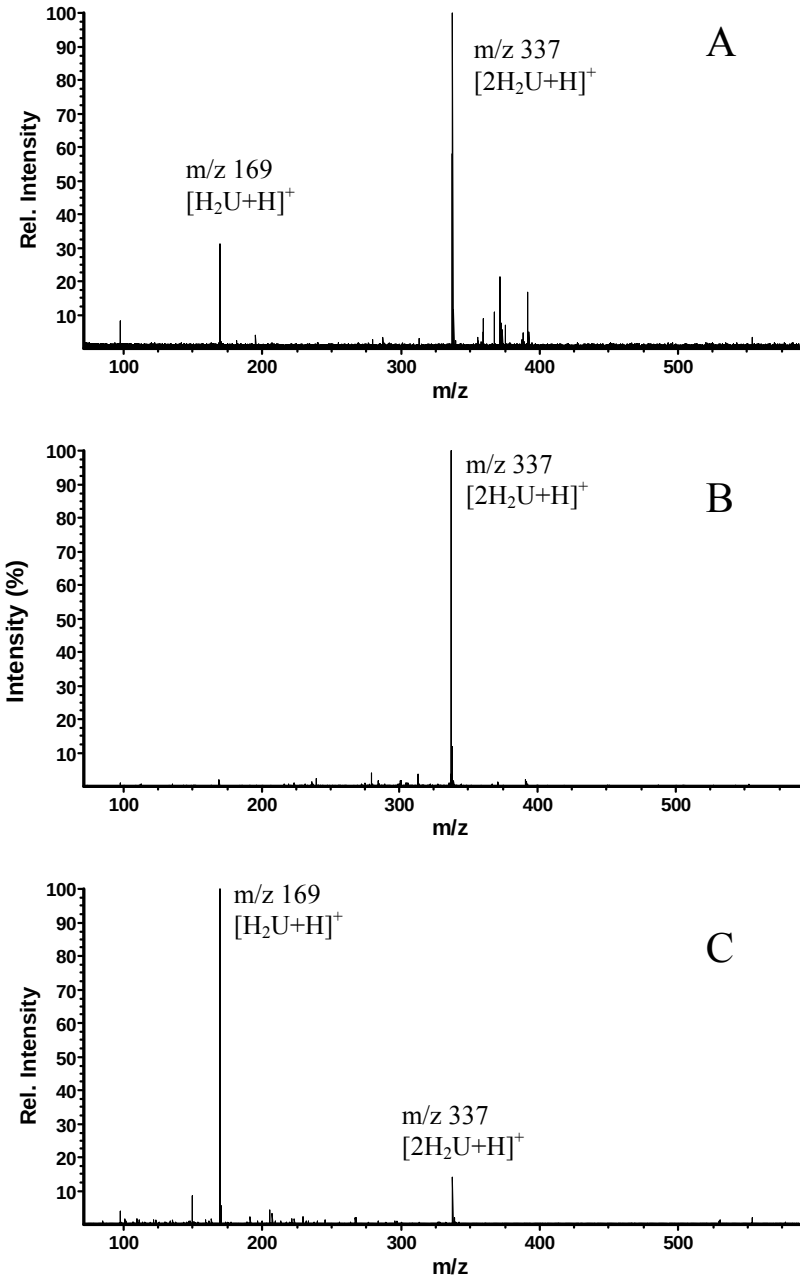

Figure 4-3. The ESI MS of 50 μM uric acid (A); ESI MS after ejection of m/z < 337 and m/z > 337 ions i.e isolation of uric acid dimer $[2H_2U+H]^+$ (m/z 337) ion (B); MS/MS of $[2H_2U+H]^+$ (m/z 337) following CO_2 laser irradiation (>0.5s) - Notice the product peak at m/z 169, likely due to $[H_2U+H]^+$ ion and smaller unassigned product peaks at m/z values <300 (C).

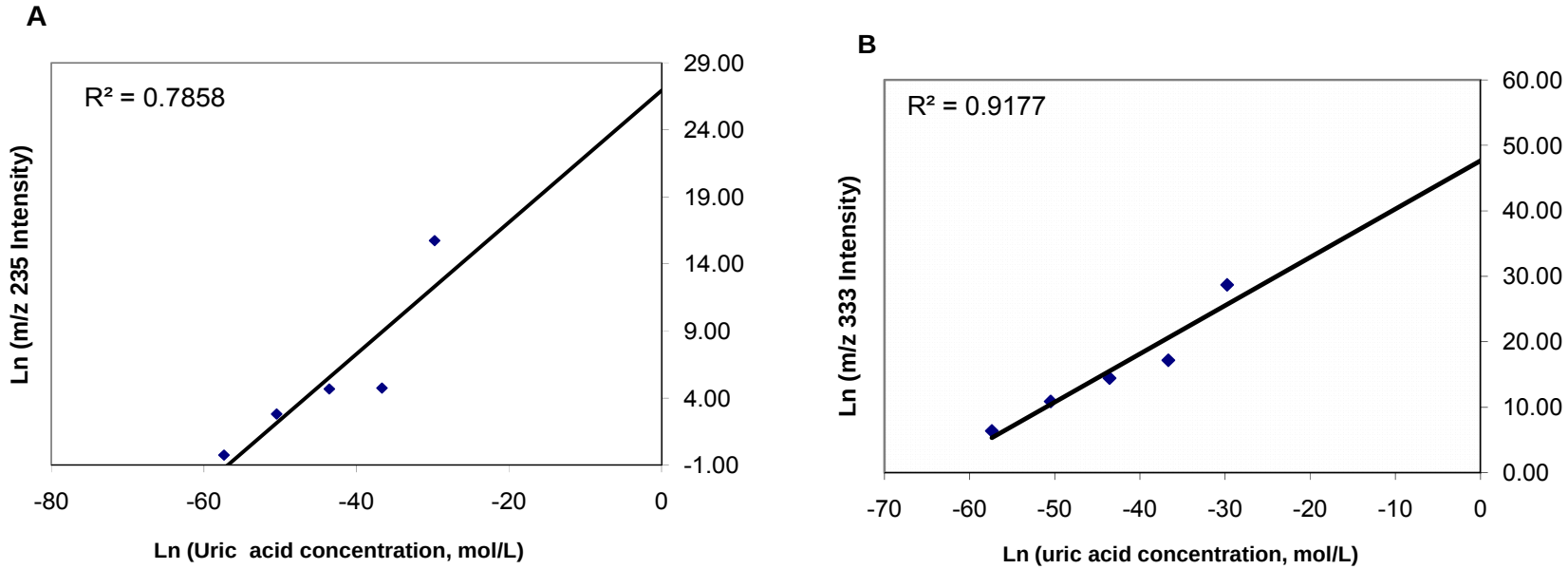

Figure 4-4. The ln (Intensity) vs ln (concentration, mol/L) plots for the ions $[K(Allnt)+K]^+$ (m/z 235) (A) and $[K(Allnt)+Ac+2K]^+$ (m/z 333) (B).

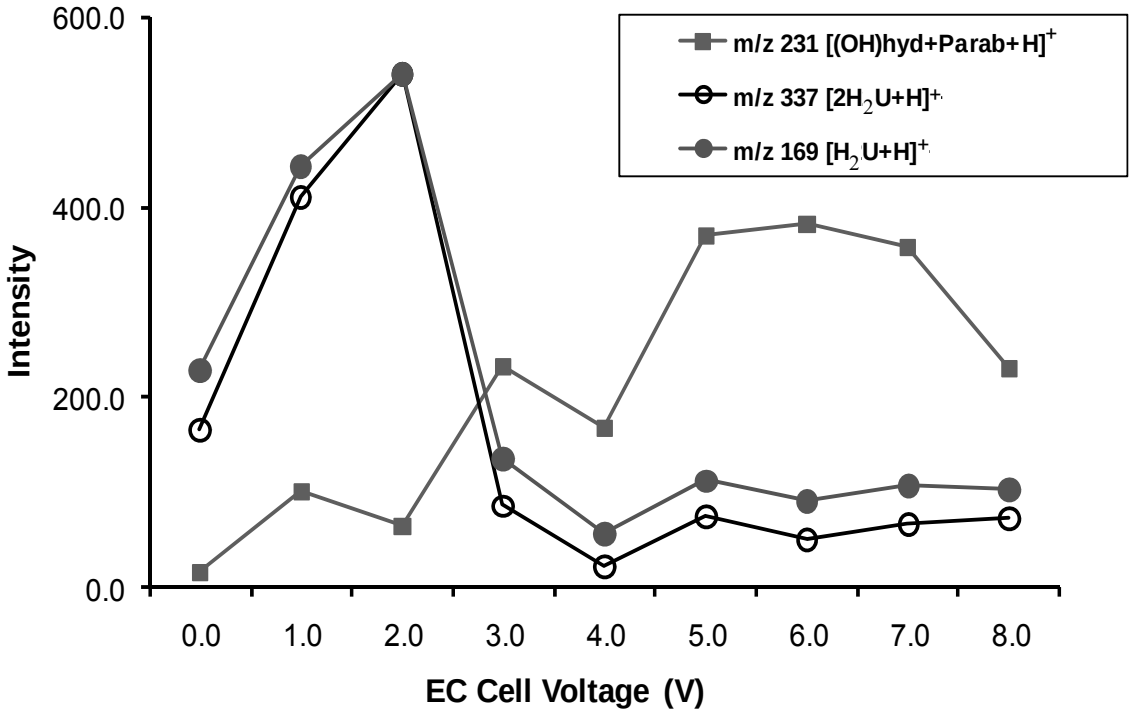

Figure 4-5. Intensity of uric acid (50 μM) ions in EC/ESI MS as a function of on-line EC cell voltage. Cone-shaped inlet; 40/60 vol%, H2O/MeOH, 10-3 M NH4Ac, pH 6.3; Flow rate 40 μL/h; HV 3 kV.

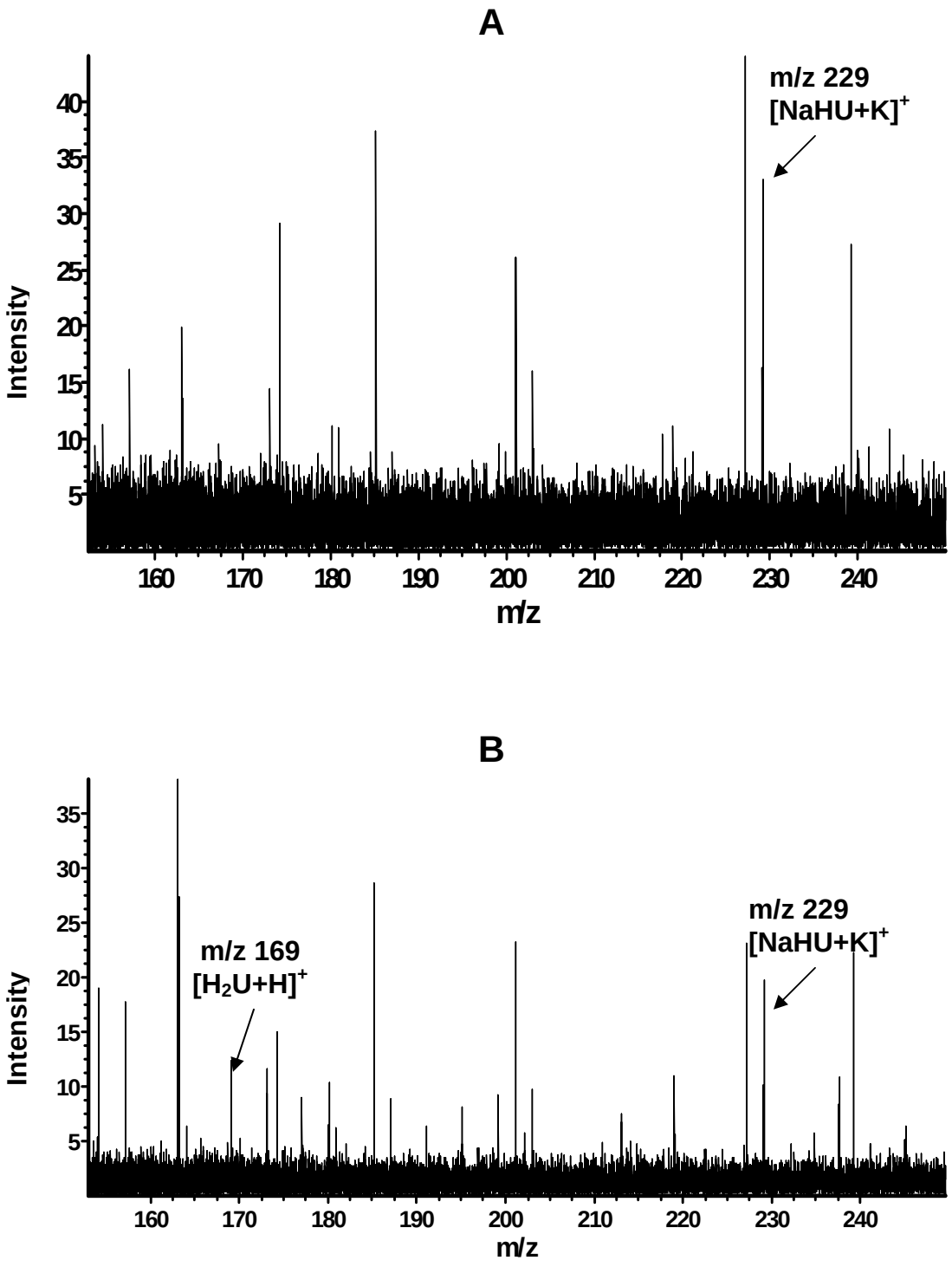

Figure 4-6. Positive ion mode ESI MS mass spectra of human urine: A) 1000 fold diluted; B) 1000 fold diluted and spiked with 20 μM uric acid. Same conditions as in Figure 4-1.

CHAPTER 5
SENSITIVITY OF POSITIVE MODE ESI AND EC/ESI MS TO THE ANALYSIS OF THIOL METABOLITES

Introduction

Disease biomarker and biological pathway discovery has led to the analysis of thiol metabolites, glutathione (GSH), cysteine (CySH) and homocysteine (hCySH) which are involved in many important physiological processes [Rahman et al., 2005]. GSH and CysH are found at millimolar concentrations in different types of cells and in blood plasma. They function as endogenous antioxidants, which protect cells against reactive oxygen species (ROS) and reactive electrophiles, and which serve to restore vital proteins to their reduced form [Forman and Dickinson, 2003]. Changes in concentrations of GSH and CysH from normal (1 – 10 mM) correlate with numerous disease conditions. For example, depletion of GSH has been reported to occur in type II diabetes [Samiec et al., 1998] and HIV [Staal et al., 1992], while elevated levels of CysH have been reported in cases of Parkinson's and Alzheimer's diseases [Shen and Dryhurst, 2001]. Elevated concentrations of hCysH, which is an intermediate in the metabolism of methionine to CysH [Nekrassova et al., 2003; Himmelfarb et al., 2002], a precursor for GSH, have been found to correlate with cardiovascular diseases such as atherosclerosis and venous thrombosis [Demuth et al., 2002; Van den Brandhof et al., 2001]. Despite this correlation of high hCySH concentrations and cardiovascular disease, the role of hCySH in the mechanism of vascular injury is unknown and could involve GSH and CysH, which share a common biosynthetic pathway with hCySH [Himmelfarb et al., 2002]. Simultaneous analysis of thiols in biological samples is important for clinical applications, as well as for understanding their roles in physiology and pathology. Since they require enzymatic catalysis to undergo oxidation reactions with H_2O_2 within the cells [Gilbert, 1995; Meister, 1983] thereby producing disulfides, it is evident that thiol metabolites are stable in vivo in their reduced form, which is consistent

with their relatively high oxidation potentials ($E^o \approx 0.92$ V vs SHE). In view of this, the GSH/GSSG concentration ratio has been proposed as an efficient measure of oxidative stress [Curello et al., 1987; Schafer and Buettner, 2001; Kemp et al., 2008].

Similarities in chemical structures, reactivity and properties between homocysteine, cysteine and glutathione (see Scheme 5-1 below) make their simultaneous analysis difficult by most analytical methods.

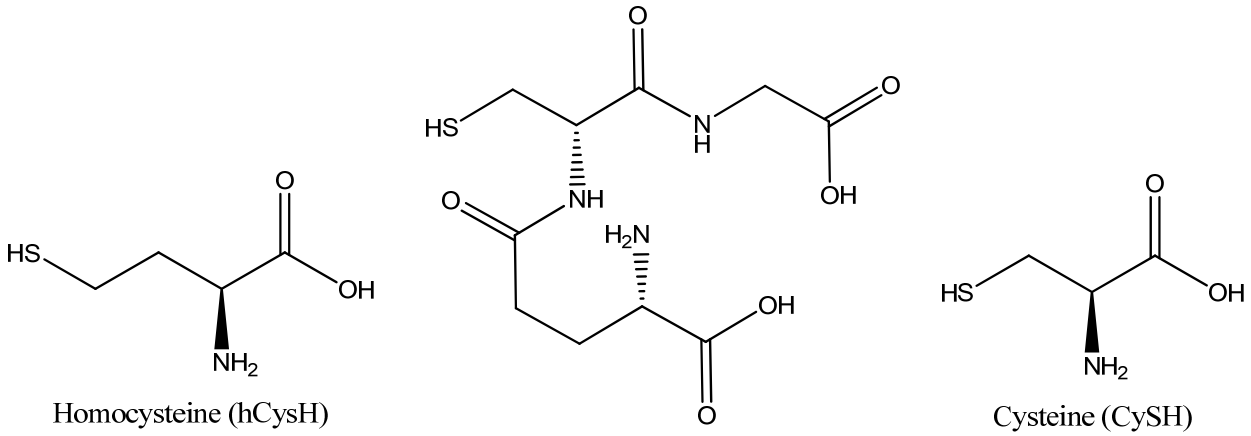

Scheme 5-1. Structures and pK_a values of thiol metabolites [Nekrassova et al., 2003; Budavari et al., 1989].

High performance liquid chromatography (HPLC) is often used for thiol separations [Garcia et al., 2008; Giustrarini et al., 2008; Nolin et al., 2007; Bald, 2004; Yoshida, 1996; Winters et al., 1995] with electrochemical detection, or with UV and fluorescence detection after derivatization because thiols are poor chromophores. Various derivatizing agents and off- and on-line derivatization methods are being evaluated in an ongoing effort to optimize derivative yields for quantitative spectrophotometric detection of thiols. However, derivatization and LC tend to be time consuming. Compton's group reported a method which involved tagging of thiols

with electrochemically generated quinoids to facilitate their quantitative determination by cyclic voltammetry [White et al., 2001a; White et al., 2001b]. However, the temporal resolution based on varying diffusion coefficients, rates of oxidation reactions ($k_{(CySH/CyS^{\cdot})} = 1.2 \times 10^3\ M^{-1}\ s^{-1}$) [Uchiyama and Sekioka, 2005] and thiol addition to the quinoid, which is associated with electrochemical (EC) methods and which could result in short analysis time, is not realized in thiol analysis. It has been observed that large overpotentials are required for the oxidation of thiols, often resulting in poorly defined and overlapping thiol or thiol adduct oxidation/reduction peaks [White et al., 2002; Zhou et al., 2007].

Furthermore, electrode materials, mostly metals, may catalyze thiol oxidation and may produce varying oxidation peak potentials for each thiol compound [White et al., 2002, Sahlin et al., 2002]. Thus measured peak potentials are seldom close to oxidation potentials calculated from thermodynamic data, such as 0.92 V vs SHE for CySH and for GSH reported by Buettner and Jerkiewicz [Buettner and Jerkiewicz, 1996]. McCarley and co-workers [Pacsial-Ong et al., 2006] used catechol-analogues (Flurone black, 1-methyl-1,2,3,4-tetrhydro-6,7-isoquionolinediol hydrobromide and 3,5-di-tert-butyl catechol) to form monothiol derivatives with GSH, CysH and hCysH, respectively. The monothiols were found to be oxidized further at different potentials to form bisthiols, allowing discrimination between GSH, CysH and hCysH. LC/EC methods with mercury electrodes allow accumulation of thiols at the surface at positive potential. The thiols are released upon reduction, thereby providing high sensitivity, but these methods are not practical because of toxicity of mercury.

Complex mediators and derivatives of hexacyanometallates and metallophthalocyanines, which catalytically oxidize thiols and are subsequently reoxidized at the electrode surface, have been used in electrochemical thiol detection [Liu et al., 2004], and their development is ongoing.

Electrospray ionization mass spectrometry (ESI MS) coupled with separation techniques is attractive for thiol analysis. Yet few reports of thiol analysis by ESI MS are found [Rubino et al., 2004; Bouligand et al., 2006; Gucek et al., 2002]. The advantage of HPLC/ESI MS in thiol analysis is selective, mass-based detection. However, long analysis time may be a limitation. With direct injection ESI MS, thiols can be resolved based on exact mass, and analysis time can be significantly reduced. However, standard calibration and quantitation with direct injection ESI MS is more challenging than with LC/MS, which allows better ion counting statistics when the mass spectrometer is focused on a single m/z value corresponding to the eluting compound [Watson, 1997]. Direct injection MS is limited to comprehensive data collection where the detection time is shared by all ions, thus producing ion count variations and S/N ratio that is less than that achieved with selected ion monitoring. But more significant are the processes undergone by analyte molecules during analysis.

Understanding the processes governing ionization of analyte molecules during electrospray and ion transmission could be useful for improving quantitatitation accuracy. Gucek et al. [2002] attempted the determination of GSH in extracts of needles of a spruce plant by positive mode ESI MS using standard addition method with limited success, at which they proposed to use an isotopically (^{15}N) labeled GSH as an internal standard. Gucek et al. attributed the difficulties in determing GSH content to the different GSH species formed even under controlled (dark, low temperature storage) conditions. However, Gucek et al. observed no change in LC/MS peak area for samples stored at 4^{o}C and considerably little amounts of decomposition products when GSH solutions were left standing in the light at 25^{o}C, when they examined the stability of GSH in aqueous solutions [Gucek et al., 2002]. The GSH species observed by Gucek et al. could be

attributed to the oxidation products of GSH formed during ESI, which the present work demonstrates.

Electrochemical processes which are inherent to electrospray ionization [Van Berkel and Kertesz, 2007; Van Berkel et al., 2000] can cause oxidation of thiols to disulfides, and poor ion collection efficiency can affect detection sensitivity. In Chapters 3 and 4 we demonstrated that metabolites with low oxidation potentials such as dopamine (E^o = -0.12 V vs SHE) and uric acid (E^o = 0.59 V vs SHE) can undergo oxidation during positive mode ESI MS. We also demonstrated that electrospray ions can be efficiently collected using a cone-shaped MS inlet [Mautjana et al., 2008a,b]. Similarly, thiols could undergo oxidation during positive mode ESI MS even though they have relatively higher E^o values (≈ 0.92V vs SHE for CySH or GSH) [Buettner and Jerkiewicz, 1996] and could form disulfide dimers. Oxidation and fragmentation, found in the present work to be the two major processes leading to the formation of different ions of thiols during positive mode ESI MS, were elucidated. This was achieved through on-line electrochemistry ESI MS which can enhance ion formation and increase sensitivity.

Sensitivity of reduced thiols was also increased by adding dopamine, which may undergo $1e^-$, $1H^+$ electrochemical oxidation and may be further oxidized chemically to DAQ by thiol radicals as proposed [Mautjana et al., 2008a]. In turn, thiol radicals can be reduced to thiols and form a thiol/DAQ adduct through nucleophilic addition. This chapter presents the ESI MS spectra of GSH, CySH and hCySH obtained under high sensitivity conditions brought about by the use of cone-shaped metal capillary inlet and on-line electrochemistry. The formation of different ions due to electrochemical processes of the ES ion source is discussed, and the application of ESI MS for thiol mixture analysis is described.

Results and Discussion

The ESI MS of glutathione (GSH), cysteine (CySH) and homocysteine (hCySH)

ESI mass spectra of GSH, CySH and hCySH in 40/60 vol% H_2O/MeOH, 1 mM NH_4c, pH 6.3 with which relatively high detection sensitivity for all three thiols was obtained, are shown in Figure 5-1. GSH (Figure 5-1A) produces ions of m/z 308, 330 and 346, which have been assigned to proton, sodium and potassium adducts of GSH, respectively. Other ion peaks at m/z 613 and 615 (Figure 5-1A *insert*) are assigned to proton adducts of the covalently bound (radical-radical) dimer [GSSG] and the hydrogen bound dimer [2GSH]. The structure of GSSG is shown in Scheme 5-2.

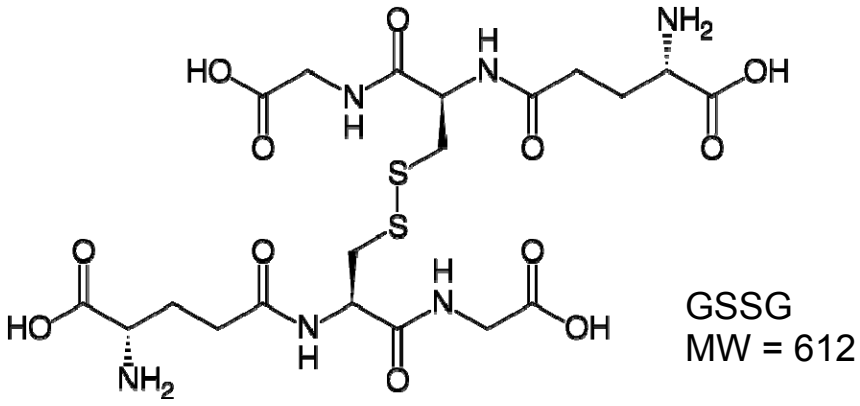

Scheme 5-2. Glutathione disulfide dimer detected as $[GSSG+H]^+$ (m/z 613) in ESI MS

The peak at m/z 154 (Figure 5-1A) is assigned to the proton adduct of an oxygen-centered glutathione cation radical $[GSH^{\bullet}+H]^{2+}$, which is proposed to form by one-electron oxidation of the zwitterion form of GSH (Scheme 5-3). Although it is formed with a +1 charge and m/z of 307 (Scheme 5-3), the oxygen-centered glutathione radical was detected as a doubly-charged proton adduct $[GSH^{\bullet}+H]^{2+}$ (m/z 154). The formation of the oxygen-centered glutathione cation radical (MW 307) is supported by H/D exchange data which indicate that this GSH radical (m/z 154) has five exchangeable hydrogens (Figure 5-2), implying an intramolecular H-bonding of the

sulfhydryl hydrogen (Scheme 5-3). In addition to H/D exchange, the structure of the oxygen centered radical $[GSH^{\cdot}+H]^{2+}$ (m/z 154) is supported by its relative isotope distribution.

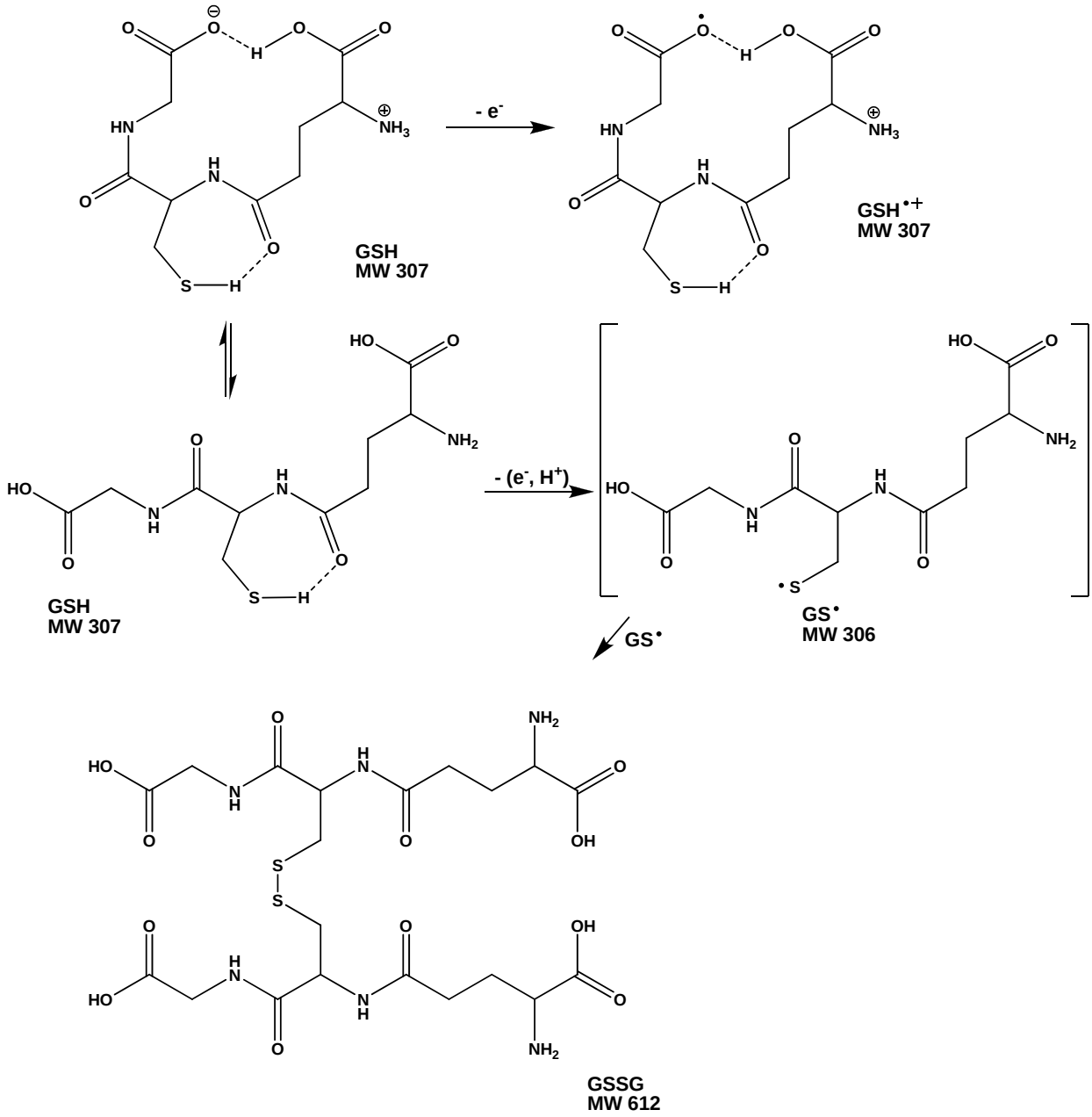

Scheme 5-3. Proposed oxidation of GSH during positive mode ESI MS. Hydrogens that form H-bonds are not exchangeable with deuterium in the presence of D_2O (see the mass spectrum in Figure 5-2).

The detection of a disulfide dimer, assigned as $[GSSG+H]^{+}$ (m/z 613), suggests oxidation of the thiol group in a non-zwitterionic form of the thiol by a loss of one electron and one proton,

despite intramolecular H-bonding of the sulfhydryl hydrogen. The intermediate thiol radicals ($GS^{\cdot}$) couple rapidly to form the dimer (Scheme 5-3).

ESI MS of cysteine (CySH) produces peaks at m/z 122 and 241 which have been assigned to the proton adduct $[CySH+H]^+$ and the disulfide dimer $[CySSCy+H]^+$ as in Figure 5-1B. In the 40/60 vol% H_2O/MeOH, 1 mM NH_4Ac, pH 6.3 carrier solution, the small ion peak at m/z 243, assigned to the proton adduct of a hydrogen bound dimer $[2CySH+H]^+$, which was not detected when 50/49/1 vol% H_2O/MeOH/HAc was used (Chapter 3), is detected. This is attributed to a different tuning of the instrument parameters to optimize thiol detection, whereas in Chapter 3, parameters were tuned for DA detection. A different mobile phase may also cause this increase in sensitivity to $[2CySH+H]^+$ m/z 243 ion. This assignment is supported by the observed isotopic distribution. Homocysteine (hCySH; Figure 5-1C), produces ion peaks that have been assigned to the proton adduct $[hCySH+H]^+$ (m/z 136) and the proton adduct of its disulfide dimer $[hCSSCh+H]^+$ (m/z 269). All solutions were freshly prepared and kept at ~4^oC until their injection, and all oxidation products observed are electrochemically generated.

The ESI MS detection sensitivity for GSH is high relative to that for CySH and hCySH, possibly because in a protein-like folded state GSH is more hydrophobic and forms gas phase ions more easily than CySH and hCySH. That CySH is detected with higher sensitivity than hCySH could be due to the ability of CySH to form an intramolecular H-bond between the sylfhydryl hydrogen and the carbonyl oxygen rendering CySH less polar (or more hydrophobic) than hCySH. Intramolecular H-bonding is difficult within the hCySH structure.

Effect of GSH Concentration on ESI MS

With dilution of 50 μM GSH solution, all the proton adducts including $[GSH+H]^+$ (m/z 308) and $[GSSG+H]^+$ (m/z 613) decrease in intensity. Similar to previous observations made during uric acid analysis in 40/60 vol%, H_2O/MeOH carrier solution containing 10^{-3} M NH_4Ac,

pH ~6.3 (Chapter 4) [Mautjana et al., 2008b], sodium and potassium adducts $[GSH+Na]^+/[GSH+K]^+$ (m/z 330/ m/z 346) and $[GSSG+Na]^+$ (m/z 635) have higher intensities than the proton adducts in large (up to 20 fold) dilutions with the same carrier solution; and $[GSH+Na]^+$ (m/z 330) becomes the base peak (Figure 5-3). This is so because at pH ~6.3 the H^+ concentration (~10^{-6} M) is less than that of Na^+ and K^+ estimated to be 10^{-5} M [Kebarle, 1997] and the [thiol][proton] ion product is simply low. The other prominent peak observed at m/z 372 is assigned to the ammonium adduct of the glutamate-less glutathione disulfide $[(GSSG-2Pyr)+NH_4]^+$. The lowest GSH concentration detected with 40/60 vol% H_2O/MeOH, 10^{-3} M NH_4Ac, pH 6.3 carrier solution, is 2 μM which is ten times lower than the lowest detected concentration of dopamine (20 μM) with 50/49/1 vol% H_2O/MeOH/HAc, pH 4.2 carrier solution (Chapter 3). The difference in sensitivity could be attributed to relative hydrophilicity of DA (which exists as a cation in solution) or relative hyrophobicity of GSH; and relative volatility of MeOH promotes the transfer of GSH to the gas phase. GSH, CySH and hCySH were generally detected with better sensitivity in 40/60 vol% H_2O/MeOH, 10^{-3} M NH_4Ac, pH 6.3 than in the 50/49/1 vol% H_2O/MeOH/HAc, pH 4.2 carrier solution.

Being a tripeptide, GSH can be folded, like proteins, thus becoming hydrophobic [Forman and Dickinson, 2003] given that the $[GSH+H]^+$ ion signal remains strong during ESI MS (Figure 5-4), and that relatively low signals of GSH fragment ions are observed. The little GSH fragmentation that is observed, could occur during transition to the gas phase in the inlet, in the same manner as described previously for dopamine [Mautjana et al., 2008a]. GSH fragmentation seen at high concentrations (≥ 0.5 mM) (Figure 5-4) occurs through the loss of the amino acid glutamate as pyroglutamic acid (Pyr; MW = 129) as well as loss of glycine (Gly; MW = 75)

(Scheme 5-4) to produce cysteinyl glycine and cysteinyl glutamate which are observed as $[(GSH\text{-}Pyr)+H]^+$ (m/z 179) and $[(GSH\text{-}Gly)+H]^+$ (m/z 233), respectively (Figure 5-4).

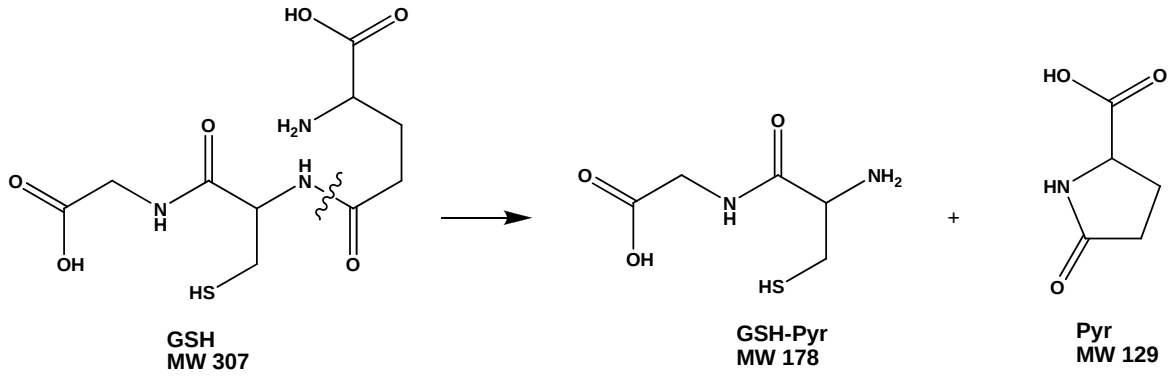

Scheme 5-4. Fragmentation of GSH during ESI MS [adapted from Rubino et al., 2006].

In contrast, glutathione disulfide appears to fragment relatively easily through the loss of glycine and glutamate leading to fragment ions of various m/z values given its relatively large size. The loss of (2Pyr) from GSSG (Scheme 5-5) produces $[(GSSG\text{-}2Pyr)+H]^+$ (m/z 355) at high concentration (Figure 5-4) or $[(GSSG\text{-}2Pyr)+NH_4]^+$ (m/z 372) at low concentration (Figure 5-3).

The ESI MS of GSH, CySH and hCySH Mixture

A mass spectrum of a mixture of thiols is shown in Figure 5-5. Ions observed in Figure 5-5 are those of the disulfide dimers, $[CySSCy+H]^+$ (m/z 241) and $[hCySSCyh+H]^+$ (m/z 269), proton adducts of glutathione $[GSH+H]^+$ (m/z 308), and interestingly, a mixed disulfide $[hCySSCy+H]^+$ (m/z 255) formed by hCySH and CySH, which may suggest a kinetically facile reaction between $hCyS^{\cdot}$ and $CyS^{\cdot}$ radicals. The formation of a mixed disulfide $[hCySSCy+H]^+$ (m/z 255) was significantly inhibited by the addition of dopamine (Table 5-1). However, more work is necessary to investigate ways to exploit or prevent its formation for analytical purposes.

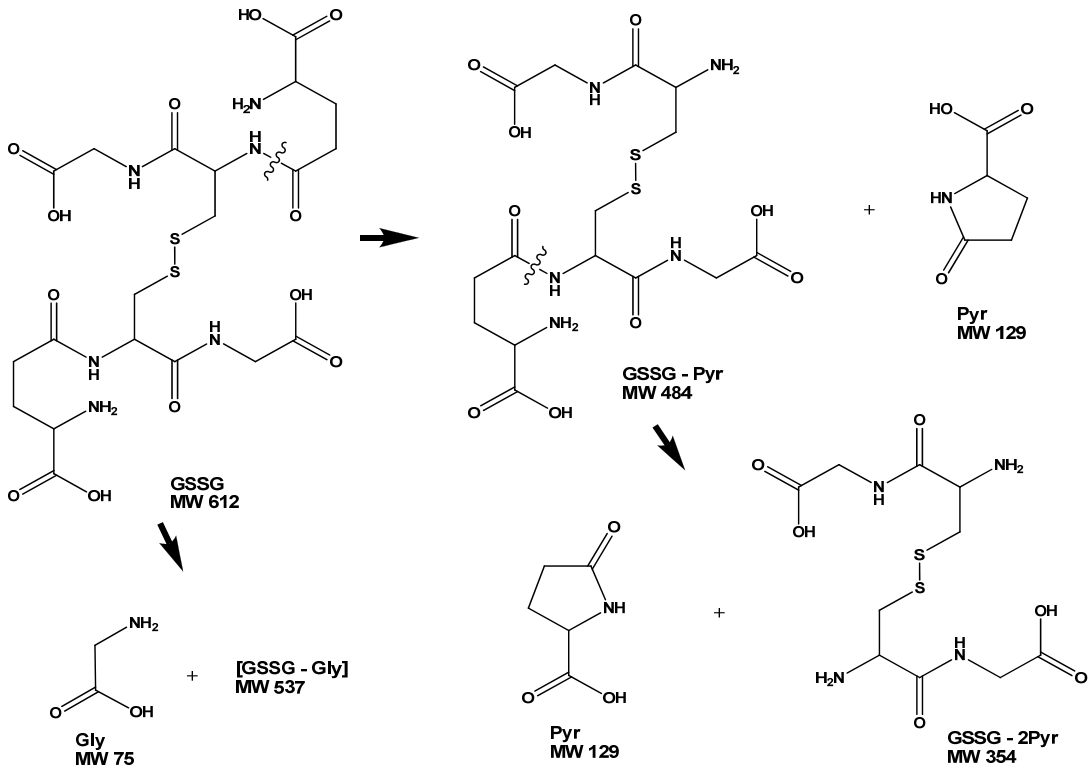

Scheme 5-5. The GSSG fragmentations observed during ESI MS [Adapted from Rubino et al., 2006].

The EC/ESI MS of GSH

Changes in signal intensities of GSH-derived ions, which occur with increase in applied low EC cell voltage in on-line electrochemistry ESI MS (EC/ESI MS) can be seen in Figure 5-6. The ion of m/z 308 $[GSH+H]^+$ remains the base peak over the tested EC cell voltage range. The formation of oxygen-centered radical $[GSH^{\cdot}+H]^{2+}$ (m/z 154) appears to compete with generation of the dimers, $[GSSG+H]^+$ and $[2GSH+H]^+$, when the low EC cell voltage is applied. The increase in relative intensity of m/z 154 ion at higher applied EC cell voltage (Figure 5-6) suggests that the formation of $[GSH^{\cdot}+H]^{2+}$ is facilitated during on-line EC/ESI MS, which may be so because $[GSH^{\cdot}+H]^{2+}$ ion is produced electrochemically and its ionization by proton adduct formation is promoted by the increase in applied EC cell voltage. Relative ion signal intensities

of $[GSSG+H]^+$ (m/z 613) and $[2GSH+H]^+$ (m/z 615) increase to a maximum, likely due to increased ionization efficiency, and then they decrease gradually as the applied EC cell voltage is increased. The latter, a hydrogen bound dimer - not an electrochemical product - decreases much more sharply compared to $[GSSG+H]^+$ (m/z 613), presumably because GSH is oxidizeable. GSSG appears to undergo oxidation as more peaks at higher m/z values were observed at EC cell voltages >3.5 V (data not shown), indicating GSH/GSSG decomposition accompanied possibly by high mass adducts, trimers, tetramers and so on.

The hydrogen/deuterium (H/D) exchange experiment indicates that the m/z 154 ion has five exchangeable hydrogens, which implies intramolecular H-bonding (of the sulfhydryl hydrogen) as proposed in Scheme 5-3 whereas GSH has six exchangeable hydrogens (Figure 5-2).

The ESI MS of GSH and hCySH in the Presence of Dopamine (DA)

It has been proposed that one-electron oxidation of thiols and of DA, in the presence of each other, which occurs during positive mode ESI MS, leads to chemical oxidation of dopamine by the thiol radical to dopamine quinone (DAQ) [Mautjana et al., 2008a], given the low oxidation potential of DA (E^o = -0.12V vs SHE) relative to the oxidation potential of thiols ($E^o_{(GSH\ or\ CySH)}$ = 0.92V vs SHE) [Buettner and Jerkiewicz, 1996]. It has been proposed in Chapter 3 that oxidation of DA by CySH results in a small increase in the intensity of CySH signal as $[CySH+H]^+$ (m/z 122) in addition to forming a CySH/DAQ adduct. Given the possibility of improving thiol sensitivity by addition of DA, a study of ESI MS and EC/ESI MS of GSH and hCySH in the presence of DA was conducted. Furthermore, the thiol/DAQ reaction has been proposed as part of the toxicity mechanism causing Parkinson's disease [Shen et al., 1996, Shen and Dryhurst, 1996a,b; Whitehead et al., 2001; LaVoie and Hastings, 1999] and EC/ESI MS is used here to determine possible roles of GSH and hCySH in the mechanism.

ESI mass spectra of GSH (0.4 mM) and hCySH (0.5 mM) with DA (2.5mM) are shown in Figure 5-7. A 50/49/1 vol% H_2O/MeOH/HAc, pH 4.2 carrier solution was chosen because it was found to give relatively high sensitivity of DA and thiol/DA adduct ions. ESI mass spectra of CySH/DA in the same carrier solution were discussed in Chapter 3 [Mautjana et al., 2008a]. For both GSH/DA and hCySH/DA solutions, ions observed include previously reported DA derived ions namely, $[DA\text{-}NH_3]^+$ (m/z 137), $[DA]^+$ (m/z 154) and $[2DA\text{-}H]^+$ (m/z 307). In the presence of DA, the GSH derived ions, $[GSH+H]^+$ (m/z 308), $[GSH+Na]^+$ (m/z 330), $[(GSSG\text{-}Gly)+H]^+$ (m/z 538) and $[GSSG+H]^+$ (m/z 613) are observed with (apparent) improved intensity (Figure 5-7A) compared to the absence of DA (Figure 5-1A) in agreement with the effect of DA on CySH mass spectra reported in Chapter 3. Homocysteine (hCySH) derived ions, i.e $[hCySH+H]^+$ and $[hCSSCh+H]^+$, are suppressed in the presence of DA (Figure 5-7B) but the low sensitivity may also be due, in part, to different mobile phase than that used in Figure 5-1C.

The adducts of GSH with DAQ $[GSH+DAQ]^+$ (m/z 459) (Figure 5-7A) and hCySH with DAQ $[hCySH+DAQ]^+$ (m/z 287) (Figure 5-7B) are detected as observed for cysteine/DAQ. The radical formation pathway reported previously [Mautjana et al., 2008a] may be responsible for the adduct formation.

Effect of GSH Concentration on Thiol/DA Mass Spectra

The adduct $[DAQ+GSH]^+$ (m/z 459) increases as the GSH concentration increases from 0.1 to 0.5mM (Figure 5-8) while DA concentration is kept constant at 2.5 mM. A plot of ion intensity vs GSH concentration (Figure 5-8), where DA concentration (2.5 mM) is held constant, shows that the adduct signal intensity increases with an increase in GSH concentration. There is an increase in intensities of DAQ adduct, $[DAQ+GSH]^+$ (m/z 459), and $[GSH+H]^+$ (m/z 308), as well as the H-bonded GSH dimer, $[2GSH+H]^+$ (m/z 615) (Scheme 5-6). There is similar increase in $[2DA\text{-}H]^+$ and $[GSSG+H]^+$ dimers (Figure 5-8).

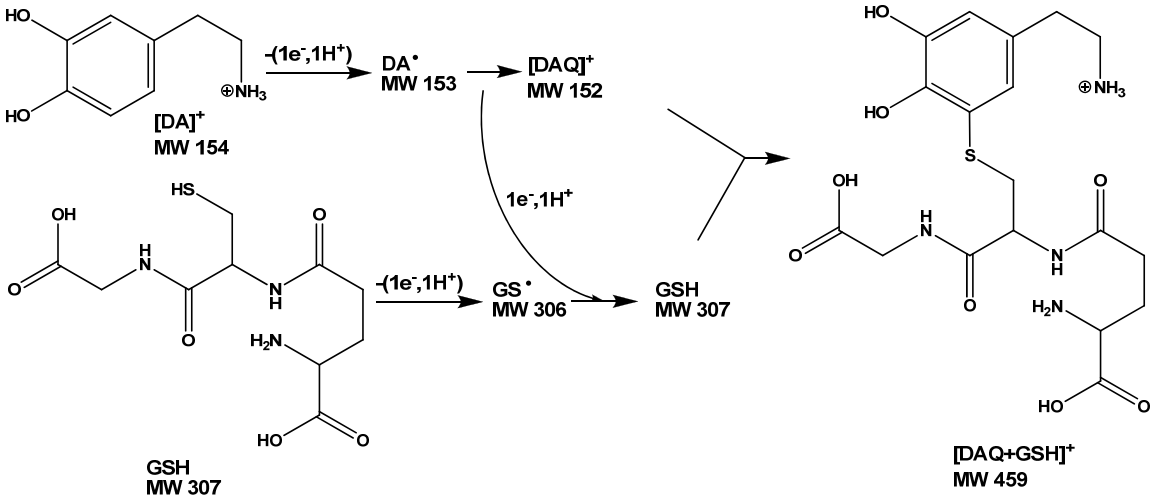

Scheme 5-6. Formation of [DAQ+GSH] adduct in positive ion mode ESI MS.

The ESI MS of GSH in the Presence of Uric Acid

A possible formation of an adduct between thiols and diimine, a product of $2e^-$, $2H^+$ oxidation of uric acid, proposed by Dutt et al. [2003] based on changes in UV absorption spectra with addition of thiol, was investigated. An ESI mass spectrum of a solution containing GSH (10 μM) and H_2U (60 μM) in 40/60 vol%, H_2O/MeOH, 10^{-3} M ammonium acetate, pH~6.3, is shown in Figure 5-9. Solutions with increasing uric acid/GSH concentration ratio, where uric acid (H_2U) concentration (60 μM) was kept constant while GSH was increased from 10 through 60 μM, were analyzed. None of the observed signals in the mass spectrum could be ascribed to GSH and H_2U adduct or their oxidation products. Observed in Figure 5-9 are H_2U derived ions, $[H_2U+H]^+$ (m/z 169) and $[2H_2U+H]^+$ (m/z 337) as well as GSH derived ions that have already been discussed. It is worth noting that under these conditions, the dimer $[GSSG+H]^+$ (m/z 613) increases and becomes the base peak. Whether this increase is due to the presence of uric acid is yet unclear. The apparent inability of GSH to form an adduct with UA could be due to the fact that the second oxidation of H_2U radicals by GS radicals would produce a diimine which is unstable [Volk et al., 1992; Volk et al.; 1999].

The ESI MS of GSH, CySH and hCySH Mixture in Presence of DA

Analysis of all three thiols, mixed in solution, in presence of DA was also performed (Figure 5-10). While both CySH $[CySH+H]^+$ (m/z 122) and hCySH $[hCySH+H]^+$ (m/z 136) ions are observed in the mass spectra of individual CySH (Figure 5-1B) and hCySH (Figure 5-1C), these monomeric ions are not detected in the mass spectrum of the thiol mixture in the presence of 2.5 mM DA (Figure 5-10), and the signal intensity of hCySH disulfide dimer $[hCySSCyh+H]^+$ (m/z 269) ion is very low. The monomeric ions of CySH and hCySH, $[CySH+H]^+$ (m/z 122) and hCySH $[hCySH+H]^+$ (m/z 136), are not detected in the mass spectrum of the thiol mixture in the absence of DA (Figure 5-5) either.

The absence of $CySH+H]^+$ (m/z 122) and hCySH $[hCySH+H]^+$ (m/z 136) ions in the thiol mixture without DA, may be an indication of facile cross-coupling of radicals given the presence of a mixed disulfide dimer $[hCySSCy+H]^+$ (m/z 255). The absence of $CySH+H]^+$ (m/z 122) and hCySH $[hCySH+H]^+$ (m/z 136) ions could also be due to the relatively poor sensitivity of ESI MS to the monomeric $[CySH+H]^+$ (m/z 122) and $[hCySH+H]^+$ (m/z 136) ions compared to $[GSH+H]^+$ (m/z 308) whose signal is observed. In the presence of DA, only a small peak of the mixed disulfide dimer $[hCySSCy+H]^+$ (m/z 255) is observed, which may indicate suppression of this ion, and the monomeric $CySH+H]^+$ (m/z 122) and hCySH $[hCySH+H]^+$ (m/z 136) ions by DA ions, or it could indicate competitive thiol/DA adduct formation where the thiols are completely consumed considering that DA is present in excess. The intensity of the disulfide dimer $[hCySSCyh+H]^+$ (m/z 269) decreases (from 37 to 5 counts; Table 5-1) in the hCySH/DA mixture because of formation of $[DAQ+hCySH]^+$ (m/z 287) adduct which competes with thiol dimerization.

The EC/ESI MS of Thiols in the Presence of DA

Similar to CySH/DAQ adduct, the adducts of $[GSH+DAQ]^+$ (m/z 459) (Figure 5-7A) and $[hCySH+DAQ]^+$ (m/z 287) (Figure 5-7B) increase in intensity with applied EC cell voltage (Figures 5-11A&B). The DAQ/thiol adducts increase with applied EC cell voltage while the respective signal intensities of disulfide dimers, $[GSSG+H]^+$ (m/z 613; Figure 5-11A) and $[hCySSCyh+H]^+$ (m/z 269; Figure 5-11B), appear to be unchanging.

The CySH disulfide dimer, with relatively high intensity (Chapter 3) than observed here for GSSG and hCySSCyh, but lower than the DAQ/CySH adduct intensity, appear to increase along with the DAQ/CySH adduct as EC cell voltage is increased. It is possible that the formation of CySSCy is kinetically competitive with DAQ/CySH formation as discussed in Chapter 3, whereas the formation of GSSG and hCySSCyh is slow. In either case, the radical pathway mechanism proposed previously for the DAQ/CySH adduct formation [Mautjana et al., 2008a] is supported by the experimental results. Briefly, both GSH (or hCySH) and DA undergo $1e^-$, $1H^+$ oxidation during ESI to form their respective radicals which, given the difference in oxidation potentials ($E^o_{(GSH\ or\ hCySH)}$ = 0.92 V vs SHE and $E^o_{(DA)}$ = -0.12 V vs SHE), undergo chemical oxidation reaction where the GSH- or hCySH-radical gets reduced and DA-radical oxidized. The resulting products, GSH (or hCySH) and DAQ, undergo a nucleophilic, 1,4-Michael addition reaction to give the adduct $[DAQ+GSH]^+$ (Scheme 5-6) or [hCySH+DAQ].

The additional adduct formed by two hCySH molecules and DAQ $[DAQ+2hCySH]^+$ (m/z 420) is observed in the mass spectrum of hCySH/DA solution (Figure 5-7B) and its intensity increases with applied EC cell voltage too. The same 50/49/1 vol% H_2O/MeOH/HAc, pH 4.2, carrier solution was used for all thiol/DA mass spectra compared above.

Summary of Thiol Mixture Analysis

The presence of DA in 50/49/1 vol% H_2O/MeOH/HAc, pH 4.2 carrier solution used in these experiments, and application of on-line EC cell voltage affect the different thiol ions and adducts in different ways. In EC/ESI MS described below the $[DAQ+hCySH]^+$ adduct ion intensity increases from 70 to 111 counts when the EC cell is turned on and is the highest hCySH related signal produced (Table 5-1). The highest signal for CySH is that of the CySSCy disulfide dimer (m/z 241) (with EC cell ON) whereas for GSH it is that of GSH proton adduct $[GSH+H]^+$ (m/z 308) (with EC cell OFF). The $[DAQ+GSH]^+$ (m/z 459) has the least signal intensity even with the EC cell ON, which could be due to the slow kinetics of the nucleophilic addition of GSH to DAQ relative to CySH and hCySH. Close inspection of data shown in Table 5-1 reveals that the best experimental conditions for thiol analysis, with which all thiol species can be detected, are when DA is present in the carrier solution and about 1.5 V EC cell voltage is applied. However, at 2.5 mM concentration in the mixture, DA appears to suppress monomeric thiol ions. Additional studies could be conducted in the future to determine the DA concentration that can allow maximum thiol detection sensitivity.

Evidence of Catalysis of CySH Oxidation by Metal Ions

Off-line cyclic voltammetry of CysH (0.5 mM) in the presence of Fe^{2+} (1 mM) shows increase in anodic current for CySH at ~1.1 V vs SCE (Figure 5-12), which indicates that CySH oxidation is likely catalyzed, and this is further supported by ESI MS data (Table 5-2). The mechanism of catalysis of CySH oxidation by the Fe^{2+} ion likely involves the Fe^{2+}/CySH complex [Tanaka et al., 1955a; Tanaka et al., 1955b; Wang and Stanbury, 2008]. The ESI MS spectra of CySH (0.5 mM) show an increase in intensity of the CySH disulfide dimer (m/z 241) when Fe^{2+} (100 μM) is added to CySH (50 μM) in 50/49/1 vol% H2O/MeOH/HAc, pH 4.2 carrier solution (Table 5-2). Signal intensities of $[CySH+H]^+$ (m/z 122) and $[CySSCy+H]^+$ (m/z

241) in the presence of Fe^{2+} or Cu^{2+} are much higher compared to those obtained without these ions (compare intensities in Table 5-1 to those in Table 5-2).

The base peak in the mass spectra of Fe^{2+}/CySH solution appears at m/z 538 (Figure 5-13), and has been assigned to the redox active $[Fe(CySH)_4]^+$ [Rose et al.; 1998; Cotton et al., 1987] formed in solution. Addition of Cu^{2+} (100 μM) has even greater catalytic effect on CySH given the high intensity of $[CySSCy+H]^+$ (m/z 241) relative to that obtained in presence of Fe^{2+} (Table 5-2). The intensity of cysteine disulfide dimer (m/z 241) in the presence of Cu^{2+} (100 μM), increases with EC cell ON (Table 5-2.

Proposed Mechanism of Catalysis of CySH Oxidation by Iron (II)

Much research on catalytic oxidation of thiols such as cysteine, by iron and copper ions is being done [Wang and Stanbury, 2008; Tyapochkin and Kozliak, 2005] to understand the mechanisms involved, which might be beneficial for analysis of thiol compounds, and undertansing metal catalyzed oxidation reactions of endogenous thiols including proteins (with sulfhydryl groups) which may occur in vivo, leading to disease. In the case of iron, however, iron-sulfur centers in some proteins such as rubredoxin (found in bacterium *C. Pasturianum*) have been well characterized [Rose et al.; 1998; Cotton et al., 1987].

Rubredoxins are relatively low-molecular weight proteins (~6000Da) which contain one iron atom surrounded by a distorted tetrahedron of cysteinyl sulfur atoms [Cotton et al., 1987]. Iron is normally in the Fe(III) oxidation state but can be reduced to the Fe(II) oxidation state (E^o = 0.77 V vs SHE) with only a slight increase in the Fe–S distances and no change in the tetrahedral coordination [Rose et al.; 1998; Cotton et al., 1987]. Iron in both oxidation states has been shown through the Mossbauer spectroscopy (which detects magnetic resonance shifts of gamma-irradiated nuclei) to be in the unpaired, high spin state [Phillips et al., 1970; Rose et al., 1998]. The high spin state with unpaired electrons allows rubredoxins to participate in electron

transfer reactions. Therefore, it is possible that the CySH ligands of the $Fe(CySH)_4$ complex can be exchanged with free cysteine in solution, with the released cysteine in oxidized form (i.e. as thiol radicals), which couple to form the cysteine disulfide dimer. This mechanism is seemingly supported by the increase in the disulfide dimer $[CySSCy+H]^+$ (m/z 241) as applied EC cell voltage is increased (Table 5-2).

Conclusions

Reduced thiols, GSH, CySH and hCySH and their oxidized forms GSSG, CySSCy and hCSSCh were detected by positive mode ESI MS. Electrospray induces oxidation of these analytes leading to formation of sulfur-centered thiol radicals which dimerize rapidly to form the disulfide dimers. On-line electrochemistry improves the detection sensitivity of ESI MS to the thiols. Relatively low concentration of ~2 μM GSH was detected. Relatively stable oxygen-centered radicals are also formed. The stability of oxygen-centered GSH radicals likely results from the intramolecular hydrogen bonding, and the resultant electron delocalization along the O-C-O-H-O-C-O chain (Sheme 5-3). The formation of GSSG observed from the pH ~6.3 solution (of GSH, $pK_a(SH) = 8.7$) suggests that electrolytic oxidation of thiol proceeds regardless of pH seeing that it is relatively low with respect to the pK_a.

In the presence of DA, GSH (and hCySH) together with DA undergo $1e^-$, $1H^+$ oxidation. The respective radicals can react to form the dimers, $[2DA-H]^+$ (m/z 307) and $[GSSG+H]^+$ (m/z 612), $[CySSCy+H]^+$ (m/z 241) or $[hCSSCh+H]^+$ (m/z 269), and can also undergo chemical redox reaction (given $E^o_{(GSH)} = 0.92$ V vs SHE and $E^o_{(DA)} = -0.12$ V vs SHE) which leads to formation of GSH (CySH or hCySH) and DAQ and subsequent nucleophilic addition of GSH (CySH or hCySH) to the electron deficient DAQ to form dopamine adducts as already described. It is possible that GSH and uric acid radicals undergo redox reaction as well but unlike DAQ, the diimine formed from oxidation of uric acid radicals is unstable. Thus no adduct is formed.

Table 5-1. Average intensities (n = 3) of thiol derived ions in the presence of DA.

m/z Value	Assignment	Intensity (without dopamine) EC Cell OFF	Intensity (without dopamine) EC Cell ON (1.5V)	Intensity (with dopamine) EC Cell OFF	Intensity (with dopamine) EC Cell ON (1.5V)
122	$[CySH+H]^+$	Not detected	Not detected	Not detected	Not detected
136	$[hCySH+H]^+$	Not detected	Not detected	Not detected	6
137	$[DA\text{-}NH_3]^+$	n/a	n/a	2	4
154	$[GSH^-]^{2+}$; *incl. $[DA]^+$	5	5	151*	214*
241	$[CySSCy+H]^+$	41	98	51	56
255	$[hCSSCy+H]^+$	131	196	29	25
269	$[hCSSCh+H]^+$	37	47	6	5
273	$[DAQ+CySH]^+$	n/a	n/a	158	244
275	$[GSH^-+CySH]^{2+}$; *incl.$[DA+CySH]^+$	3	3	5*	8*
287	$[DAQ+hCySH]^+$	n/a	n/a	70	111
307	$[2DA-H]^+$	n/a	n/a	4	4
308	$[GSH+H]^+$	135	115	37	32
459	$[DAQ+GSH]^+$	n/a	n/a	6	8

Table 5-2. Average intensities (n = 3) of cysteine disulfide dimer (m/z 241) indicating metal ion catalysis of cysteine oxidation.

m/z Value	Assignment	Intensity (without metal ions) EC Cell OFF	Intensity (without metal ions) EC Cell ON (1.5V)	Intensity (with Fe(II)) EC Cell OFF	Intensity (with Fe(II)) EC Cell ON (1.5V)	Intensity (with Cu(II)) EC Cell OFF	Intensity (with Cu(II)) EC Cell ON (1.5V)
122	$[CySH+H]^+$	8.7	64.1	83.4	104.7	10.7	26.3
241	$[CySSCy+H]^+$	49.7	213.9	88.7	280.0	231.4	290.0
296.7	$[CySFeSCy]^+$	2.6	12.1	16.5	20.4	n/a	n/a
538	$[Fe+4CySH]^+$	2.8	6.2	222.4	394.2	14.9	8.1
304	$[CySSCy+Cu]^+$	n/a	n/a	n/a	n/a	9.7	10.9

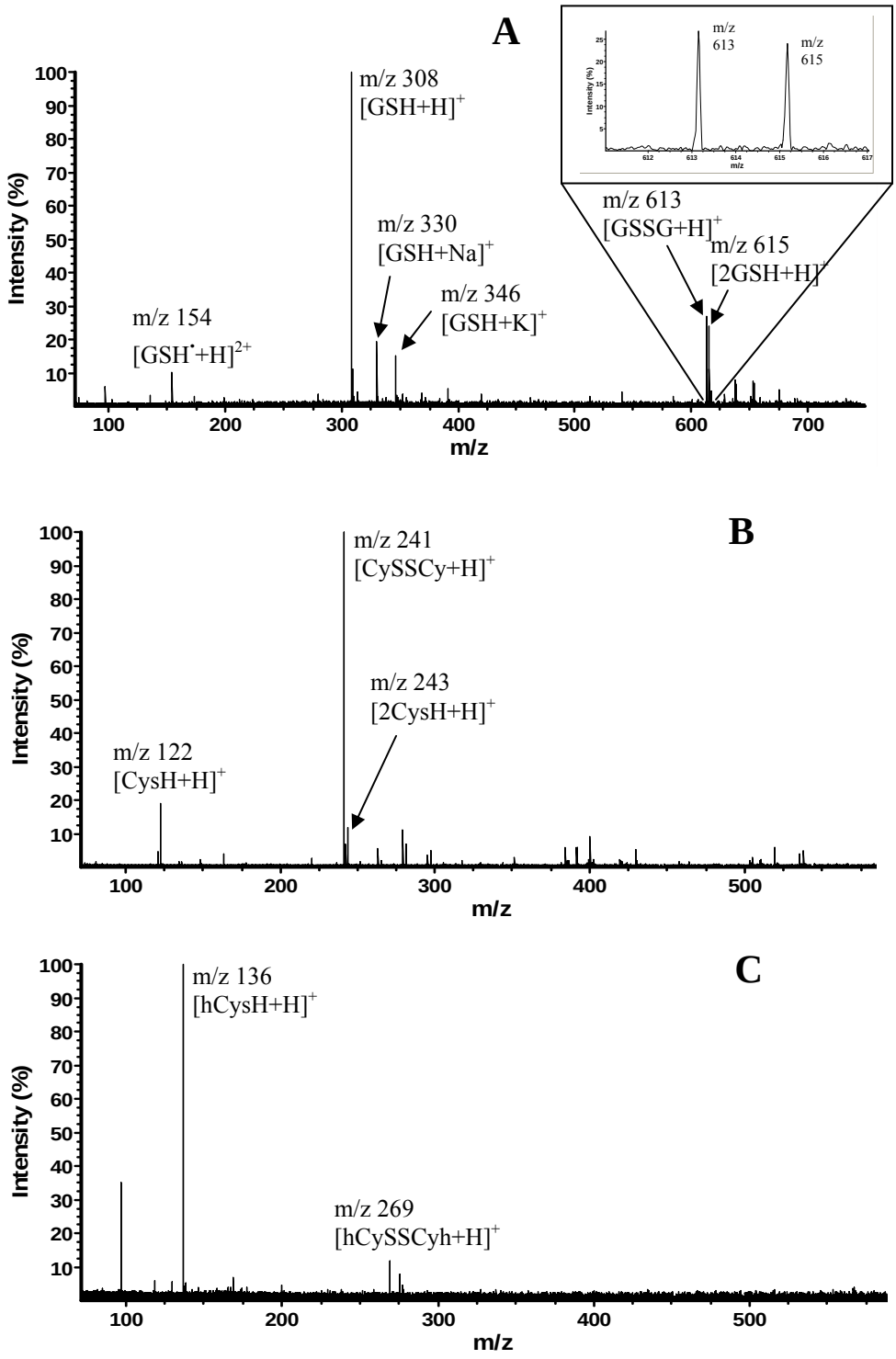

Figure 5-1. Positive mode ESI MS of (A) GSH (0.05 mM), (B) CySH (0.05 mM) and (C) hCySH (0.5 mM) in 40/60 vol%, H_2O/MeOH containing 1 mM NH_4Ac, pH~6.3; Flow rate 50 µL/h; HV 3 kV.

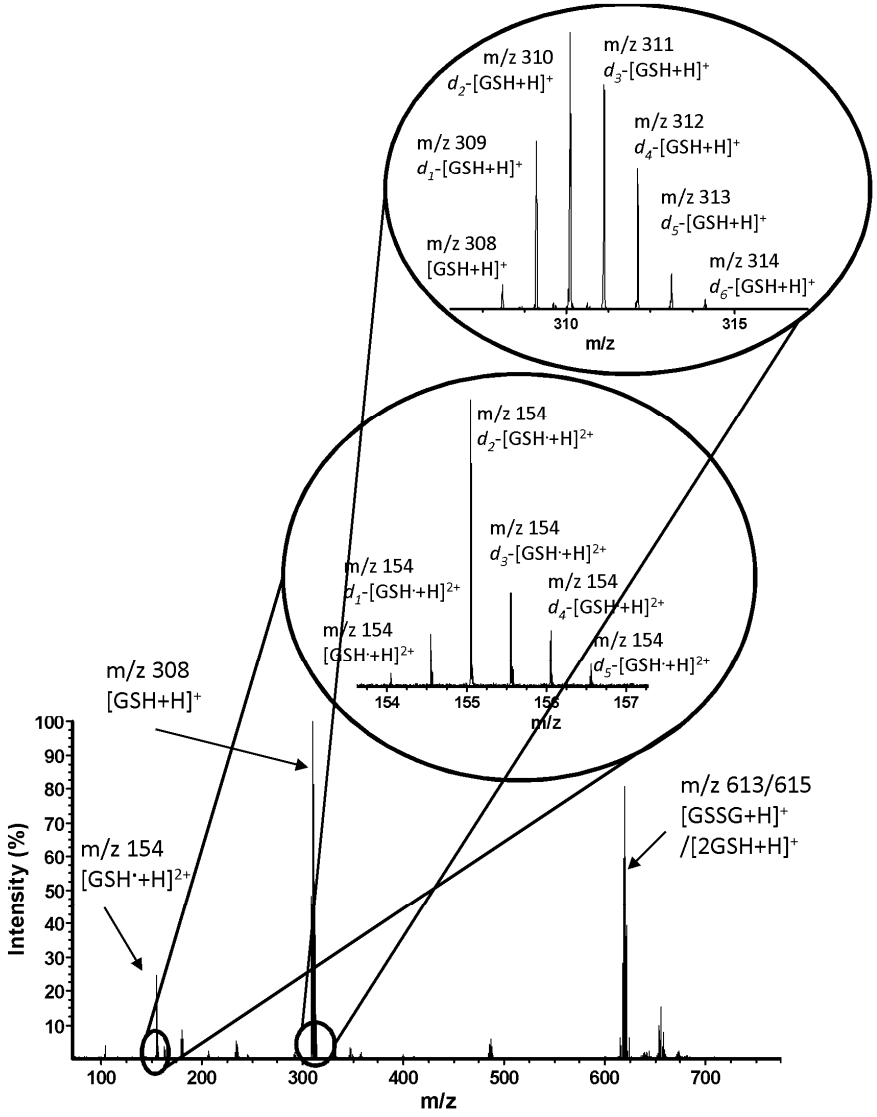

Figure 5-2. The H/D exchange ESI MS of GSH (0.05 mM) in 40/60 vol%, D_2O/MeOH, 1 mM NH_4Ac, pH 6.3; Flow rate 50 μL/h; HV 3 kV. See structures in Scheme 5-3.

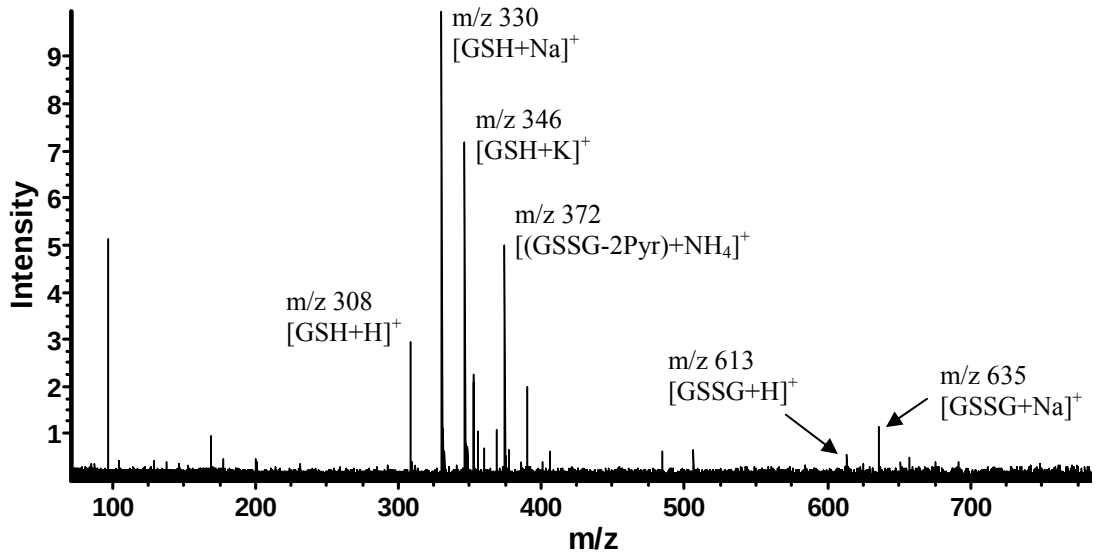

Figure 5-3. Lowest concentration of GSH (2 x 10^{-3} mM or 2 μM) detected with positive mode ESI MS; Same conditions as in Figure 5-1.

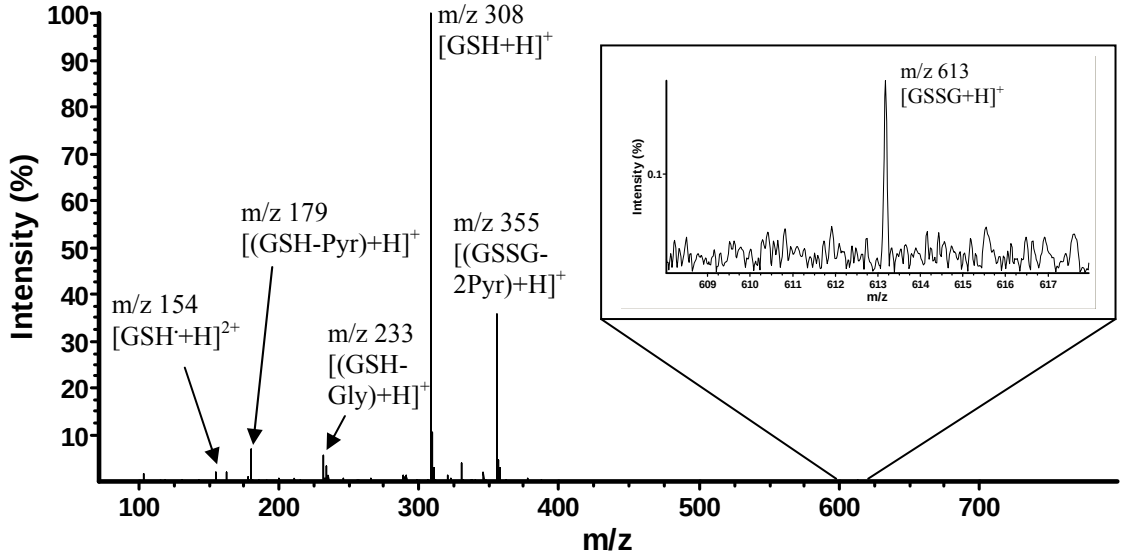

Figure 5-4. Positive mode ESI MS of GSH (0.5 mM); Same conditions as in Figure 5-1.

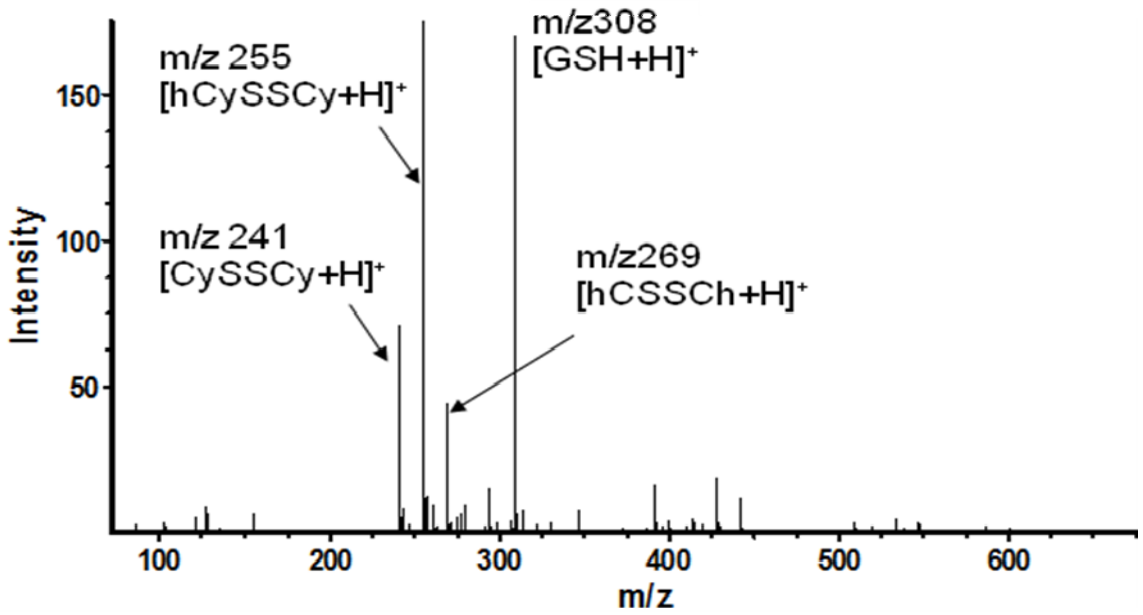

Figure 5-5. The ESI MS of mixed thiols, GSH (0.05 mM), CysH (0.05 mM) and hCySH (0.5 mM). Same conditions as in Figure 5-1

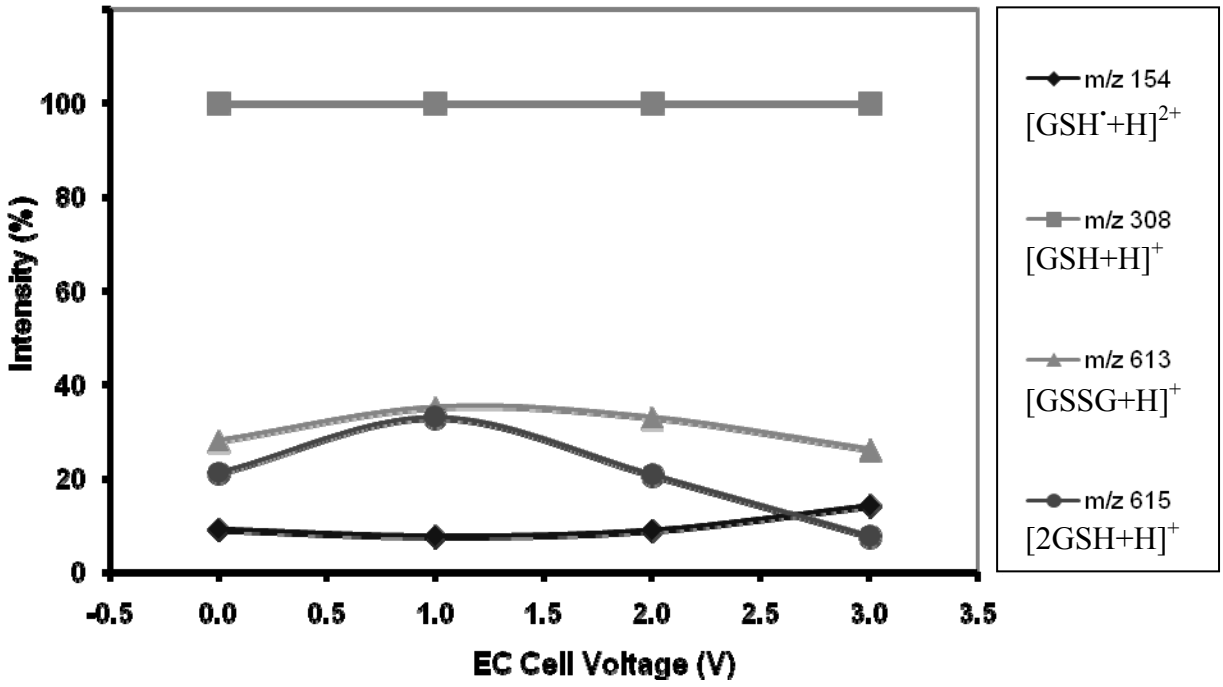

Figure 5-6. Effect of on-line EC cell voltage on ESI MS of GSH (0.05 mM); Same conditions as in Figure 5-1.

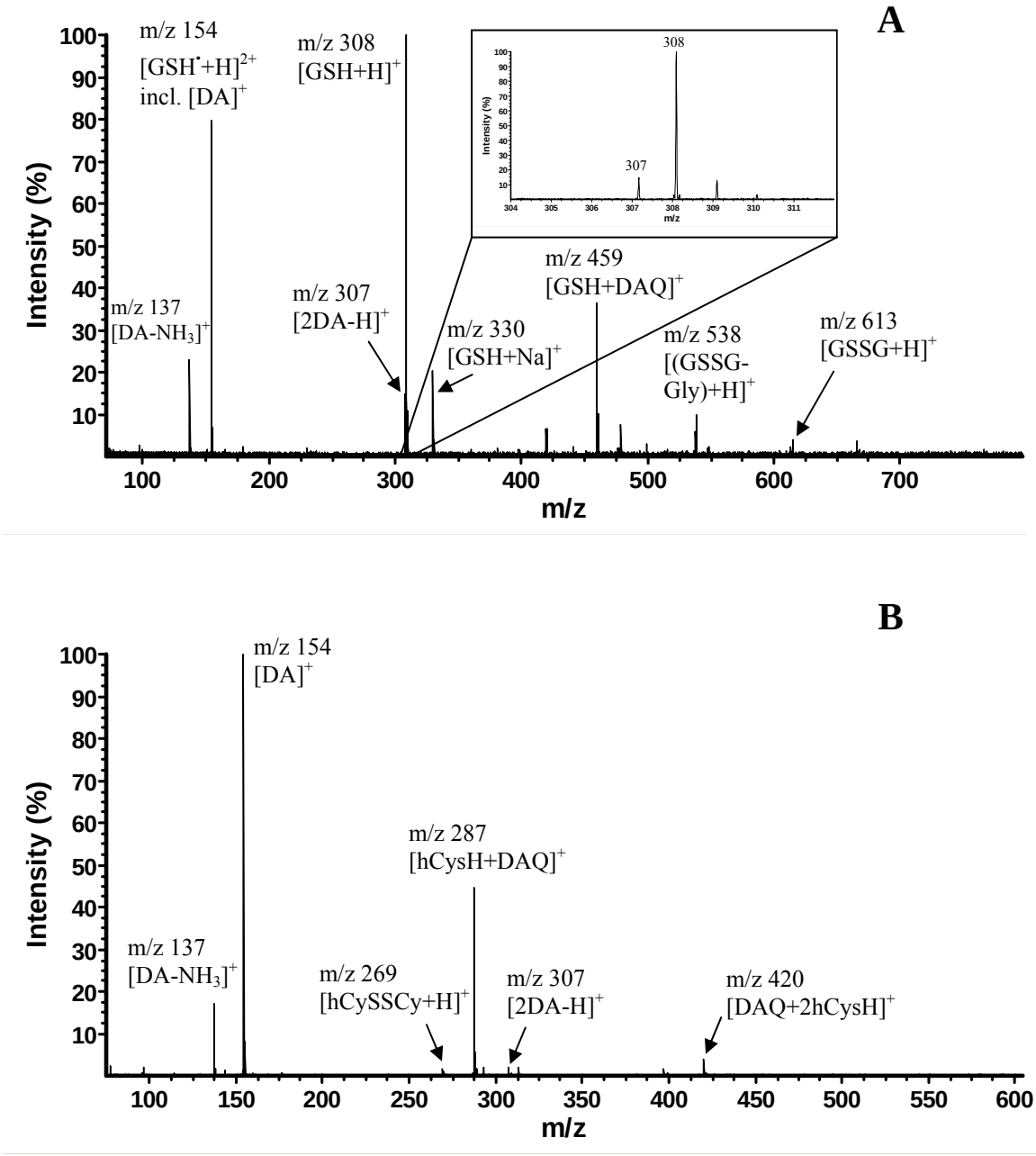

Figure 5-7. Positive mode ESI MS of (A) GSH (0.5 mM) and (B) hCysH (0.5 mM), each in the presence of DA (2.5 mM); 50/49/1 vol%, H_2O/MeOH/HAc, pH~4.2; flow rate 50µL/h; HV 3 kV.

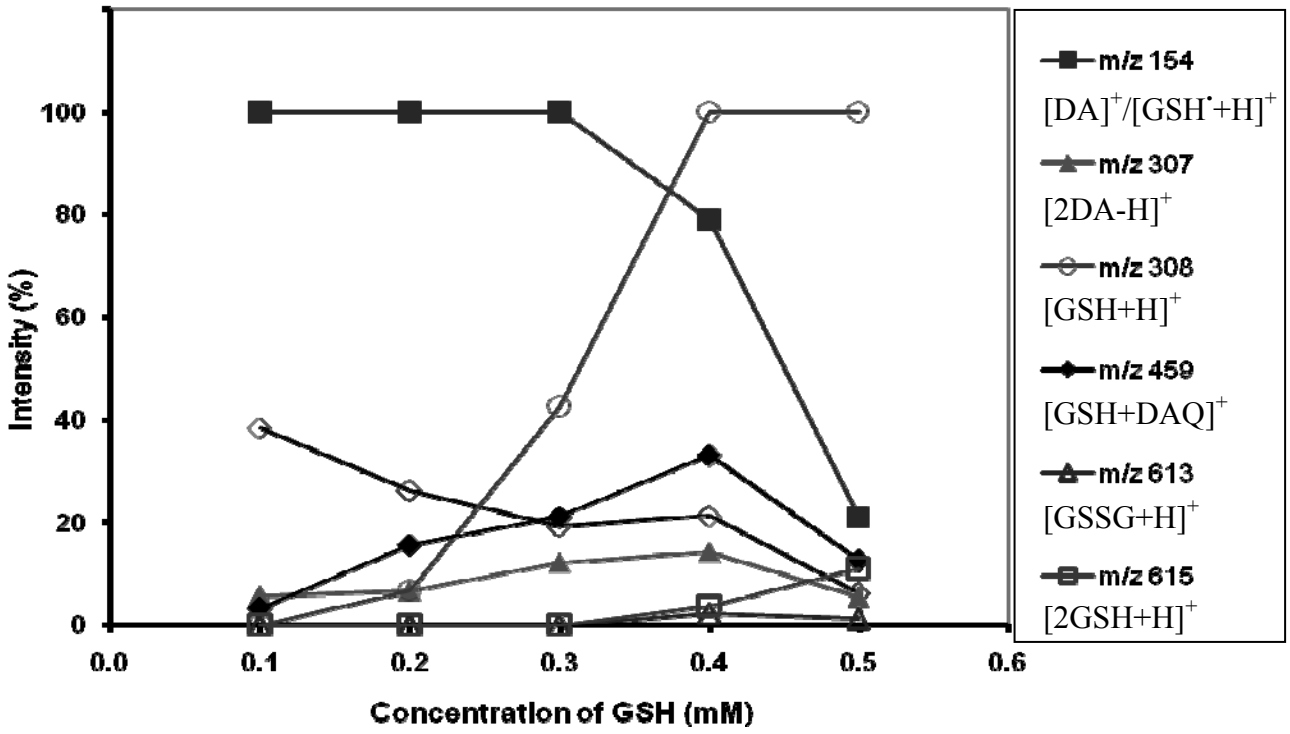

Figure 5-8. Positive mode ESI MS of GSH (various concentrations) in the presence of DA (2.5 mM); Same conditions as in Figure 5-7.

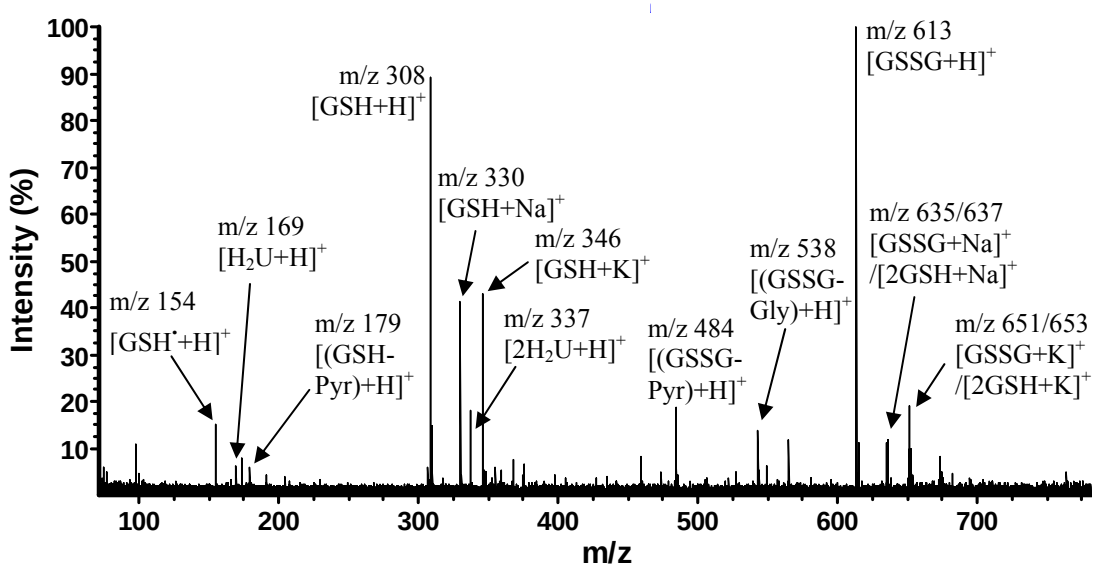

Figure 5-9. Positive mode ESI MS of GSH (0.01 mM or 10 μM) in the presence of uric acid (0.06 mM or 60 μM); Same conditions as in Figure 5-1.

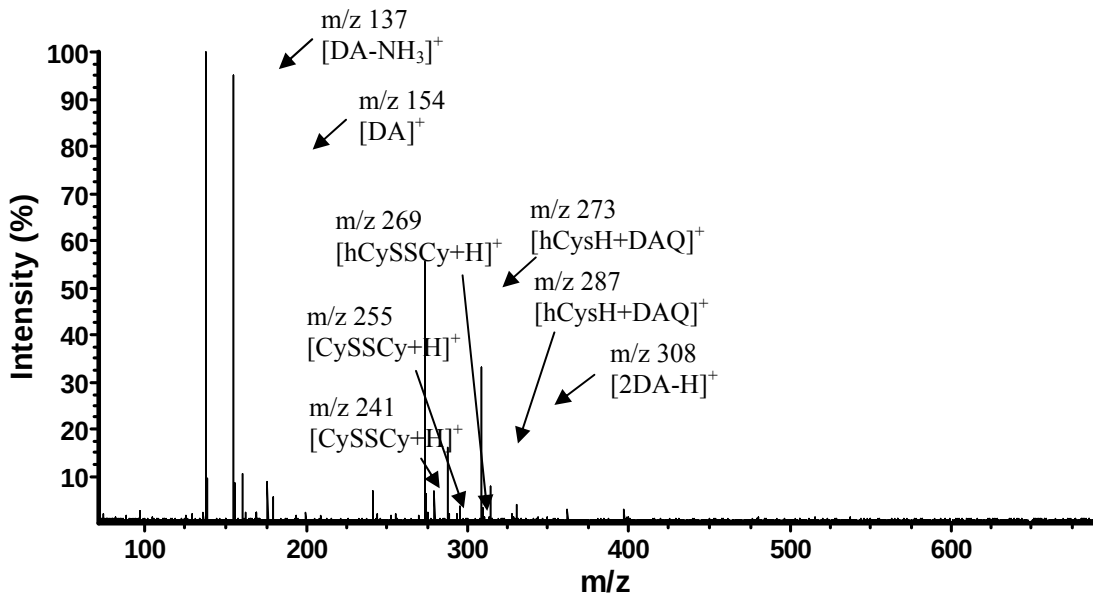

Figure 5-10. Positive mode ESI MS of a thiol mixture, GSH (0.05 mM), CySH (0.05 mM) and hCySH (0.5 mM), in the presence of DA (2.5 mM). Same conditions as in Figure 5-7.

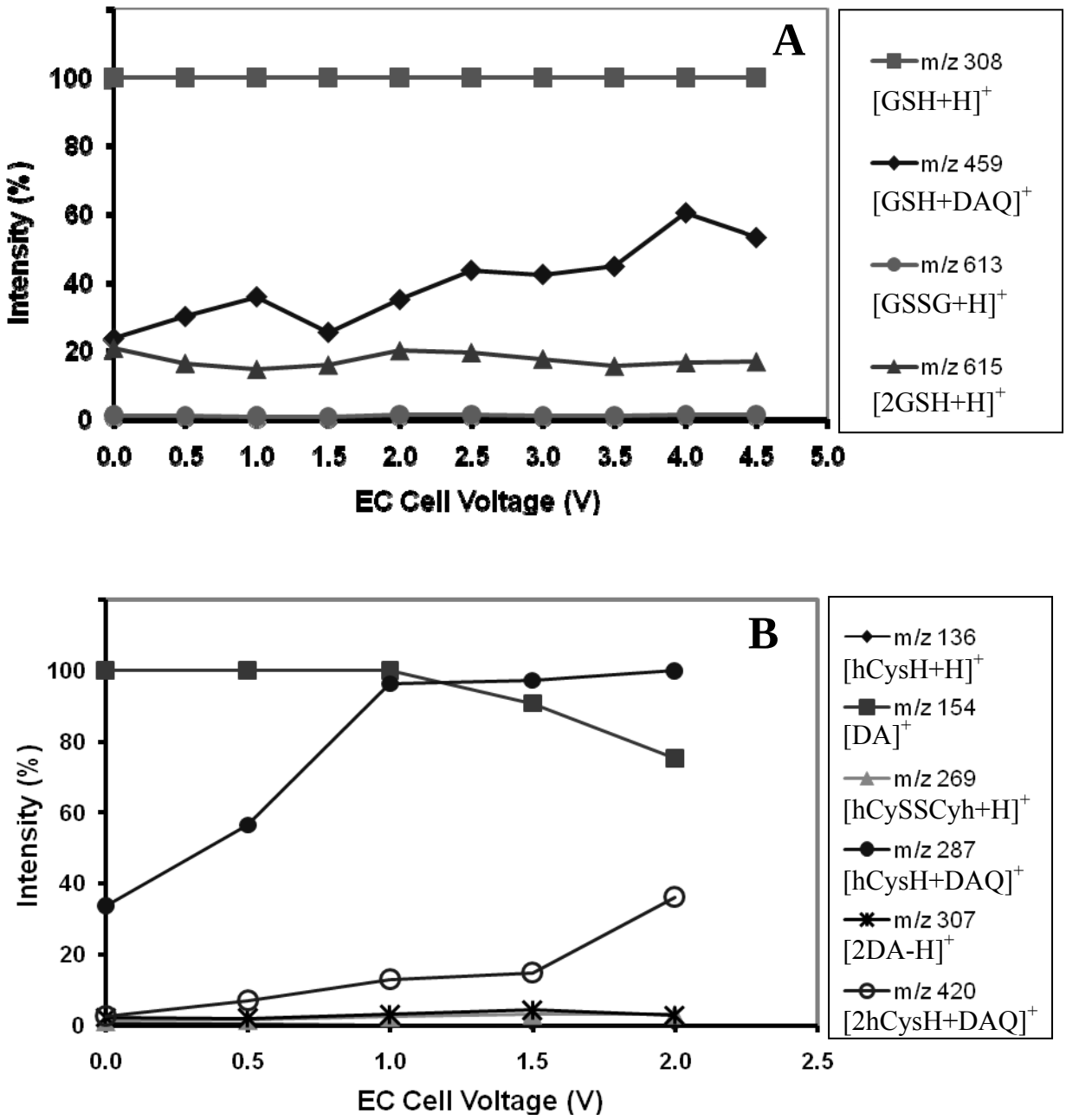

Figure 5-11. Effect of applied EC cell voltage on oxidation products of (A) GSH and (B) hCySH, each in presence of DA (2.5 mM); Same conditions as in Figure 5-7.

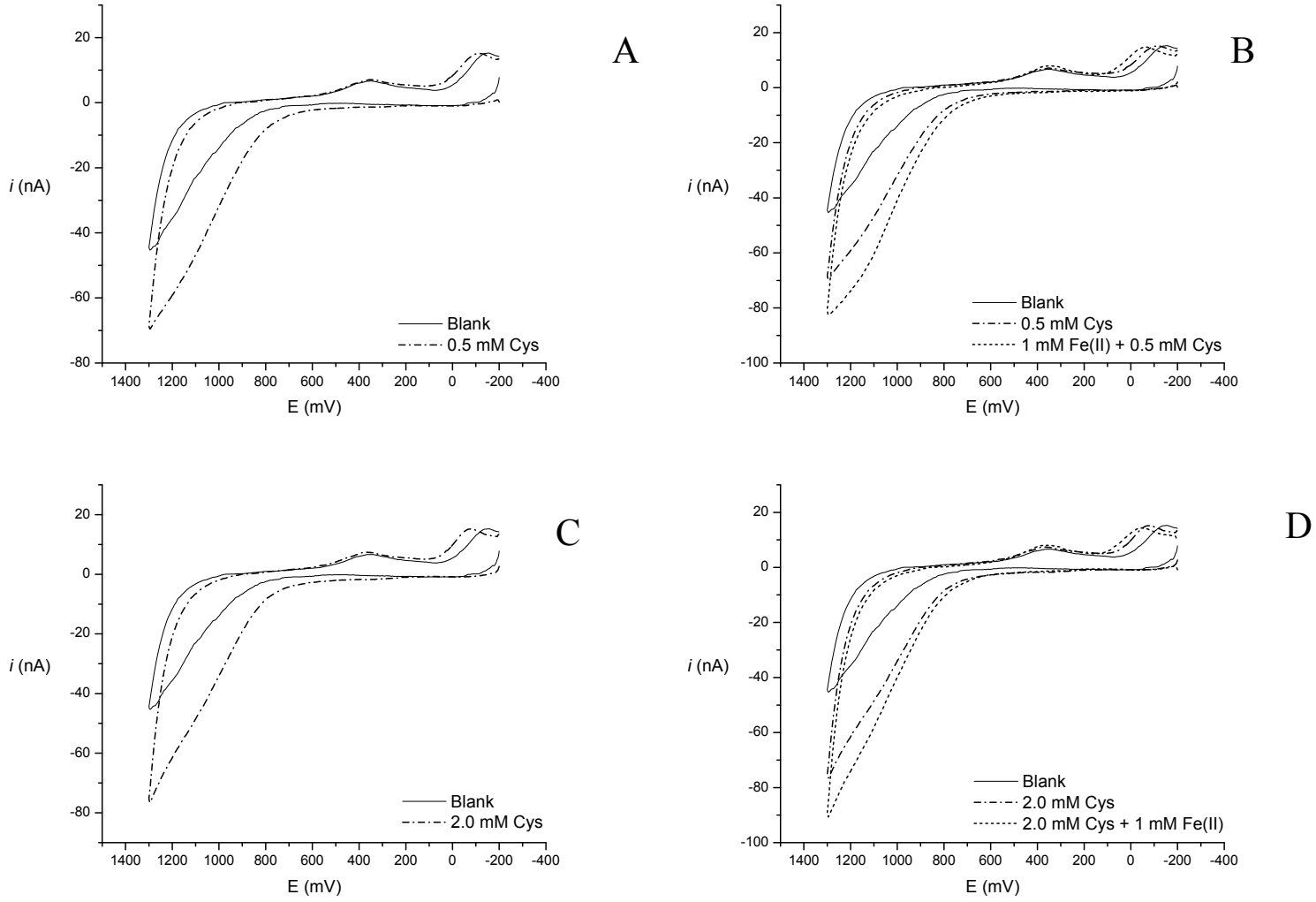

Figure 5-12. Cyclic voltmmograms (ν = 50 mV/s) of cysteine (0.5 mM) alone (A) and with Fe^{2+} (1 mM) (B); cysteine (2.0 mM alone) (C) and with Fe^{2+} (1 mM) (D) on stainless steel electrode (r=50 μm); Ref = SCE. Blank = 50/49/1 vol%, H_2O/MeOH/HAc.

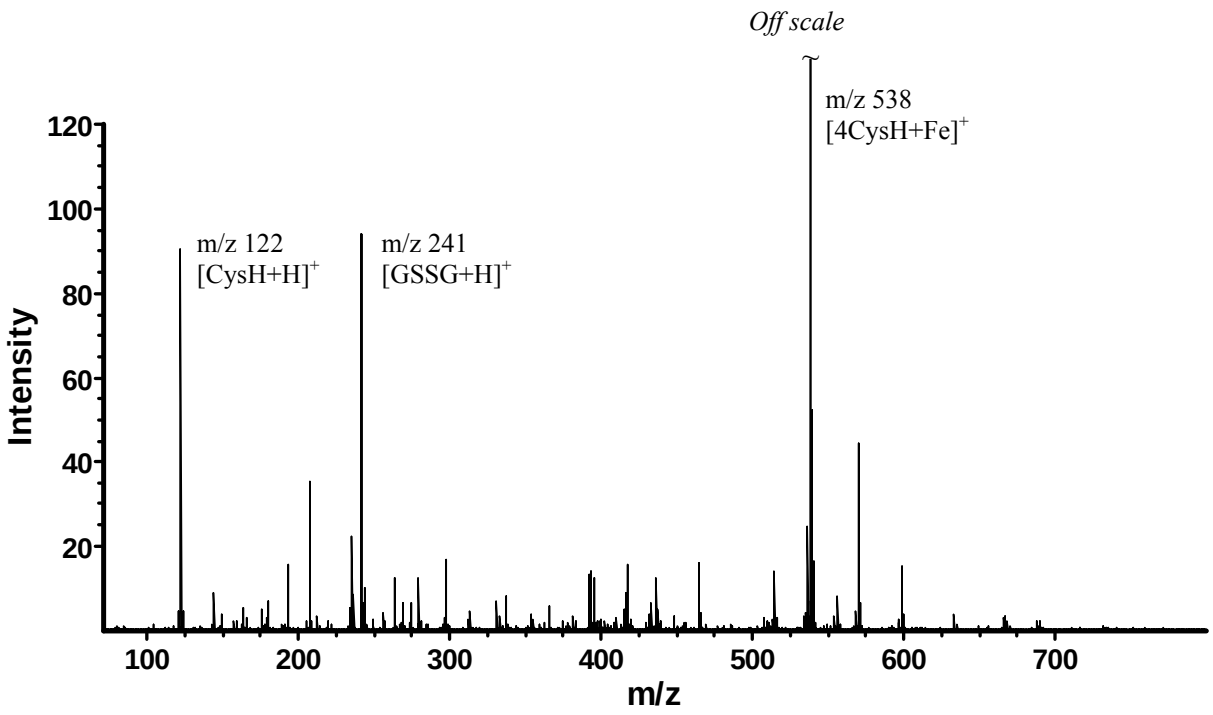

Figure 5-13. Positive mode ESI MS of CySH (0.5 mM) with Fe^{2+} (100 μM).

CHAPTER 6
OXIDATION OF PURINES DURING ESI MS AND EC/ESI MS

Introduction

Emil Fischer won the 1902 Nobel Prize in chemistry for synthesis of purines [http://Nobelprize.org/nobel_prizes/chemistry/1902/fischer-lecture.pdf], a group of heterocyclic organic compounds with fused pyrimidine and imidazole rings, including adenine, guanine, hypoxanthine, xanthine, and uric acid. Adenine and guanine bases are found incorporated in deoxyribonucleic acid (DNA) and ribonucleic acid (RNA) molecules, whereas hypoxanthine and xanthine are formed as intermediates of nucleotide catabolism which, in man, ends with uric acid as a final product [Waring et al., 2000] (see Chapter 1, Scheme 1-4).

In DNA and RNA, adenine or guanine is attached to a sugar (2-deoxyribose or ribose) unit with an N-glycosidic bond between C_1 of the sugar unit and N_9 of the purine to form a nucleoside (see Chapter 1, Scheme 1-2, for numbering in the purine structure). The purine nucleosides are adenosine and guanosine, as well as inosine and xanthosine, which are not in DNA or RNA. Addition of one or more phosphate groups to the nucleoside (via a phosphate ester bond to $C_{5'}$ of the sugar or via an acid anhydride linkage if more than one phosphate is present) results in purine nucleotides: adenosine monophosphate (AMP), guanosine monophosphate (GMP), inosine monophosphate (IMP) and xanthosine monophosphate (XMP). Purines are produced from the breakdown of adenosine triphosphate (ATP, Scheme 6-1) and guanosine triphosphate (GTP), the energy-carrying molecules in the body [Jencks and Wolfenden, 2000]. The ultimate source of ATP and GTP is catabolism of food.

Various enzymes catalyze the different metabolic reactions shown in Chapter 1, Scheme 1-4. [Simmonds et al., 1997]. These enzymes regulate purine levels within healthy limits in the

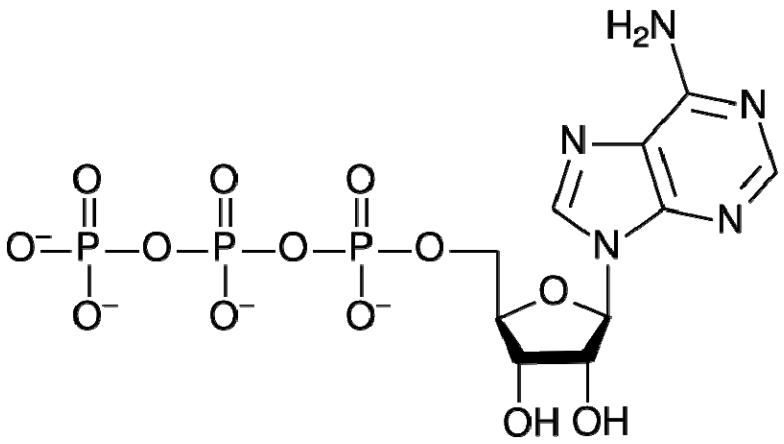

Scheme 6-1. Structure of the nucleotide, adenosine triphosphste (ATP).

body via catalysis of biosynthesis (in case of purine deficiency) and salvage pathways (if excess of purines is produced). Abnormal conditions in cells, such as hypoxic stress and enzyme deficiency (or super-activity), can lead to accumulation of purines in various organs, such as the brain [Ford et al., 2007], heart and kidneys [Zvi et al., 2007; Ejaz et al., 2007], leading to disease [Simmonds et al., 1997; Kathiwala et al., 2008]. Manifestations of metabolic disorders in the purine pathway in man include immunological, haematological, neurological and renal problems [Nyhan, 2005; Simmonds et al., 1997].

The analytical techniques used for purine analysis include high performance liquid chromatography (HPLC) and capillary electrophoresis (CE) using either ultraviolet (UV) light absorbance or electrospray ionization mass spectrometry (ESI MS) for detection [Ito et al., 2000; La Marca et al., 2006; Edwards et al., 2006] and cyclic voltammetry (CV) [Cavalheiro and Brajter-Toth, 1999]. Selectivity difficulties experienced with CV, long analysis times associated with HPLC are some of the limitations of these techniques in clinical analysis of purines and screening of biological samples. One of the strategies for improving throughput involves direct injection ESI MS with high resolution mass analyzers, such as Fourier transform ion cyclotron resonance (FT-ICR), to identify metabolites without need for chromatographic separation.

However, electrochemical processes of the ES ion source can affect the sensitivity with which analytes of low oxidation potentials such as purines are detected. Complete electrochemical oxidation of purines may involve oxygen, multiple electrons and protons, and is affected by pH [Cavalheiro and Brajter-Toth, 1999; Owens and Dryhurst, 1977]. It is apparent that electrochemical oxidation of purines can be slow and complex, which may affect their detection sensitivity. Literature peak oxidation potential (Ep) values [Dryhurst and Elving 1968; Oliviera-Brett et al., 2002; Cavalheiro and Brajter-Toth, 1999] of purine bases (see structures in Scheme 6-2), at similar electrodes and pH values, can be arranged as uric acid < xanthine < guanine < hypoxanthine < adenine. This chapter describes electrochemical oxidation reactions that purines may undergo during positive ion mode ESI MS.

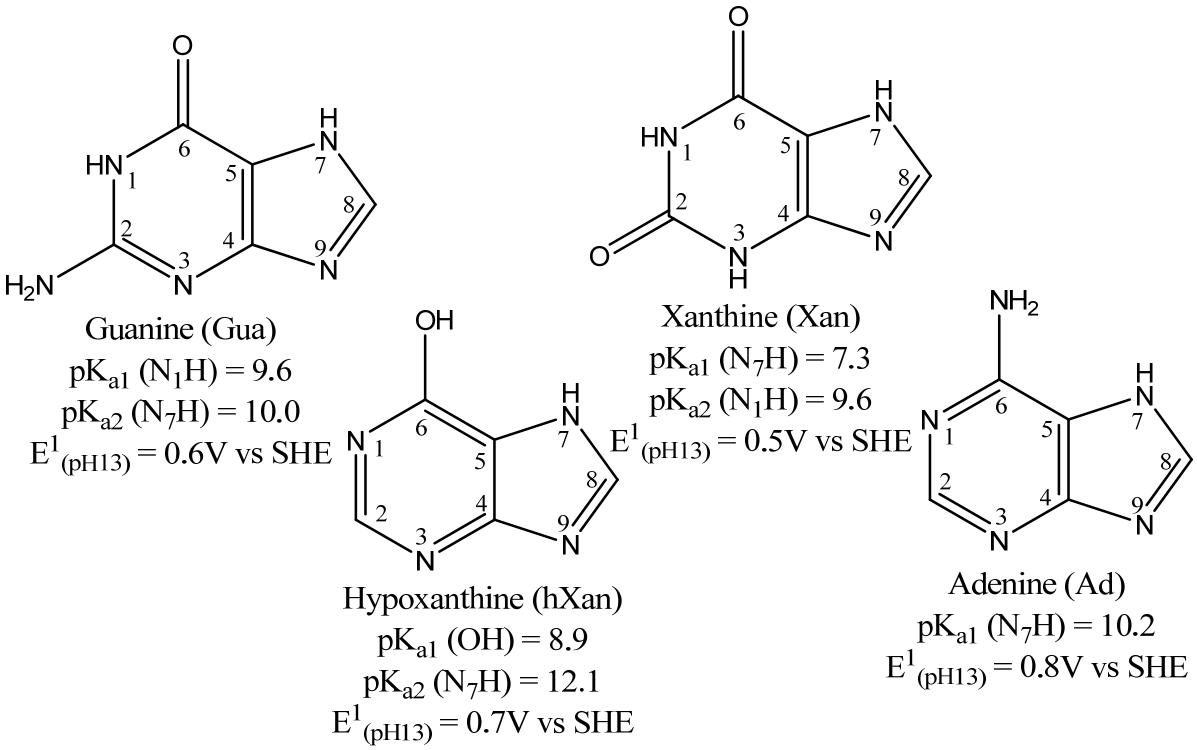

Scheme 6-2. Structures of purine bases, pK$_a$ values [Budavari, 1989; Rogstad et al., 2003] and one-electron oxidation potentials (E^1 vs SHE) [Jovanovic and Simic, 1986]

Results and Discussion

The ESI MS and EC/ESI MS of Guanine (Gua)

The ESI mass spectrum of guanine prepared in 50/49/1 vol%, H_2O/MeOH/HAc, pH 4.2, is shown in Figure 6-1. The peaks observed at m/z 152 and 302 are assigned to proton adducts, $[Gua+H]^+$ and $[2Gua+H]^+$, while those at m/z 174 and 325 are sodium adducts $[Gua+Na]^+$ and $[2Gua+Na]^+$ of guanine and guanine dimer, respectively. The potassium adduct of guanine dimer $[2Gua+K]^+$ (m/z 341) is also observed. Informed by the mechanism of oxidation of guanine proposed by Dryhurst, [1969], the small peak at m/z 168 was identified as 8-oxoguanine $[OxoGua+H]^+$, a hydrolyzed $2e^-$, $2H^+$ oxidation product of guanine. A larger ESI MS signal is obtained for 8-oxoguanine $[OxoGua+H]^+$ (m/z 168) peak when the EC cell is turned ON (Figure 6-2). Its intensity increases as applied EC cell voltage is increased (Figure 6-3), while the intensity of the guanine dimer decreases. Intensities of guanine $[Gua+H]^+$ (m/z 152) and the deaminated guanine $[(Gua-NH_3)+H]^+$ (m/z 135) increase with applied EC cell voltage, a behavior similar to that of DA discussed in Chapter 3.

In 40/60 vol%,, H_2O/MeOH, 1 mM NH_4Ac, pH 6-3, peaks due to hydrogen bonded guanine tetramers (see Scheme 6-3) with Na^+ and K^+ metal ions in the center (m/z 627 and 643, respectively) [Manet et al., 2001] are observed (Figure 6-4), along with their adducts with Na^+ and K^+ ions. It should be noted that a high flow rate (50 μL/h) was reached in this experiment to achieve a stable electrospray current. Based on flow rate vs intensity (of DA) data described in Chapter 3, more analyte ions, hence high intensity, may be detected. It is also possible that the presence of a guanine dimer peak indicates the tendency of the carrier solution composition to promote dimer formation, particularly in presence of alkali-metal ions [Manet et al., 2001] at concentrations that are relatively higher than that of protons (H^+), at pH values below pK_a.

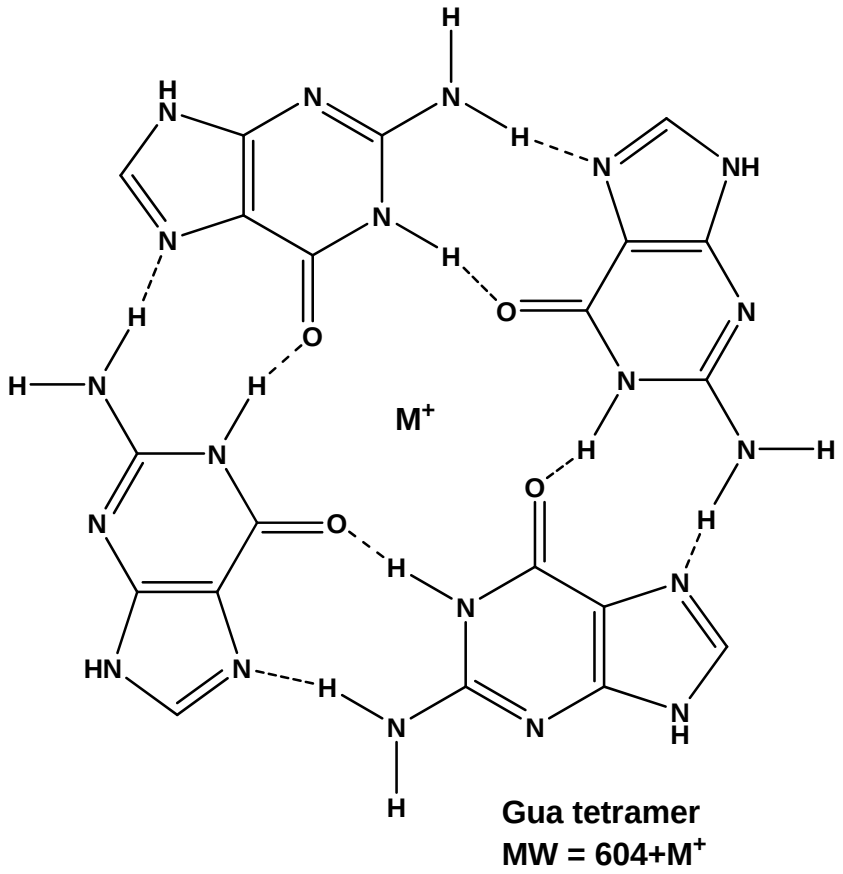

Scheme 6-3. The H-bonded guanine tetramer with a metal ion center (M^+ = sodium ion, Na^+ or potassium ion, K^+)

The proposed mechanism of formation of guanine dimer and 8-oxoguanine during positive ion mode ESI MS is shown in Scheme 6-4, where the initial loss of $1e^-$, $1H^+$ leads to a dimeric radical which is stabilized by hydrogen atom transfer through H-bonding with the third unoxidized guanine molecule (Chapter 4, Scheme 4-4) for uric acid. A neutral guanine radical generated in this step can be oxidized further by loss of $1e^-$, $1H^+$, followed rapidly by hydrolysis to 8-oxoguanine.

The instability of $2e^-$, $2H^+$ oxidation product observed here is not peculiar to guanine. The same level of instability is demonstrated by the $2e^-$, $2H^+$ oxidation product of uric acid, the uric

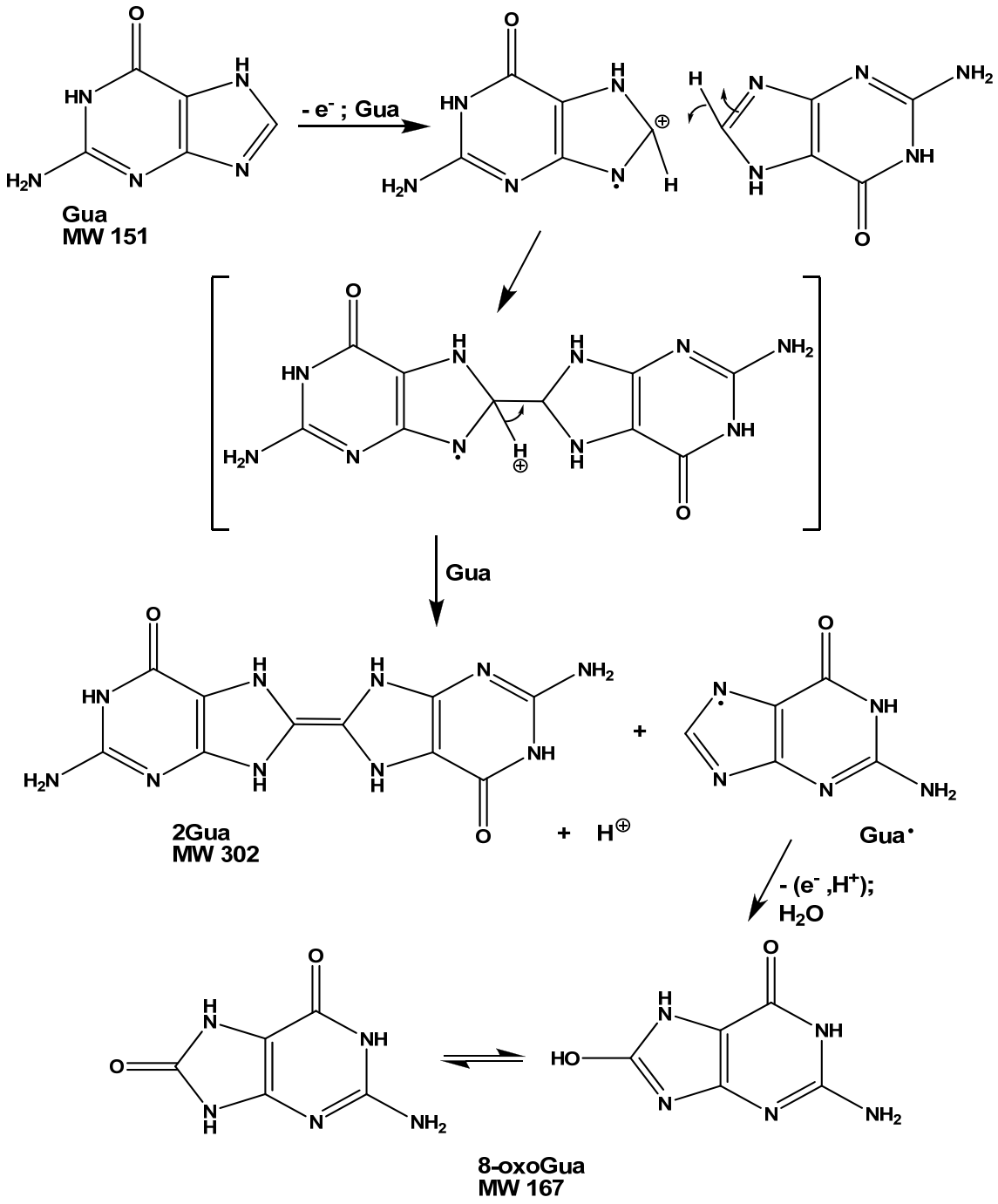

Scheme 6-4. Proposed mechanism of oxidation of guanine in 40/60 vol%, H_2O/MeOH, 10^{-3} M NH_4Ac, pH 6.3, during positive mode ESI MS.

acid diimine, which is also hydrolyzed upon formation [Volk et al., 1992]. The absence of 8-oxoguanine in 50/49/1 vol%, H_2O/MeOH/HAc, pH 4.2, (Figures 6-1 and 6-2) could be due to stable tetramers with a metal ion center formed by guanine in 40/60 vol%,, H_2O/MeOH, 10^{-3} M

NH_4Ac, pH 6.3 carrier solution, which may be more difficult to oxidize than free guanine. The concentration of Na^+ and K^+ ions, which promotes aggregation of guanine [Manet et al., 2001], is relatively higher than that of the protons in the 40/60 vol%, H_2O/MeOH, 10^{-3} M NH_4Ac, pH 6.3, carrier solution. Thus the formation of guanine tetramer is favored in this carrier solution than in 50/49/1 vol%, H_2O/MeOH/HAc, pH 4.2.

The ESI MS and EC/ESI MS of Adenine (Ad)

Figure 6-5 shows the ESI MS of adenine in 50/49/1 vol%, H_2O/MeOH/HAc, pH 4.2. The peaks observed at m/z 119, 136 and 158 are assigned to the proton adduct of the deaminated adenine $[(Ad\text{-}NH_3)+H]^+$, and the proton and sodium adducts of adenine $[Ad+H]^+$ and $[Ad+Na]^+$, respectively. None of the peaks observed in the ESI MS of adenine in the same carrier solution (Figure 6-5) can be attributed to oxidation products of adenine (pK_a (N_7H) = 10.2) [Rogstad et al., 2003]. Neither did new peaks appear with application of EC cell voltage (up to 4 V) to this solution of adenine. Use of the relatively less acidic carrier solution 40/60 vol%, H_2O/MeOH, 1 mM NH_4Ac, pH 6.3 (Figure 6-6) revealed some new peaks, including those at m/z 271 and 309, assigned to the proton and potassium adducts of the adenine dimer $[2Ad+H]^+$ and $[2Ad+K]^+$. However, the application of EC cell voltage to the pH 6.3 solution produced multiple high mass peaks (data not shown) possibly due to adducts of multiple electron (up to $6e^-$) oxidation products of adenine with Na^+ and K^+ ions, made the mass spectrum too complex for meaningful analysis. The dimer peaks disappeared with increasing EC cell voltage, indicating oxidative decomposition. It has been reported by Dryhurst and Elving [1968] that adenine oxidation is an overall $6e^-$, $6H^+$ process, which they proposed occurred by sequential $2e^-$, $2H^+$ oxidations. The ESI MS results described here support the $1e^-$, $1H^+$ oxidation of adenine, which leads to transient $2e^-$, $2H^+$ oxidation products, similar to oxidation of uric acid (Chapter 4) and guanine (described in the preceding section).

Fragmentation and further electrochemical reactions of the intermediate $2e^-$, $2H^+$ oxidation product of adenine are known to be numerous [Dryhurst and Elving 1968] and this is reflected here by the complex EC/ESI MS mass spectra. Nevertheless, to the extent that adenine (pK_a = 10.2) undergoes $1e^-$, $1H^+$ oxidation at pH~6.3, to form the detected adenine dimer $[2Ad+H]^+$ (m/z 271) or $[2Ad+K]^+$ (m/z 309), a mechanism is proposed (Scheme 6-5).

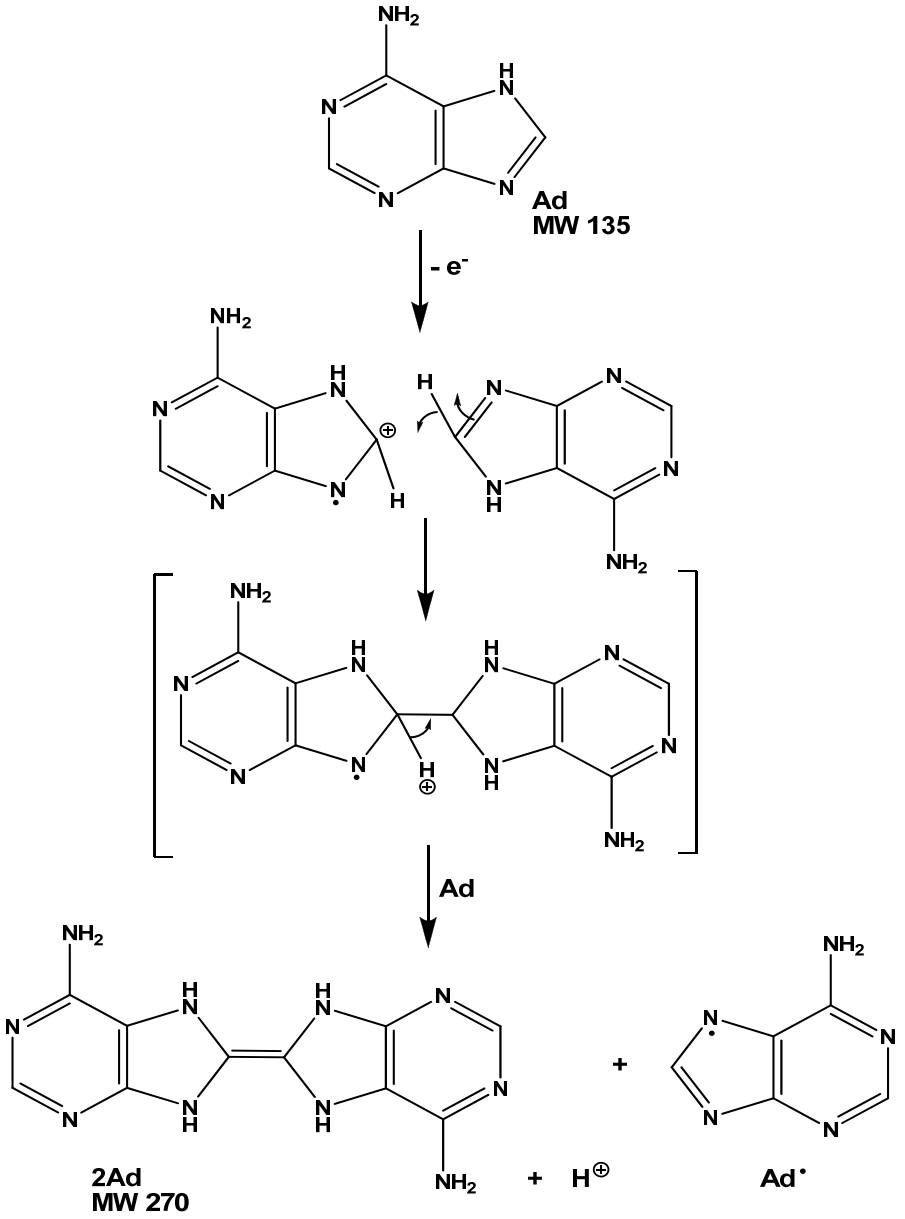

Scheme 6-5. Proposed mechanism of oxidation of adenine during positive mode ESI MS.

The ESI MS and EC/ESI MS of Hypoxanthine (hXan)

Because hypoxanthine is much less soluble in 50/49/1 vol%, H_2O/MeOH/HAc, pH 4.2 than in 40/60 vol%, H_2O/MeOH, 1 mM NH_4Ac, pH 6.3, this latter carrier solution was chosen for ESI MS and EC/ESI MS experiments. When prepared in 40/60 vol%, H_2O/MeOH, 1 mM NH_4Ac, pH 6.3 carrier solution, hypoxanthine (pK_{a1} = 8.6) [Budavari, 1989] gives two prominent peaks in the ESI MS mass spectrum (Figure 6-7). The peaks at m/z 137 and 273 are due to proton adducts of hypoxanthine $[hXan+H]^+$ and hypoxanthine dimer $[2hXan+H]^+$. Only a small $[hXan+H]^+$ (m/z 137) peak, which could not be reproduced well enough for meaningful analysis, was observed when using 50/49/1 vol%, H_2O/MeOH/HAc, pH 4.2 carrier solution, and the hypoxanthine dimer $[2hXan+H]^+$ (m/z 273) peak was not observed.

Like the other purines analyzed thus far, hypoxanthine appears to undergo $1e^-$, $1H^+$ oxidation during positive ion mode ESI (proposed mechanism shown in Scheme 6-6), although no $2e^-$, $2H^+$ oxidation products of hypoxanthine were detected even when voltage was applied to the EC cell. With increasing EC cell voltage, hypoxanthine is efficiently ionized and remains the base peak. New (unassigned) peaks appear in the mass spectrum at m/z values between 137 and 550, while the relative intensity of hypoxanthine dimer $[2hXan+H]^+$ (m/z 273) decreases (Figure 6-8) in the same manner as shown for dopamine, uric acid and guanine (Chapters 3, 4, and 6). It is possible that the later $1e^-$, $1H^+$ oxidation steps of hypoxanthine are kinetically more facile than hydrolysis or hydroxylation steps which form xanthine, and highly reactive species such as diimine are formed.

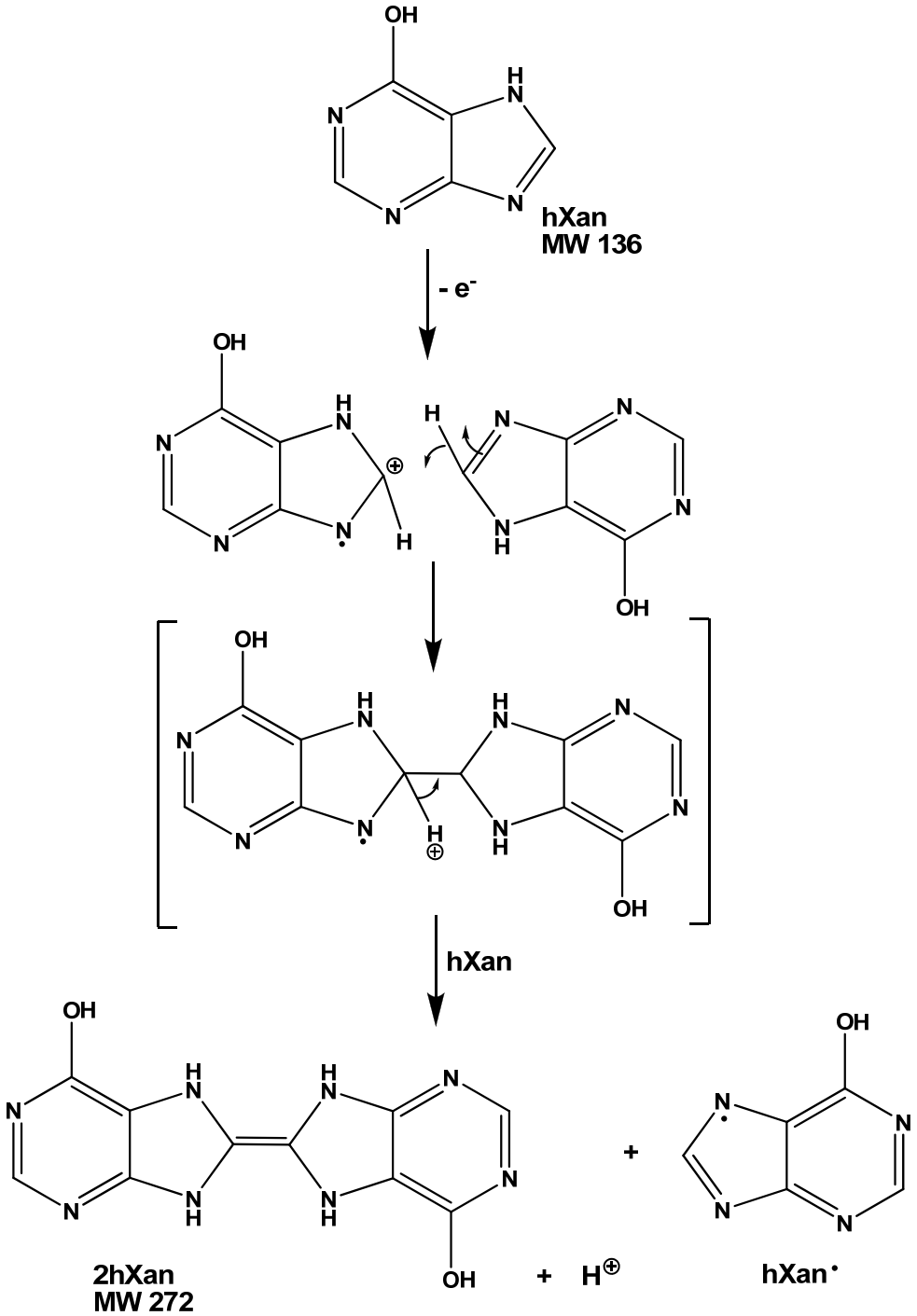

Scheme 6-6. Proposed mechanism of oxidation of hypoxanthine during positive mode ESI MS.

The ESI MS and EC/ESI MS of Xanthine (Xan)

Like hypoxanthine, xanthine is poorly soluble in low pH solutions and undergoes multiple electron (up to $4e^-$) oxidation overall [kathiwala et al., 2008]. Xanthine (50 μM) was prepared in

40/60 vol%, H_2O/MeOH, 1 mM NH_4Ac, pH 6.3, the same carrier solution used for hypoxanthine, and the mass spectrum shown in Figure 6-9 was obtained. In contrast to other purines, the ESI MS mass spectrum of xanthine indicates that it forms a dimeric radical which is detected as $[(2Xan\text{-}H)^{\bullet}+Na]^+$ (m/z 326). The presence of xanthine radicals supports a radical pathway of electrochemical oxidation of xanthine, recently proposed by Kathiwala et al [kathiwala et al., 2008] based on cyclic voltammetry. The dimeric radical intensity of xanthine increases slowly as applied EC cell voltage is increased (Figure 6-10). Similar to guanine, xanthine also forms an H-bonded tetramer with a sodium ion $[4Xan+Na]^+$ (m/z 631] at the center (Scheme 6-7).

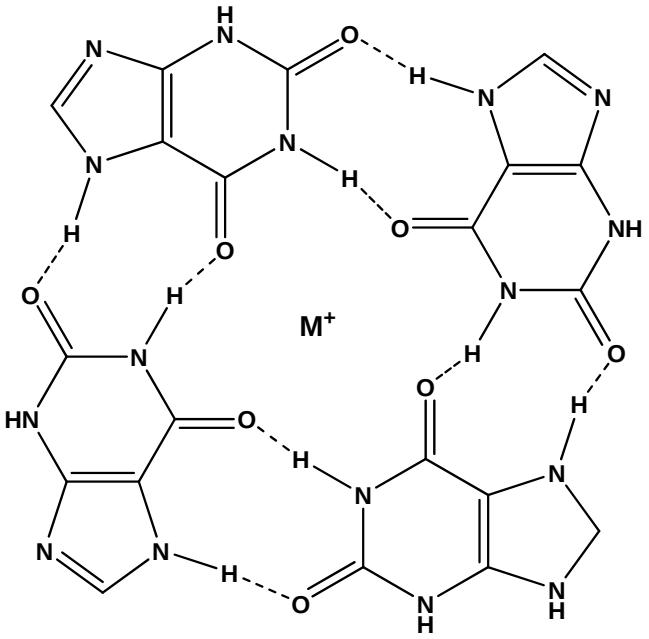

Xan tetramer
MW = 608+M+

Scheme 6-7. The H-bonded xanthine tetramer with a metal ion center (M^+ = sodium ion, Na^+)

The signal intensity of the H-bonded tetramer/sodium ion dduct $[4Xan+Na]^+$ decreases in intensity as the EC cell voltage increases (Figure 6-10), probably because it is oxidized. The proposed mechanism of formation of the dimeric xanthine radical is shown in Scheme 6-8.

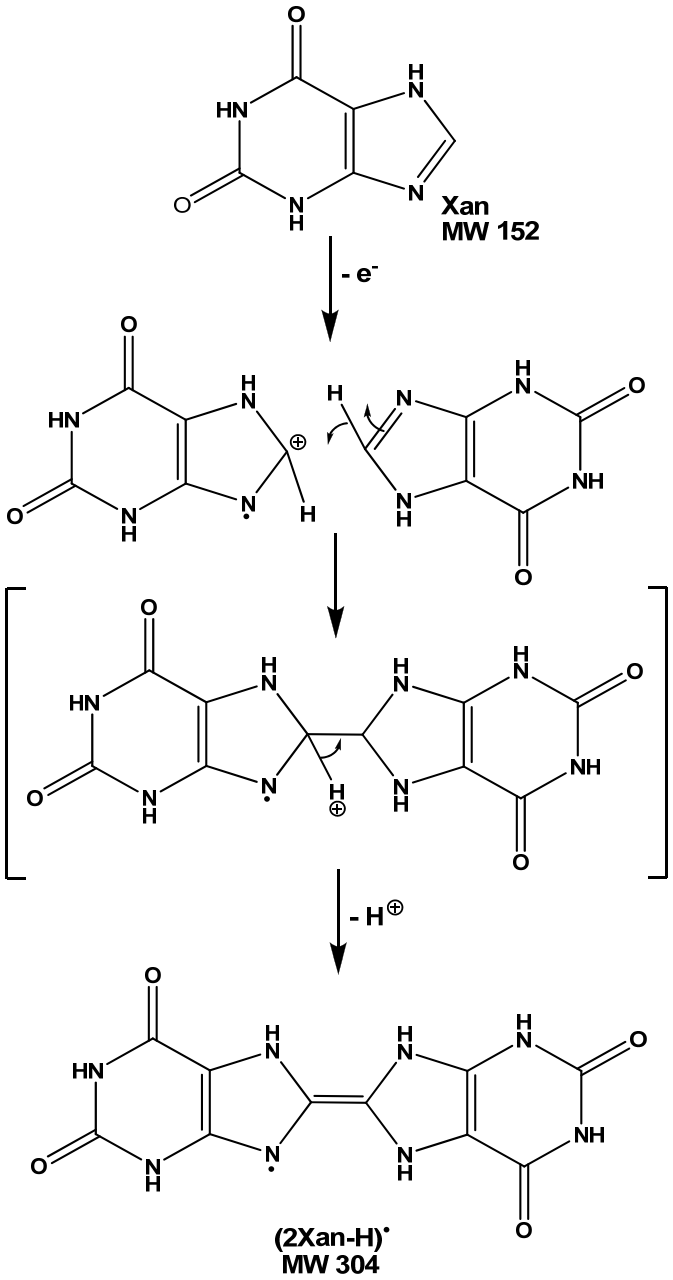

Scheme 6-8. Proposed oxidation mechanism of xanthine to xanthine radicals [Adapted from Kathiwala et al., 2008]. The final product (2Xan-H) is detected as a $[(2Xan\text{-}H)^{\bullet}+Na]^{+}$ (m/z 326).

Conclusions

The ESI MS and EC/ESI MS data presented in this chapter indicate that oxidation of purines does occur during positive ion mode ESI by stepwise $1e^{-}$, $1H^{+}$ losses. With the exception of xanthine, oxidations of purines appear to follow a general path illustrated in Scheme 6-9,

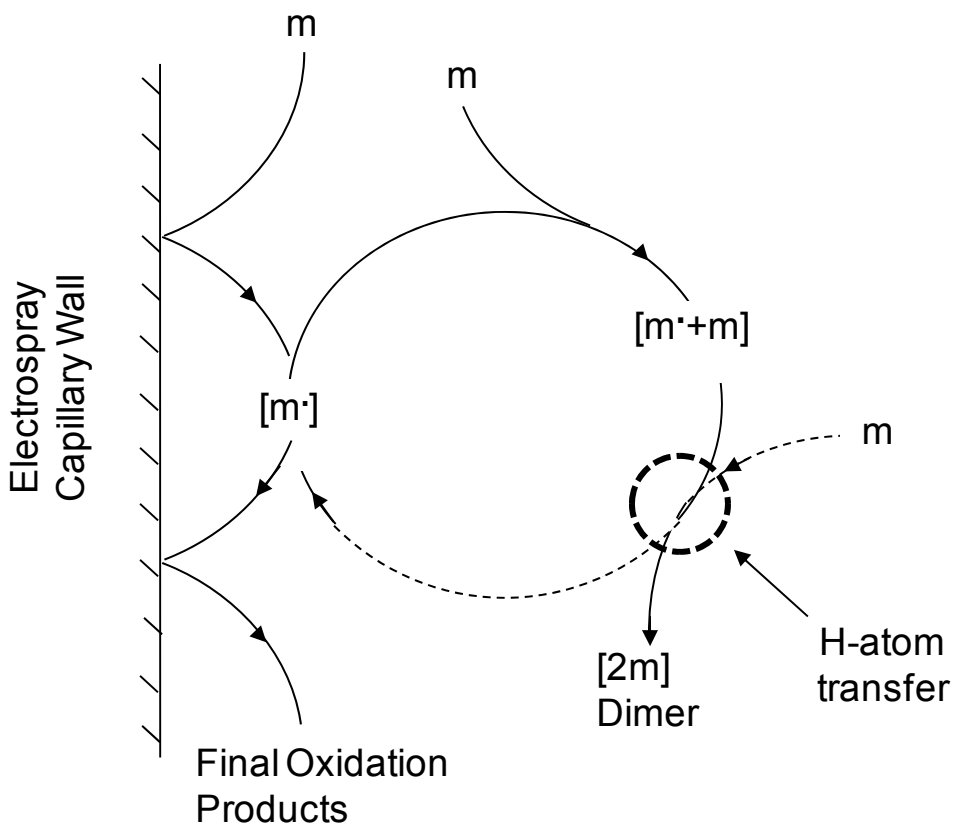

Scheme 6-9. Proposed general path of oxidation of purines during positive mode ESI MS (m = purine metabolite).

where the radical generated by the initial $1e^-$, $1H^+$ oxidation step attacks an unoxidized purine to stabilize and by so doing forms the dimeric radical.

Through hydrogen bonding with a third unoxidized purine, a hydrogen atom is transfered to the dimeric radical thereby forming a neutral purine dimer. The neutral purine radical resulting from H-atom transfer to the dimeric radical either combines with another unoxidized purine molecule in a cycle (Scheme 6-9), or it undergoes the second $1e^-$, $1H^+$ oxidation step to form a $2e^-$, $2H^+$ oxidation product and subsequent products, if the $2e^-$, $2H^+$ oxidation product is not stable.

Hydrogen bonding between two purine molecules is apparently not favored because the two molecules are required to be perpendicular to one another. The favorable H-bonding arrangement is one where four purine molecules form a square. Higher stability is reached with a metal ion in the center. The tetramer arrangement observed in the guanine and xanthine cases is evidence of this peculiar H-bonding. Antecedent also supports the proposition that the observed purine dimers are electrochemically generated, which is also indicated by the positive response when voltage is applied to the EC cell leading to the observed $2e^-$, $2H^+$ products.

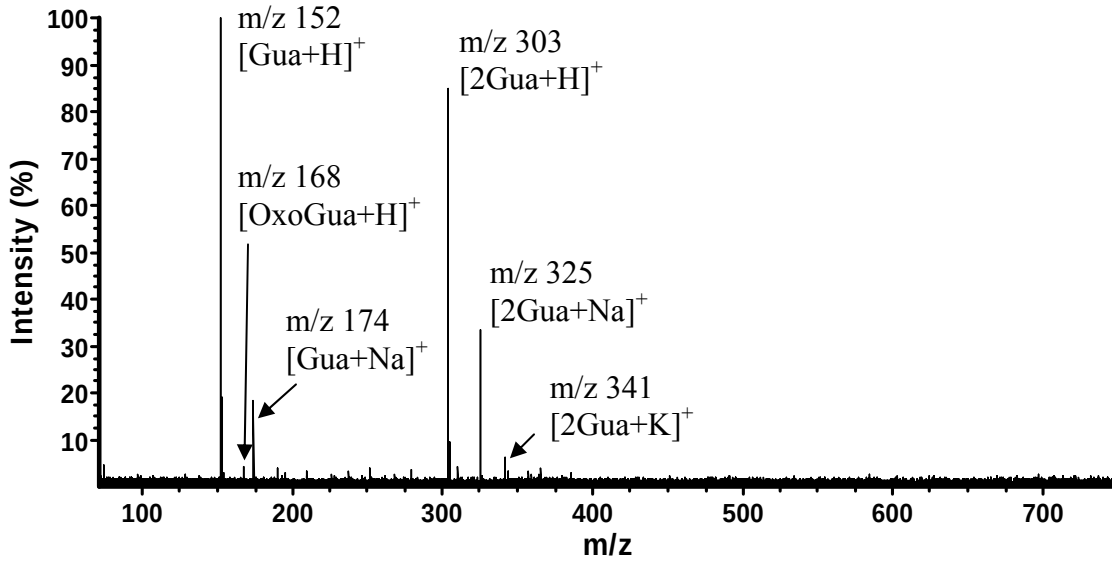

Figure 6-1. The ESI MS of guanine (50 μM) in 50/49/1 vol%, H_2O/MeOH/HAc, pH~4.2; HV 3 kV; Flow rate 30 μL/h.

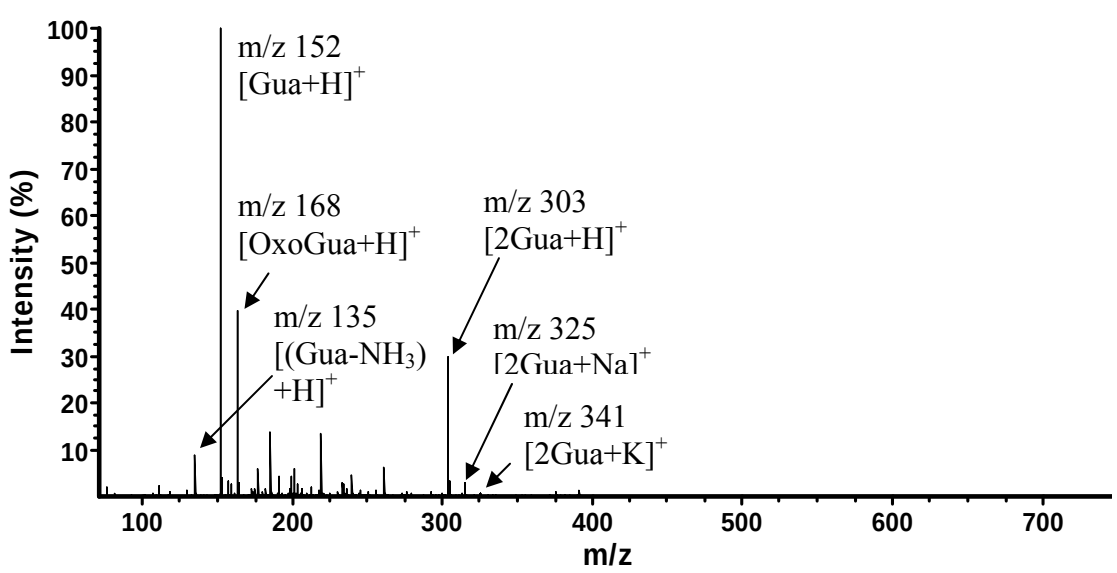

Figure 6-2. The EC/ESI MS of guanine (50 μM) in 50/49/1 vol%, H_2O/MeOH/HAc, pH~4.2; HV 3 kV; Flow rate 30 μL/h; EC cell voltage 1.5V.

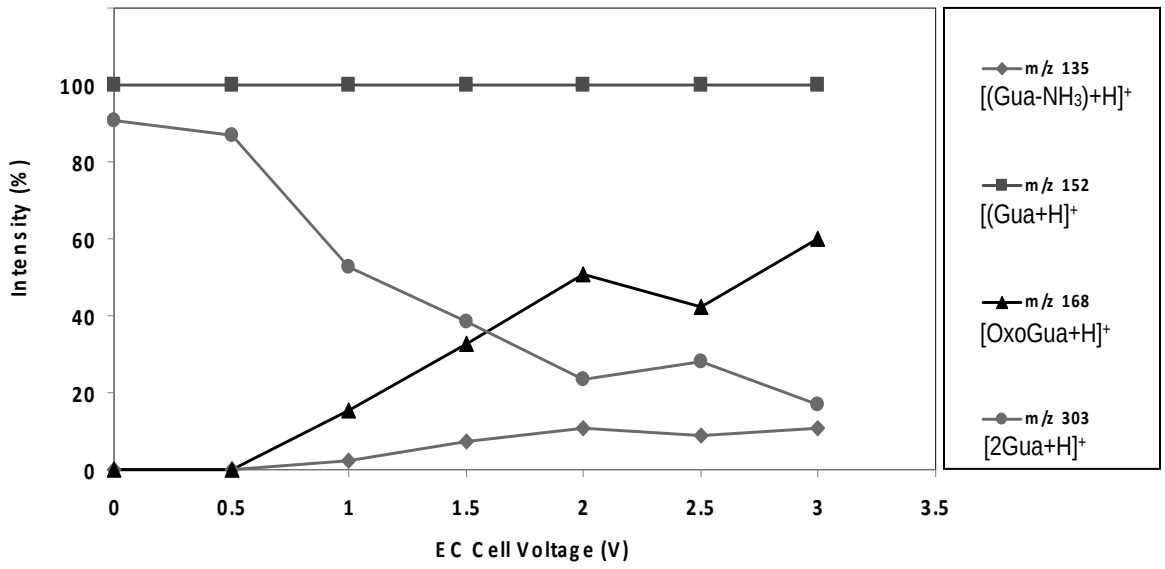

Figure 6-3. The EC/ESI MS of guanine (50 μM). Other conditions as in Figure 6.2.

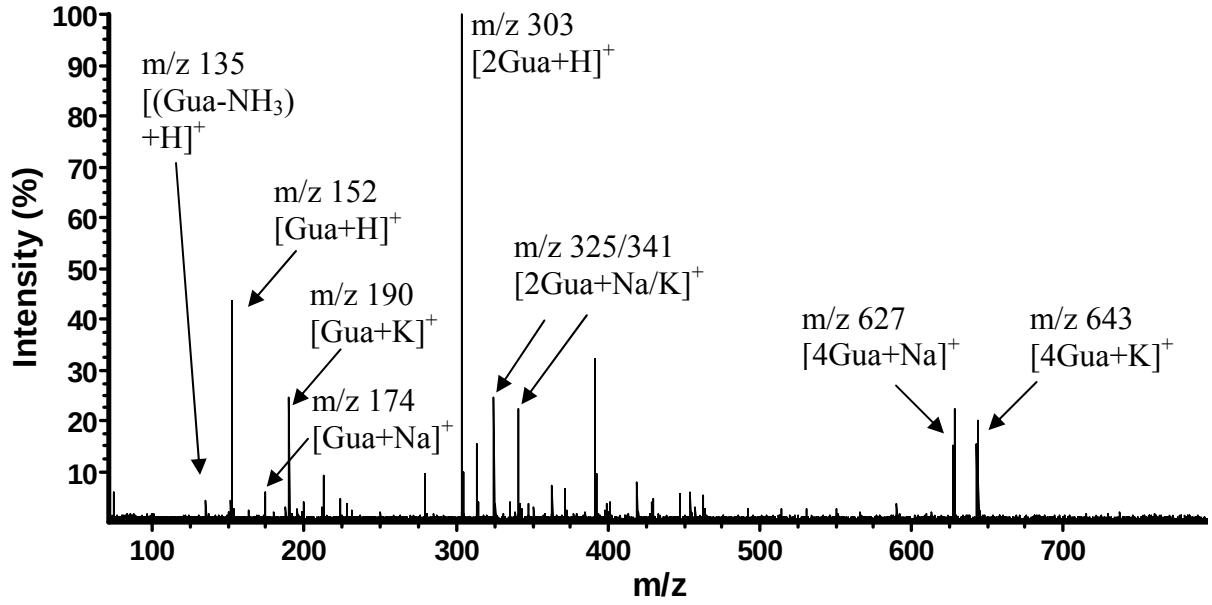

Figure 6-4. The ESI MS of guanine (50 μM) in 40/60 vol%, H_2O/MeOH, 1 mM NH_4Ac, pH~6.3; HV 3 kV; Flow rate 50 μL/h.

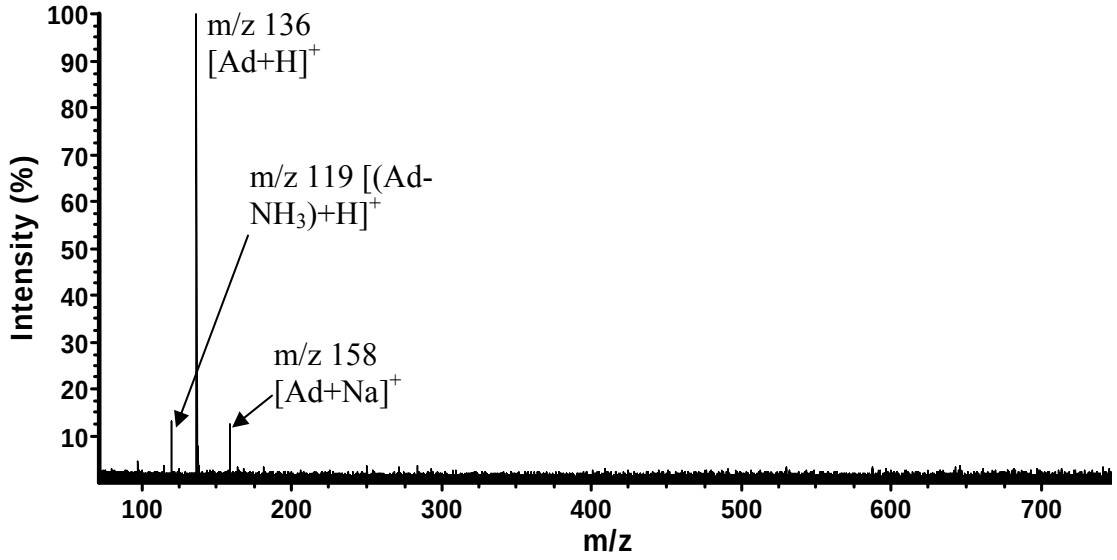

Figure 6-5. The ESI MS of adenine (50 μM) in 50/49/1 vol%, H_2O/MeOH/HAc, pH 4.2; HV 3 kV; Flow rate 30 μL/h; EC cell voltage 1.5V.

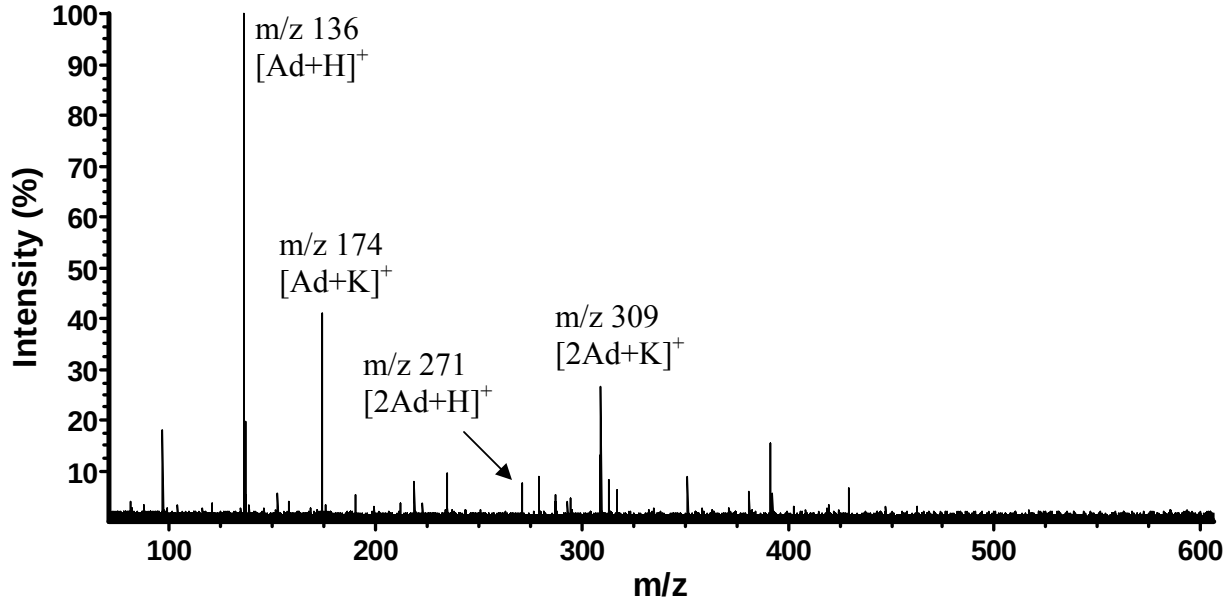

Figure 6-6. The ESI MS of adenine (50 μM) in 40/60 vol%, H_2O/MeOH, 1 mM NH_4Ac, pH 6.3. Other conditions as in Figure 6-4.

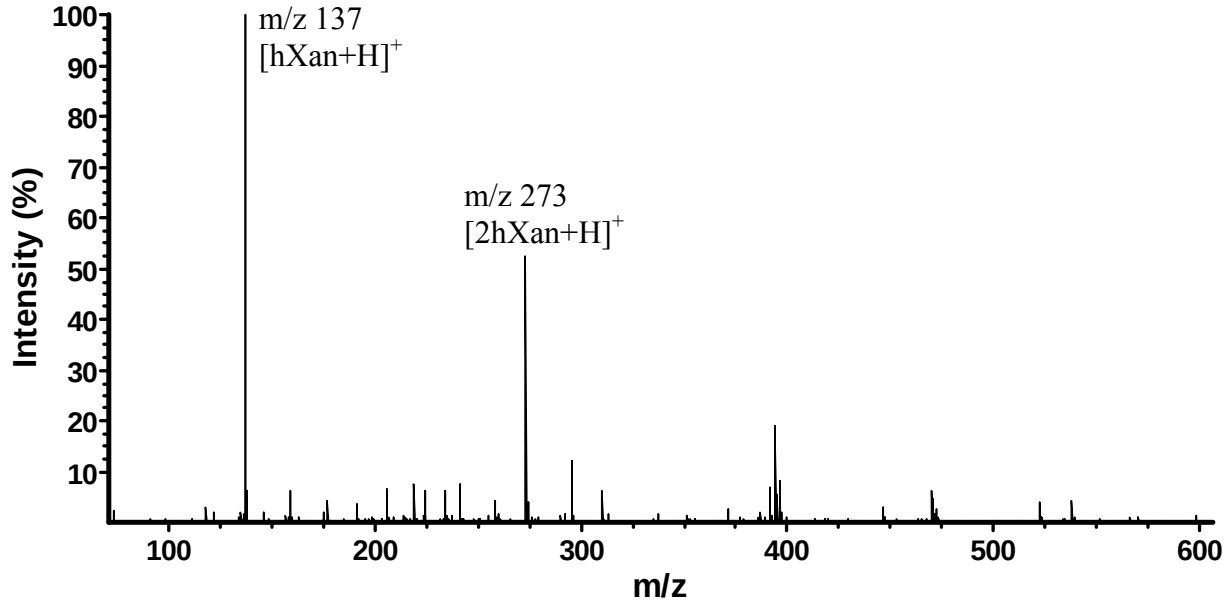

Figure 6-7. The ESI MS of hypoxanthine (50 μM) in 40/60 vol%, H_2O/MeOH, 1 mM NH_4Ac, pH 6.3. Other conditions as in Figure 6-4.

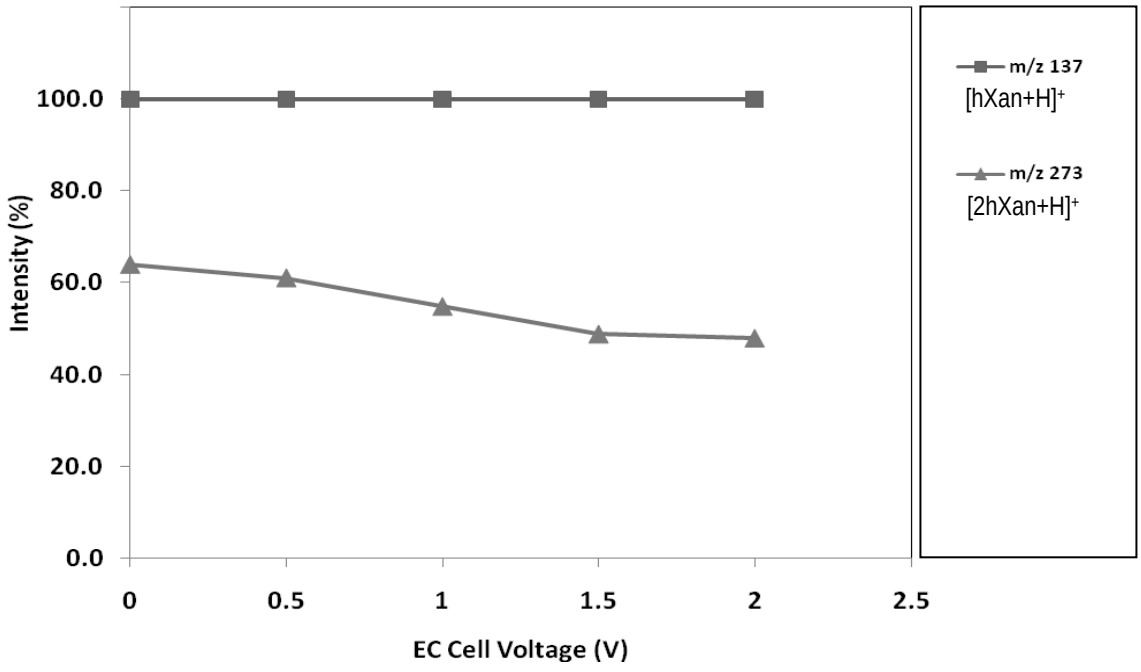

Figure 6-8. The EC/ESI MS of hypoxanthine (50 μM). Other conditions as in Figure 6-4.

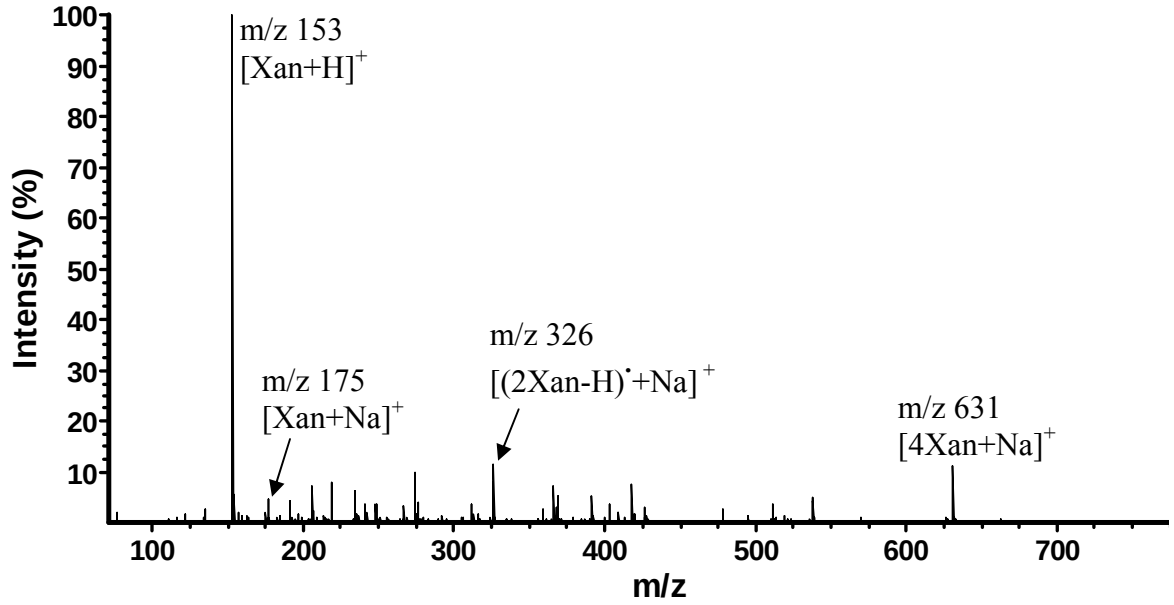

Figure 6-9. The ESI MS of xanthine (50 μM) in 40/60 vol%, H_2O/MeOH, 1 mM NH_4Ac, Other conditions as in Figure 6-4.

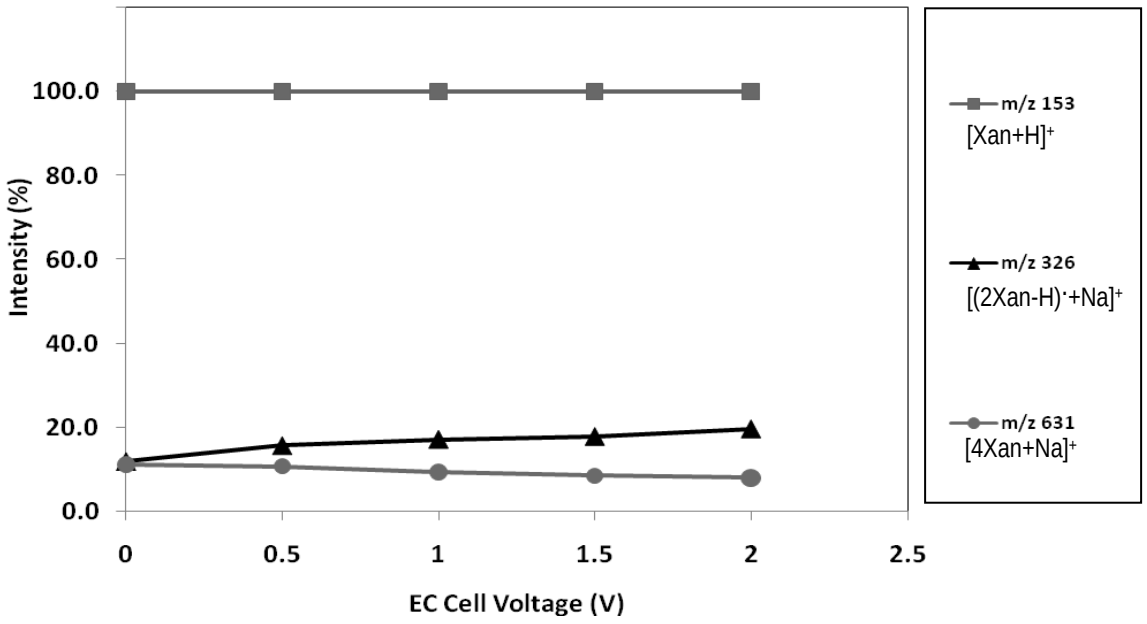

Figure 6-10. The EC/ESI MS of xanthine (50 μM). Other conditions as in Figure 6-4.

CHAPTER 7
CONCLUSIONS

A novel, integrated on-line EC/ESI MS system with adjustable EC cell voltage was developed in this work. It is a robust system for detection of many types of analytes, including neutrals and negatively charged analytes, which were previously regarded as outside the domain of positive ion mode ESI MS. The on-line electrochemical cell was integrated into the electrospray needle by dividing the needle into two sections and joining them with plastic tubing as described in Chapter 2. The EC cell voltage made it possible to augment the electrochemical processes that are inherent to the ESI operation for sensitivity enhancement and elucidation of electrochemical reactions. As indicated by the cited literature, others have sought to suppress electrochemistry of the electrospray ion source to avoid oxidation of analytes with limited success. The approach adopted in the present work was to augment this inherent electrochemistry and actually understand how it affects analytes in order to use ESI MS more effectively for bioanalytical work and chemical analysis in general. The EC/ESI MS results of dopamine discussed in Chapter 3 showed that applied EC cell voltage allows electrochemical reactions at the back-end of the ESI needle, in addition to those occurring at the tip. This increases the active surface area of the electrode (i.e. the ES needle), as reflected by up to 100% increase in ES current and improved ionization efficiency.

While substantial, the extent to which the ESI MS signal was enhanced by application of EC cell voltage in EC/ESI MS was a factor of eight less than the signal enhancement achieved by using a cone-shaped MS capillary inlet instead of a standard cylindrical inlet. The large, cone-shaped orifice (about 2.5 cm depth) allows 100% collection of the electrospray vapor from an 80 μm internal diameter (i.d.) electrospray needle positioned 0–5mm away. The ES needle can be 0 mm away from the MS inlet and still allow an air gap for electrospray, because the needle

diameter (~ 100 μm) is much smaller than the 6.1 mm orifice diameter of the MS inlet. With appropriate carrier solution flow rate and conductivity, it is believed that this arrangement can ensure 100% collection of the electrospray plume. However, collection efficiency does not exactly translate into ion transmission efficiency, because of electrostatic attraction of positively charged ions to the relatively negative MS inlet and subsequent neutralization. More precisely, the MS inlet is held at a positive potential which is less than the applied needle voltage. It is more appropriate then, to talk of electrostatic repulsion from the ES needle tip and migration of ions in the electric field gradient across the interface, rather than electrostatic attraction to the MS inlet. If the latter were the predominant case, most ions would simply be pulled from the axial center to the MS inlet surface/wall and not enter the mass spectrometer.

Ion formation mechanisms have been elucidated to varying degrees in this work. The validity of assignments of various ions was verified by close matches of measured and throretical isotope distributions, as well as by hydrogen/deuterium (H/D) exchange experiments. In the case of dopamine and uric acid, infra-red multiple photon dissociation (IRMPD) followed by tandem mass spectrometric (MS/MS) analyses was also performed. By itself, MS/MS evidence was not conclusive but did not disprove the covalent nature of the electrochemically generated dopamine and uric acid dimers. The numbers of exchangeable hydrogens, determined by H/D exchange experiments, were in perfect agreement with those in proposed covalently linked dimers which differ by at least two hydrogens (i.e. 2 mass units) from their hydrogen bonded counterparts. In the case of dopamine, a hydrogen-bonded dimer would be doubly charged in the carrier solution used, considering the pH of the solution and the pK_a values of dopamine. The clear effect of applied EC cell voltage reflected in the signal intensity vs applied EC cell voltage curves, as well as the appearance of both covalently bonded disulfide dimers and hydrogen bonded thiol dimers,

are evidence of electrochemical activity and the presence of electrochemically generated covalently bonded dimers.

Mechanisms of formation of ions of the different analytes observed in their ESI MS mass spectra were proposed in this work, both individually and in generic terms. The ESI MS data indicate, as reflected by the proposed mechanisms, that oxidation of all the analytes considered in this work proceeds by discrete $1e^-$, $1H^+$ losses. Positive ion mode ESI is a radiation-free technique to generate radicals and study their reactions, particularly those involving biological molecules in aqueous milieu. Analytes with pendant groups, such as dopamine and glutathione, undergo fragmentation with cleavage of the pendant groups. More fragments are observed for larger molecules such as glutathione. Products from the second $1e^-$, $1H^+$ losses, where applicable, were observed as minor peaks, which could be an indication that this step is kinetically slow during ESI. Analytes known to involve more than $2e^-$, $2H^+$, which have relatively high oxidation potentials, such as adenine and xanthine, tend to produce complex mass spectra, and further work is required to elucidate all the oxidation steps using ESI MS.

Future work could include the application of the EC/ESI MS system developed in this work to analysis of real biological samples such as cells. With better understanding of all factors affecting analyte detectability in ESI MS, particularly ion intensity/ES current as a function of concentration, calibration curves could be constructed for analytical determinations.

> Understanding is a mental process. If mental processes are electrochemical in nature, then the answer to the question, 'Is electrochemistry essential to the understanding of electrospray ionization?' would be 'Yes,' irrespective of any relation, or lack thereof, between electrochemistry and the electrospray process. – John Fenn [in Electrochemical processes in electrospray ionization mass spectrometry – Special Feature: Discussion, J. Mass Spectrom. 2000, 35, 939 – 952]

LIST OF REFERENCES

Aebersold, R.; Mann, M. *Nature* **2003**, *422*, 198.

Alderman, M. Kala, J. V. A. *Curr. Med. Res. Opinion* **2004**, *20*, 369.

Allen, R. N.; Shukla, M. K.; Leszczynski, J. *Int. J. Quant. Chem.* **2004**, *100*, 801.

Ames, B. N.; Cathcart, R.; Schwiers, E.; Hochstein, P. *Proc. Nat. Acad. Sci.USA*, **1981**, *78*, 6858.

Anderson, R. F.; Harris, T. A.; *Free Rad. Res.* **2002**, *37*, 1131.

Aplin, K. L. *Rev. Sci. Instrum.* **2005**, *76*, 104501-1.

Arakawa, R. Yamaguchi, M. Hotta, H. Osakai, T. Kimoto, T. *J. Am. Soc. Mass Spectrom.* **2004**, *15*, 1228.

Arnobe, M. G.; Luth, M. S.; Roitzsch, M.; Cerda, M. M.; Lax, P.; Kampf, G.; Sigel, H.; Lippert, B. *Chem. Eur. J.* **2004***, 10*, 1046.

Bald, E. B. *J. Chromatogr. A* **2004**, *1032*, 109.

Bard, A. J.; Faulkner, R. L. *Electrochemical Methods*, 2nd ed, John Wiley & Sons, 2001.

Baykut, G.; Eyler, J. R. *Trends Anal. Chem.* **1986**, *5*, 44.

Becerra, A.; Lazcano, A. *Orig. Life Evol. Bios.* **1998**, *28*, 539.

Benavente, F. van der Heijden, R. Tjaden, U. R. van der Greef, J. Hankemeier, T. *Electrophoresis* **2006**, *27*, 4570.

Binyamin, G. Chen, T. Heller, A. *J. Electroanal. Chem.* **2001**, *500*, 604.

Blackley, C. R.; Vestal, M. L. *Anal. Chem.* **1983**, *55*, 750.

Blades, T.; Ikonomou, M. G.; Kebarle, P. *Anal. Chem.* **1991**, *64*, 2109.

Blakney, G. T.; Robinson, D. E.; Ly, N. V.; Kelleher, N. L., Hendrickson, C. L.; Marshall, A. G. *Predator: PCI Data Station for FT-ICR Mass spectrometry, 53rd Amer. Soc. Mass Spectrom. Ann. Conf. on Mass Spectrom. & Allied Topics,* San Antonio, TX, June 4-9 (2005) *(Poster)*.

Blank, C. L.; McCreery, R. L.; Wightman, R. M.; Chey, W.; Adams, R. N.; Reid, J. R. E. E. Smissman, *J. Med. Chem.* **1976**, *19*, 178.

Bogdanov, B.; Smith, R. D. *Mass Spectrom. Rev.* **2005**, *24*, 168.

Bond, A. M.; Colton, R.; D'Agostino, A.; Downard, A. J.; Traeger, J.C. *Anal. Chem.* **1995**, *67*, 1691.

Bouligand, J.; Deroussent, A.; Paci, A.; Morizet, J.; Vassal, G. *J. Chromatogr. B* **2006**, *832*, 67.

Bravo, R.; Hsueh, C.; Jaramillo, A.; Brajter-Toth, A. *Analyst* **1998**, *123*, 1625.

Brockman, T. J.; Anderson, L. B. *Anal. Chem.* **1984**, *88*, 2.

Bruckenstein, S.; Gadde, R. R. *J. Am. Chem. Soc.* **1971**, *93*, 793.

Budavari, S.; O'Neil, M. J.; Smith, A.; Heckelman, P. E., Eds. *The Merck Index*, 11th ed. Merck & Co. Inc., New Jersey, 1989.

Buettner, G. R.; Jerkiewicz, A. A. *Radiation Res.* **1996**, *145*, 532.

Camera, E.; Picardo, M. *J. Chromatogr. B* **2002**, *781*, 181.

Cappiello A.; Bruner, F. *Anal. Chem.* **1993**, *65*, 1281.

Cavalheiro, E, T. G.; Brajter-Toth, A. *J. Pharm. Biomed. Anal.* **1999**, *19*, 217.

Cech, N. B.; Enke, C. G. *Mass Spectrom. Rev.* **2001**, *20*, 362.

Constentin, C.; Robert, M.; Saveant, J. *J. Am. Chem. Soc.* **2007**, *129*, 5870.

Cotton, F. A.; Wilkinson, G.; Gaus, P. L. *Basic Inorganic Chemistry 2nd Ed.*, John Wiley & Sons, New York 1987, p672.

Creaser, C. S.; Stygal, J. W. *Analysis* **1993**, *118*, 1467.

Curello, S.; Ceconi, C.; Cargnoni, A; Cornacchiari, A.; Ferrari, R.; Albertini, A. *Clin. Chem.* **1987**, *33*, 1448.

de la Mora J. F. *J. Fluid Mech.* **1992**, *243*, 561.

Demuth, K.; Drunat, S.; Girerd, X.; Moatti, N; Paul, J-. L.; Safar, M; Boutouyrie, P. *Atherosclerosis* **2002**, *165*, 167.

Deng, H.; Van Berkel, G. J. *Electroanalysis* **1999**, *11*, 857.

Diehl, G.; Karst, U. *Anal. Bioanal. Chem.* **2002**, *373*, 390.

Dole, M.; Mack, L. L.; Hines, R. L.; Mobley, R. C.; Ferguson, L. D.; Alice, M. B. *J. Chem. Phys.* **1968**, *49*; 2240.

Dryhurst, G. *J. Electrochem. Soc.* **1969**, *116*, 1411.

Dryhurst, G.; Elving, P. *J. Electrochem. Soc.* **1968**, *115*, 1014.

Dutt, J. S. N.; Cardosi, M. F.; Davis, J. *Analyst*, **2003**, *128*, 811.

Edwards, J. L.; Chisolm, C. N.; Shackman, J. G.; Kennedy, R. T. *J. Chromatogr. A* **2006**, *1106*, 80.

Ejaz, A. A.; Mu. W.; Kang, D. H.; Roncal, C.; Sautin, Y. Y.; Henderson, G.; Tabah-Fisch, I.; Keller, B.; Beaver, T. M.; Nakagawa, T.; Johnson, R. J. *Clin. J. Am. Soc. Nephrol.* **2007**, *2*, 16.

Fenn, J. B. *Angew. Chem. Int. Ed.* **2003**, *42*, 3871.

Fenn, J. B.; Mann, M.; Meng, C. K.; Wong, S. F.; Whitehouse, C. M. *Mass Spectrom. Rev.* **1990**, *9*, 37.

Fenn, J. B.; Mann, M.; Meng, C. K.; Wong, S. F.; Whitehouse, C. M. *Science* **1989**, *246*, 64.

Ford, E. S.; Li, C. Y.; Cook, S.; Choi, H. K. *Circulation*, **2007**, *115*, 2526.

Forman, H. J.; Dickinson, D. A. *Biofactors* **2003**, *17*, 1.

Gamache, P. H. Meyer, D. F. Granger, M. C. Acworth, I. N. *J. Am. Soc. Mass. Spectrom.* **2004**, *15*, 1717.

Garcia, S. C.; Schott, K.; Charao, M.; Moro, A.; Bulcao, R.; Grotto, D.; Valentini, J.; Bohrer, D.; Cardoso, S.; Pomblum, V. *Biomed. Chromatogr.* **2008**, *22*, 460.

Gerhardt, R.; Adams, N. *Anal. Chem.* **1982**, *54*, 2618.

Getek, T. A.; Korfmacher W. A.; McRae, T. A.; Hinson, J. A. *J. Chromatogr. A* **1989**, *474*, 245.

Gilbert, H. F. *Methods Enzymol.* **1995**, *251*, 8.

Giustrarini, D.; Milzani, A.; Dalle-Donne, I.; Rossi, R. *Blood Cells, Molecules & Diseases* **2008**, *40*, 174.

Glish, G. L.; Vachet, R. W.; *Nature*, **2003**, *2*, 140.

Grosshans, P. B.; Marshall, A. G. *Int. Mass Spectrom.* **1991**, *107*, 49.

Gucek, M.; Makuc, S.; Mlakar, A.; Berincnik-Vrbovsek, J.; Marsel, J. *Rapid Commun. Mass Spectrom.* **2002**, *16*, 1186.

Hambitzer, G.; Heitbaum, J. *Anal. Chem.* **1986**, *58*, 1067.

Harris, D. C. *Quantitative Chemical Analysis*, 4th ed, W.H. Freeman & Co., New York 2007.

Hartman, S. Okun, J. G. Schmidt, C. Langhans, C. Carbade, S. F. Burgard, P. Haas, D. Sass, J. O. Nyhan, W. Hoffmann, G. F. *Clin. Chem.* **2006**, *526*, 1127.

Hawley, M. D.; Tatawadi, S. V.; Piekarski, S.; Adams, R. N. *J. Am. Chem. Soc.* **1967**, *89*, 447.

Hayden, M. R.; Tyagi, S. C. *Nutrition & Metabolism*, 2004, 1:10, http://www.nutritionandmetabolism.com/content/pdf/1743-7075-1-10.pdf

Hicks, M. Wong, L. S. Day, R. O. *Free Rad. Res. Comms.*, **1993**, *18*, 337.

Himmelfarb, J.; McMenamin, E.; McMongle, E. *Kidney Int.* **2002**, *61*, 705.

Hooper, D. C. Scott, G. S. Zborek, A. Mikheeva, T. Kean, R. B. Koprowski, H. Spitsin, S. V. *FASEB* **2000**, *14*, 691.

Ikonomou, M. G.; Blades, A. T.; Kerbale, P. *Anal. Chem.* **1991**, *63*, 1989.

Iribane, J. V.; Thomson, B. A. *J. Chem. Phys.* **1976**, *64*, 2287.

Ito, T. van Kuilenburg, A. B. P. Bootsma, A. H. Haasnoot, A. J. van Cruchten, A. Wada, van Y. Gennip, A. H. *Clin. Chem.* **2000**, *46*, 445.

Griffiths, M. *J. Biol. Chem.* **1952**, *197*, 399.

Jackson, G. S.; Enke, C. G. *Anal. Chem.* **1999**, *71*, 3777.

Jencks, W. P.; Wolfenden, R. V. *Biogr. Mems Fell. R. Soc.* **2000**, *46*, 335.

Jiang, H.; Dolan, A. R.; Li, M.; Moy, M. A.; Gong, B.; Wood, T. D. Int. J. Mass Spectrom. **2007**, *261*, 13.

Jovanovic, S. C.; Simic, M. G. *J. Phys. Chem.* **1986**, *90*, 974.

Karas, M.; Hillenkamp, F. *Anal. Chem.* **1988**, *60*, 2299.

Karst, U. *Angew. Chem. Int. Ed.*, **2004**, *43*, 2476.

Kathiwala, M.; Affum, A. O.; Perry, J.; Brajter-Toth, A. *Analyst*, **2008**, *133*, 810.

Kebarle, P. *J. Mass. Spectrom.* **1997**, *32*, 922.

Kelly, R.; Page, J.; Tang, K.; Smith, R. *Anal. Chem.* **2007**, *79*, 4192.

Kemp, M.; Go, Y. -M. Jones D. P. *Free Radical Biol. Med.* **2008**, *44*, 921.

Kertesz, V.; Van Berkel, G. J. *J. Am. Soc. Mass Spectrom.* **2006**, *17*, 953.

Kertesz, V.; Van Berkel, G. J. *J. Solid State Electrochem.* **2005**, 9, 390.

Kertesz, V.; Van Berkel, G. J.; *J. Mass Spectrom.* **2001**, *36*, 204.

Kim, T.; Udseth, H.; Smith, R.; *Anal. Chem.* **2000**, *72*, 5014.

Konermann, L.; Silva, E. A.; Sogbein, O. F. *Anal. Chem.* **2001**, *73*, 4836.

Kupeli, S. Yurdakok, M. Kilinc, G. Bilgetekin, E. *Pediatr. Nephrol.* **2005**, *20*, 1361.

la Marca, G. B. Casetta, S. Malvagia, E. Pasquini, M. Innocenti, M. A. Donati, E. Zammarchi, *J. Mass Spectrom.* **2006**, *41*, 1442.

LaVoie, M. J.; Hastings, T. G. *J. Neurosci.* **1999**, *19*, 1484.

Li, Y.; Pozniak, B. P.; Cole, R. B. *Anal. Chem.* **2003**, *75*, 6987.

Liao, C. -Y.; Zen, J. –M. *Sens. Actuators B* **2008**, *129*, 896.

Liljegren, G.; Dahlin, A.; Zettersten, C.; Bergquist, J.; Nyholm, L. *Lab Chip* **2005**, *5*, 1008.

Linert, W.; Herlinger, E.; Jameson, R. F.; Kienzl, E.; Jellinger, K.; Youdim, M. B. H. *Biochim. Biophys. Acta* **1996**, *1316*, 160.

Liu, D. Q.; Wu, L.; Sun, M.; MacGregor, P. A. *J. Pharm. Biomed. Anal.* **2007**, *44*, 320.

Liu, M.; Li, P.; Cheng, Y.; Xian, Y.; Jin, L. *Anal. Bioanal. Chem.* **2004**, *380*, 742.

Lohman, W.; Karst, U. *Anal. Bioanal. Chem.* **2008**, *391*, 79.

Lu, W.; Xu, X.; Cole, R. B. *Anal. Chem.* **1997**, *69*, 2478.

Mack, L. L.; Kraklik, P.; Rheude, A.; Dole, M. *J. Chem. Phys.* **1970**, *52*; 4977.

Maleknia, S. D.; Chance, M. R.; Downard, K. M. *Rapid Commun. Mass Spectrom.* **1999**, *13*, 2352.

Manet, I.; Francini, L.; Masiero, S.; Pieraccini, S.; Spada, G. P.; Gottarelli, G. *Helvetica Chim. Acta*, **2001**, *84*, 2096.

Maples, K. R. Mason R. P. *J. Biol. Chem.* **1988**, *263*, 1709.

Marshall, A. G.; Comisarow, M. *Chem. Phys. Lett.* **1974**, *25*, 282.

Marshall, A. G.; Hendrickson, C. L.; Jackson, G. S. *Mass Spectrom. Rev*. **1998**, *17*, 1.

Mautjana, N. A. Estes, J. Eyler, J. R. Brajter-Toth, A. *Electroanalysis* **2008a**, 20, 1959.

Mautjana, N. A.; Estes, J.; Eyler, J. R.; Brajter-Toth, A. *Electroanalysis* **2008b**, *In Press*.

Meister, A. *Science* **1983**, *220*, 472.

Mentasti, E. Rinaudo, C. Boistelle, R. *J. Chem. Eng. Data* **1983**, *28*, 247.

Moini, M.; Cao, P.; Bard, A. J.; *Anal. Chem.* **1999**, *71*, 1658.

Mutoh, M.; Kieda, S.; Kmimura, K. *J. Appl. Phys.* **1979**, *50*, 3174.

Nekrassova, O.; Lawrence, N. S.; Compton, R. G. *Talanta*, **2003**, *60*, 1085.

Nemes, P.; Marginean, I.; Vertes, A. *Anal. Chem.* **2007**, *79*, 3105.

Nolin, T. D.; McMenamin, M. E.; Himmelfarb, J. *J. Chromatogr. B* **2007**, *852*, 554.

Nyhan, W. L.; *Mol. Genet. Metab*., **2005**, *86*, 25.

Ochran, R. A.; Konermann, L. *J. Am. Soc. Mass Spectrom.* **2004**, *15*, 1747.

Ogasawara, Y.; Mukai, Y.; Togawa, T.; Suzuki, T.; Tanabe, S.; Ishii, K. *J. Chromatogr. B* **2007**, *845*, 157.

Okumura, L. L.; Stradiotto, N. R.; Rees, N. V.; Compton, R. G. *Electroanalysis* **2008**, *8*, 916.

Oliviera-Brett, A. M.; Diculescu, V.; Piedade, J. A. P. *Bioelectrochemistry* **2002**, *55*, 61.

Owens, J. L.; Dryhurst, G. *Anal. Chim. Acta* **1977**, *89*, 609.

Pacsial-Ong, E. J.; McCarley, R. L.; Wang, W.; Strongin, R. M. *Anal. Chem.* **2006**, *78*, 7577.

Pascual, E.; Batlle-Gualda, E.; Martínez, A.; Rosas, J.; Vela, P. *Ann. Internal Med.* **1999**;*131*, 756.

Permentier, H.; Bruins, A. P.; Bischoff, R. *Mini-Rev.Med. Chem.* **2008**, *8*, 46.

Phillips, W. D.; Poe, M.; Weiher, J. F.; McDonald, C. C.; Lovenberg, W. *Nature*, **1970**, *227*, 574.

Pozniak, B. P.; Cole, R. B. *J. Am. Soc. Mass Spectrom.* **2004**, *15*, 1737.

Pozniak, B. P.; Cole, R. B. *J. Am. Soc. Mass Spectrom.* **2007**, *18*, 737.

Price, W. D.; Schnier, P. D.; Williams, E. R. *Anal. Chem.* **1996**, *68*, 859.

Rahman, I.; Biswas, S. K.; Jimenez, Luis, A.; Torres, M.; Forman, H. J. *Antioxid. Oxidation Signal.* **2005**, *7*, 42.

Regino, M. C. S.; Brajter-Toth, A. *Anal. Chem.* **1997**, *69*, 5067.

Rogstad, K. N.; Jang, Y. H.; Sowers, L. C.; Goddard, W. A. *Chem. Res. Toxicol.* **2003**, *16*, 1455.

Rohner, T. C.; Lion, N.; Girault, H. H. *Phys. Chem. Chem. Phys.* **2004**, *6*, 3056.

Rose, K.; Shndle, S. E.; Eidsness, M. K.; Kurtz, D. M. Jr; Scott, R.; Hedman, B.; Hodgson, K. O.; Solomon, E. I. *J. Am. Chem. Soc.* **1998**, *120*, 10743.

Roussel, C.; Dayon, L.; Lion, N.; Rohner, T.; Josserand, J.; Rossier, J. S.; Jensen, H.; Girault, H. H. *J. Am. Soc. Mass Spectrom.* **2004**, *15*, 1767.

Rubino, F. M.; Pitton, M.; Brambilla, G.; Colombi, A. *J. Mass Spectrom.* **2006**, *41*, 1578.

Rubino, F. M.; Verduci, C.; Giampiccolo, R.; Pulvirenti, S.; Brambilla, G.; Colombi, A. *J. Am. Soc. Spectrom.* **2004**, *15*, 288.

Sahlin, E.; Beisler, A. T.; Webber, S. G.; Sandberg, M. *Electrochemical Detection of Peptides*, p367 – 398 in *Electroanalytical Methods for Biological materials*, Marcel Dekker, New York, 2002, Editors: Brajter-Toth, A.; Chambers, J. Q.

Samiec, P. S.; Drews-Botsch, C.; Flagg, E. W.; Kurtz, J. C.; Sternberg, P.; Reed, R. L.; Jones, D. P. *Free Radic. Biol. Med.* **1998**, *24*, 699.

Sanchez-Rivera, A. E.; Corona-Avendano, S.; Alarcon-Angeles, G.; Rojas-Hernandez, A.; Ramirez-Silva, M. T.; Romero-Romo, M. A. *Spectrochim. Acta. A* **2003**, *59*, 3193.

Schafer, F. Q.; Buettner, G. R. *Free Radical Biol. Med.* **2001**, *30*, 1191.

Schneider, B. B.; Douglas, D. J.; Chen, D. D. Y. *Rapid Commun. Mass Spectrom.* **2001**, *15*, 2168.

Seiwert, B.; U. Karst, *Anal. Chem.* **2007**, *79*, 7131.

Senko, M. W. Canterbury, J. D. Guan, S. Marshall, A. G. *Rapid Commun. Mass Spectrom.* 1996, *10*, 1839.

Shen, X. M.; Dryhurst, G. *Tetrahedron* **2001**, *57*, 393.

Shen, X.; Dryhurst, G. *Bioorg. Chem.* **1996a**, *24*, 340.

Shen, X.; Dryhurst, G. *J. Med. Chem.*, **1996b** *39*, 2018.

Shen, X.; Xia, B.; Wrona, Z.; Dryhurst, G.; *Chem. Res. Toxicol* **1996**, *9*, 1117.

Shen, Y.; Smith, R. D.; Unger, K. K.; Kumar, D.; Lubda, D. *Anal. Chem.* **2005**, *77*, 6692.

Shi, Y. Evans, J. E. Rock, K. L. *Nature* **2003**, *425*, 516.

Sica, D. A.; Schoolwerth, A. C. *Curr. Opin. Nephrol. Hyperten.* **2002**, *11*, 475.

Siegbahn, P. E. M. Blomberg, M. R. A. Crabtree, R. H. *Theor. Chem. Acc.* **1997**, *97*, 289.

Simic, M. G. Jovanovic, S. V. *J. Am. Chem. Soc.* **1989**, *111*, 5778.

Simmonds, H. A.; Duley, J. A. Fairbanks, L. D.; McBride, M. B. *J. Inher. Metab. Dis.* **1997**, *20*, 214.

Skinner, K. A.; Whites, C. R.; Patel, R.; Tan, S.; Barnes, S.; Kirk, M.; Darley-Usmar, V.; Parks D. A. *J. Biol. Chem.* **1998**, *273*, 24491.

Sours, R. E.; Swift, J. A. *Am. Crystallogr. Assoc. Trans.* **2004**, *39*, 83.

Spataru, N.; Sarada, B. V.; Popa, E.; Tryk, D. A.; Fujishima, A. *Anal. Chem.* **2001**, *73*, 514.

Spencer, J. P. E.; Jenner, P.; Daniel, S. E.; Lees, A. J.; Marsden, D. C.; Halliwell, B. *J. Neurochem.* **1998**, 71, 2112.

Spina, M. B.; Cohen, G. *Proc. Natl. Acad. Sci. USA* **1989**, *86*, 1398.

Staal, F. J. T.; Ela, S. W.; Roederer, M.; Anderson, M. T.; Herzenberg, L. A., *Lancet* **1992**, *339*, 909.

Starkey, J. A.; Mechref, Y.; Muzikar, J.; McBride, W. J.; Novotny, M. V. *Anal. Chem.* **2006**, *78*, 3342.

Subramanian, P. Tyagi, S. K. Dryhurst, G. *Nucleosides & Nucleotides* **1987**, *6*, 25.

Tanaka, N.; Kolthoff, I. M.; Stricks, W. *J. Am. Chem. Soc.* **1955**, *77*, 1996.

Tanaka, N.; Kolthoff, I. M.; Stricks, W. *J. Am. Chem. Soc.* **1955**, *77*, 2004.

Tang, K.; Lin, Y.; Matson, D. W.; Kim, T.; Smith, R. D.; *Anal. Chem.* **2001**, *73*, 1658.

Taylor, G. I. *Proc. R. Soc. London, A* **1964**, *280*, 383.

Taylor, M. J. Richardson, T. *J. Food Sci*. **1980**, *45*, 1223.

Terashima, C.; Rao, T. N.; Sarada, B. V.; Kubota, Y.; Fujishima, A. *Anal. Chem.* **2003**, *75*, 1564.

Thompson, J. J. *Rays of Positive Electricity and Their Application to Chemical Analyses*, Longmans, Green and Co.: London, 1913.

Tse, D. C. S.; McCreery, R. L. R.; Adams, N. *J. Med. Chem.* **1976**, *19*, 37.

Tyapochkin, E.; Kozliak, E. *J. Mol. Catal. A* **2005**, *242*, 1.

Uchiyama, S.; Sekioka, N. *Electroanalysis* **2005**, *17*, 2052.

Van Berkel, G. J.; Asano, K. G.; Granger, M. C. *Anal. Chem.* **2004**, *76*, 1493.

Van Berkel, G. J.; Asano, K. G.; Granger, M. C. *Anal. Chem.* **2005**, *77*, 4366.

Van Berkel, G. J.; Enke, C. G.; Cole, R. B.; Martinez-Sanchez, M.; Fenn, J. B. *J. Mass Spectrom.* **2000**, *35*, 939.

Van Berkel, G. J.; *J. Am. Soc. Mass Spectrom.* **2004**, *15*, 1691.

Van Berkel, G. J.; Kertesz, V.; *Anal. Chem.* **2007**, *79*, 5510.

Van Berkel, G. J.; Kertz, V. *J. Mass Spectrom.* **2001**, *36*, 1125.

Van Berkel, G. J.; McLuckey, S. A.; Glish, G. L. *Anal. Chem.* **1992**, *64*; 1586.

Van Berkel, G. J.; Zhou, F. *Anal. Chem.* **1995a**, *67*, 2916.

Van Berkel, G. J.; Zhou, F. *Anal. Chem.* **1995b**, *67*, 3958.

Van Berkel, G. J.; Zhou, F.; Aaronson, J. T. *Int. J. Mass Spectrom. Ion Processes* **1997**, *162*, 55.

Van den Brandhof, W. E.; Haks, K.; Schouten, E. G.; Verhoef, P *Atherosclerosis* **2001**, *157*, 403.

Vanhoutte, K.; Van Dongen, W.; Esmans, E. L. *Rapid Commun. Mass Spectrom.* **1998**, *12*, 15.

Vestal, M. L. *Chem. Rev.* **2001**, *101*, 361.

Volk, K.J.; Yost, R. A.; Brajter-Toth, A. *Anal. Chem.* **1986**, *60*, 720.

Volk, K.J.; Yost, R. A.; Brajter-Toth, A. *J. Electrochem. Soc.* **1990**, *137*, 1764.

Volk, K. J.; Yost, R. A.; Brajter-Toth, A. *Anal. Chem.* **1992**, *64*, 21A.

Volk, K. J.; Yost, R. A.; Brajter-Toth, A. *Anal. Chem.* **1999**, *61*, 1709.

Wang, X.; Stanbury, D. M.; *Inorg. Chem.* **2008**, *47*, 1224.

Wang, Y. H.; Goddard, W.; Noyes, K. T.; Sowers, L. C.; Hwang, S; Chung, D. S. *J. Phys. Chem. B*, **2003**, *107*, 344.

Wang, Z.; Konigsberger, E. *Thermochim. Acta*, **1998**, *310*, 237.

Waring, W. S. Webb, D. J. Maxwell, S. R. J. *Q. J. Med.* **2000**, *93*, 707.

Watson, J. T. *Introduction to Mass Spectrometry*, 3rd ed, Lippincot – Raven, New York 1997.

White, P. C.; Lawrence, N. S.; Davis, J.; Compton, R. G. *Anal. Chim. Acta* **2001a**, *447*, 1.

White, P. C.; Lawrence, N. S.; Tsai, Y. C.; Davis, J.; Compton, R. G. *Mikrochim. Acta*, **2001b**, *137*, 87.

White, P. C.; Lawrence, N. S.; Davis, J.; Compton, R. G. *Electroanalysis* **2002**, *14*, 89.

Whitehead, R. E.; Ferrer, J. V.; Javitch, J. A.; Justice, J. B. *J. Neuron. Chem.* **2001**, *76*, 1242.

Whitehouse, C. M.; Dreyer, R. N.; Yamashita, M.; Fenn, J. B. *Anal. Chem.* **1985**, *57*, 675.

Willard, H. H.; Merritt, L. L.; Dean, J. A.; Settle, F. A. *Instrumental Methods of Analaysis*, 7th ed, Wadsworth Publishing Co.: California 1988.

Willoughby, R. C.; Browner, R. F. *Anal. Chem.* **1984**, *56*, 2626.

Willoughby, R. C.; Browner, R. F. *Anal. Chem.* **1988**, *60*, 489.

Winters, R. A.; Zukowski, J.; Ercal, N.; Matthews, R. H.; Spitz, D. R. *Anal. Biochem.* **1995**, *227*, 14.

Wu, S.; Zhang, K.; Kaiser, N. K.; Bruce, J. E.; Prior, D. C.; Anderson, G. A. *J. Am. Soc. Mass Spectrom.* **2006**, *17*, 772.

Xu, X.; Lu, W.; Cole, R. B. *Anal. Chem.* **1996**, *68*, 4244.

Xu, X.; Nolan, S. P.; Cole, R. B. *Anal. Chem.* **1994**, *66*, 119.

Yoshida, T. *J. Chromatogr. B* **1996**, *678*, 157.

Yue-Dong, Y. *Biomed. Chromatogr.* **1998**, *12*, 47.

Zenely, J. *J. Phys. Rev.* **1917**, *10*, 1.

Zhang, F.; Dryhurst, G. *J. Med. Chem.* **1994**, *37*, 1084.

Zhang, T.; Palii, S. P.; Eyler, J. R.; Brajter-Toth, A. *Anal. Chem.* **2002**, *74*, 1097.

Zhang, T; Brajter-Toth, A, *Anal. Chem.* **2000**, *72*, 2533.

Zhou, F.; Van Berkel, G. J. *Anal. Chem.* **1995**, *67*, 3643.

Zhou, L.; Zhai, B.; Yue, E.; Lee, L. M. *Anal. Bioanal. Chem.* **2006**, *385*, 1087.

Zhou, M.; Ding, J.; Shang, Q. *Anal. Chem.* **2007**, *79*, 5328.

Zvi, I.; Green, Y.; Nakhoul, Y.; Kanter, Y.; Nagler, R. M.; *Nephron. Clin. Pract.* **2007**, *105*, 114.

BIOGRAPHICAL SKETCH

N. Alpheus Mautjana obtained a Bachelor of Technology (B.Tech.) degree in analytical chemistry in 1997 from Vaal Triangle Technikon, now called Vaal Triangle Technical University in South Africa. He accepted a scholarship from African Explosives and Chemicals Industry (AECI), South Africa, to study for Master of Science (M.Sc.) degree in analytical chemistry at the University of Cape Town, which he completed in December 2000. He accepted a position with African Explosives Limited (AEL), a subsidiary of AECI, as a Team Manager in January 2001 and was later promoted to Plant Technical Services Manager which was his exit position in November 2003. N. Alpheus Mautjana joined the PhD program at the University of Florida in spring 2004 and at this, the completion of his PhD, he returns to South Africa.